Evaluation of Strain in Human Flexor Digitorum Profundus and Flexor Digitorum Superficialis Tendons Under Different Ex Vivo Loading Modalities

by

Nathan William Pool

A dissertation submitted to the Graduate Faculty of
Auburn University
in partial fulfillment of the
requirements for the Degree of
Doctor of Philosophy

Auburn, Alabama
August 3, 2024

Keywords: Cyclic Loading, Creep Loading,
Sequential Transition Ordering, Human Tendons

Copyright 2024 by Nathan William Pool

Approved by

Dr. Sean Gallagher, Chair, Hal N. and Peggy S. Pennington Professor Emeritus, ISE
Dr. Richard Sesek, Tim Cook Professor, ISE
Dr. Mark Schall, Daniel F. & Josephine Breeden Associate Professor, ISE
Dr. Sa'd Hamasha, Hal N. and Peggy S. Pennington Associate Professor, ISE
Dr. Ash Abebe, Professor and Chair, Mathematics and Statistics
Dr. Michael Zabala, Auburn Alumni Engineering Council Associate Professor, ME

Abstract

Tendon is an integral part of the musculoskeletal system. Improving our understanding of tendon properties can be useful for further developing musculoskeletal injury risk assessment models. This dissertation provides fundamental data on the mechanical properties of human tendons of the hands and wrist through *ex vivo* testing. This was accomplished through first determining the most common/appropriate methods to measure and test tendons. Human tendons from 14 donors ranging in age (30 - 77 years old) were used in the described studies. Tendons from these donors were exposed to either cyclic fatigue, creep, or sequence loading (combined loading) until failure. Results of these studies found that strains at failure of (8 - 22%) were consistent with known literature (8 - 20%) suggesting that tendon is similar in how strain develops regardless of anatomical location or tendon type. Though the strains at failure were within the above expected range, average times to failure varied (0.26 - 29.53 hrs.) depending on the test. A dependent relationship between applied stress and time to failure was also observed. Differences were found in creep times to failure when comparing tendons of the hands and wrist to the Achilles tendon. A statistically significant transition effect was found in combined loading to which in both levels of ultimate tensile strength (25 and 55%) transitioning from cyclic to creep resulted in an average difference in strain of 0.4% and 0.34% than if transitioning from a creep load to a cyclic load. The presence of a transition effect does not suggest that creep load results in more damage than cyclic, but instead shows slightly larger changes in strain when transitioning. Improving our understanding of the *ex vivo* viscoelastic properties of tendon provides fundamental data to improve injury risk assessment models.

Acknowledgments

First and foremost, I would like to my mother, Joy Pool. Your unwavering support and has allowed me to pursue my dreams of becoming an engineer. I would like to thank my best friend, Mr. Jesse Lykins, who has always believed in my potential, even when I had doubts, and his constant motivation has been invaluable. I am grateful to my advisor, Dr. Sean Gallagher. Although you have been challenging at times, I have come to understand that your approach stems from your desire to see me succeed. To Dr. Richard Sesek and soon to be Dr. Bob Sesek, without either of I am not sure how I would have made it to this point. Dr. Sesek, thank you for your unwavering guidance, support, and mentorship as I have continued to learn how to be an effective safety educator and practitioner. To Bob, words cannot express how grateful I am to you. Your continued guidance, and mentorship from crafting emails to thinking like an engineer have helped me to grow. Thank you. To my OSE friends and family, thank you for your continued support. The friendships I have made with you all have made this journey enjoyable. Your encouragement has been a source of strength, and I am fortunate to have such a wonderful network of people who genuinely care about my success. As the saying goes, "It takes a village," and this has never been truer. Thank you all for being a part of my life.

Table of Contents

List of Tables

Table of Figures

List of Abbreviations

ACGIH American Conference of Governmental Industrial Hygienists

ANOVA Analysis of variance

BLS United States Bureau of Labor Statistics

CI confidence interval

COD cause of death

COPD chronic obstructive pulmonary disease

CT computed tomography

CSA cross-sectional area

CTS carpal tunnel syndrome

D distal

DUE distal upper extremity

DUET Distal Upper Extremity Tool

EDL extensor digitorum longus

EHL extensor hallucis longus

ESRD end-stage renal disease

FDL flexor digitorum longus

FDP flexor digitorum profundus

FDS flexor digitorum superficialis

HAL hand activity level

ICC interclass correlation coefficient

IgA Immunoglobulin A

IS interfiber space

KD	kinked fiber deformations
L	left
LBP	low back pain
MSD	musculoskeletal disorder
PLA	polylactic acid
P	proximal
ROI	region of interest
R	right
RSI	Revised Strain Index
SD	standard deviation
TLV	threshold limit value
TPU	thermoplastic polyurethane
UTS	ultimate tensile stress

Chapter 1: Introduction

The human musculoskeletal system consists of several types of tissue, including bone, cartilage, ligament, tendon, muscle, and other connective tissue. The function of tendon is to connect muscle to bone, providing a strong yet flexible structure to allow for the transfer of large forces between them. This transmission of muscle force to bone is an essential factor in the ability of humans to perform physical movements. Like other tissues, tendons age over time and can incur damage or degrade because of a combination of many physical factors. Damage due to loading, aging, smoking, obesity, comorbid diseases, and other physical factors can increase one's risk for a tendon-related injury and/or reduction in normal function (da Costa & Vieira, 2009; Kirkendall & Garrett, 2007). Studying the multifactorial process of injury development requires us to develop our knowledge of tendon material properties from both physiological and mechanical perspectives. Specifically, we need to further our understanding of how tendon mechanical properties influence the etiology of injury development. The knowledge acquired from research in this area could improve existing musculoskeletal disorder (MSD) risk assessment models with the goal of preventing future occupational tendon-related injuries.

This dissertation focuses on the mechanical properties of flexor tendons that traverse the carpal tunnel when exposed to different loading modalities. This chapter provides a brief background of tendon structure and biomechanics and establishes the need for such research. It suggests how data generated from this dissertation could improve current MSD risk assessment models. In addition, this introductory chapter provides an outline of the dissertation, specify the specific aims, and gives a breakdown of the topics covered in later chapters.

1.1 Tendon Related Musculoskeletal Disorders

Tendons are a form of connective tissue that joins muscle to bone. When not subjected to undue high-force high-repetition and cumulative loading, tendons are able to withstand the forces associated with physical movement. The form and function of specific tendons depend on their location. Tendons connect muscle to bone via two junctions. The myotendinous junction is the connection between muscle and tendon, while the osteotendinous junction is the connection point between tendon and bone (Kannus, 2000).

Tendons are composed of a combination of collagen (75 - 86% of the dry weight), elastin (~2% of the dry weight), and water (60 - 80% of the wet weight) (Goodman & Choueka, 2005; James et al., 2008; R. F. Ker, 2002; Kirkendall & Garrett, 2007). The structure of tendons stems from tendon-specific cells known as tenoblasts and tenocytes that produce collagen and elastin. Cross-linked collagen molecules (tropocollagen) from the tenoblasts form a microfibril or collagen fibril. Groups of microfibrils are bundled, forming subfibrils or fibrils, and groups of subfibrils form larger fibrils or fibers. Figure 1 provides a visual representation of tendon anatomy and how each bundle of fibrils combines to form a tendon.

Figure 1: Visual Representation of Tendon Anatomy

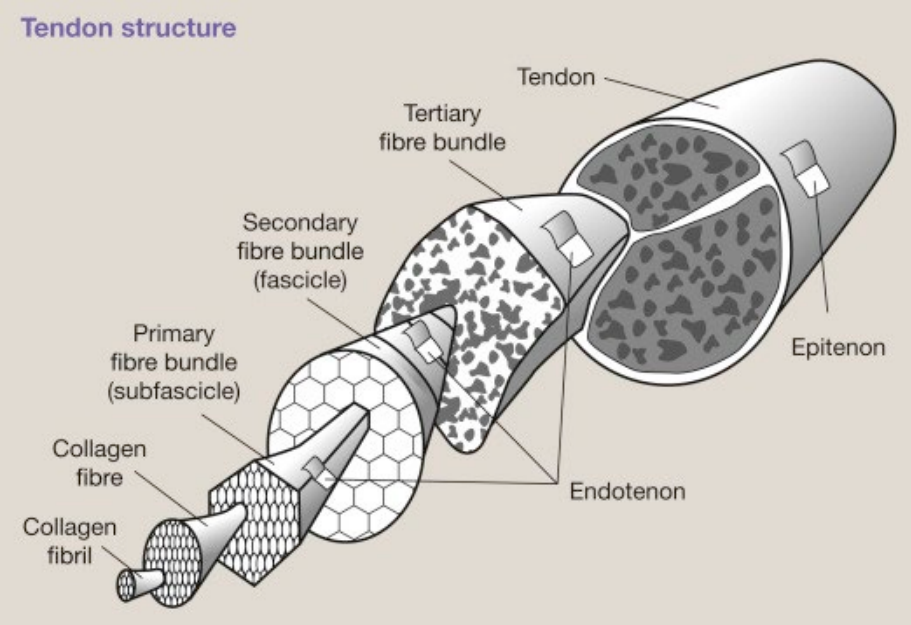

Note. Figure reprinted from "Tendon and ligament: basic science, injury and repair," by *K. Parmar, 2018, Orthopedics and Trauma,32(4), 241-244. Copyright [2018] by Elsevier.*

Tendons are encased in either a synovial membrane or paratenon. For example, tendons such as the Achilles and quadriceps are encased in a paratenon. However, tendons such as the flexor digitorum profundus (FDP) and superficialis (FDS) are encased by a synovial membrane. One function of the synovial membrane is to contain synovial fluid. This fluid enables smooth tendon gliding in the tendon sheath and provides nutrients to tendon cells through diffusion as a result of movement (Goodman & Choueka, 2005; James et al., 2008; Shepherd & Screen, 2013). The paratenon also enables smooth tendon gliding by reducing friction from tendons rubbing against each other. However, while smooth gliding likely reduces the rate of injury to the tendon, it cannot prevent all damage that might occur over time. Injuries include but are not limited to tendon rupture or tear and the development of tendon-related musculoskeletal disorders (MSDs)

such as tendonitis, tendinosis, and tenosynovitis. There are many approaches to studying the different mechanisms that may play a role in the development of MSDs, ranging from the microscopic (Zitnay et al., 2020) to the macroscopic (Schechtman & Bader, 1994, 1997, 2002; Smith, 2019). To better understand these mechanisms, it is important to consider and understand the biomechanics of tendon tissue. The section that follows provides an overview of this topic.

1.2 Tendon Biomechanics

Tendons facilitate the transmission of high muscle forces to bone, enabling motion with minimal deformation or energy loss. Tendon is stronger per unit area than muscle and its tensile strength is almost equivalent to bone (James et al., 2008). Such characteristics are attributed to the mechanical properties of collagen fibers that make up this material (Miller & Freivalds, 1995). Collagen falls into a category of materials described as “viscoelastic”. A viscoelastic material is a material that exhibits both elastic and viscous behavior when deformed. Thus, tendons demonstrate properties such as hysteresis (the reaction of a system to changes made by a past reaction), creep deformation (the elongation of a material under a constant load), stress relaxation (the decrease in stress under constant strain), and strain rate dependency. In addition to the properties mentioned above, tendons have other important mechanical properties, such as tensile and residual strength. *Ex vivo* testing of different loading modalities would be required to collect data on such properties. Examples are tests of creep (application of a constant load) or cyclic loading (the application of repeated stress or load on a material).

Another component of studying tendons' mechanical and viscoelastic properties is the stress-strain relationship (Goodman & Choueka, 2005; James et al., 2008; Shepherd & Screen, 2013). Stress (σ) is the ratio of force to the cross-sectional area (CSA) of a material, while strain (ε) is the ratio of the change in displacement (length) with respect to the material’s initial length.

The stress-strain curve for tendons has four regions: toe, linear or elastic, plastic, and failure. An example is shown in Figure 2.

Figure 2: Sample Stress Strain Curve

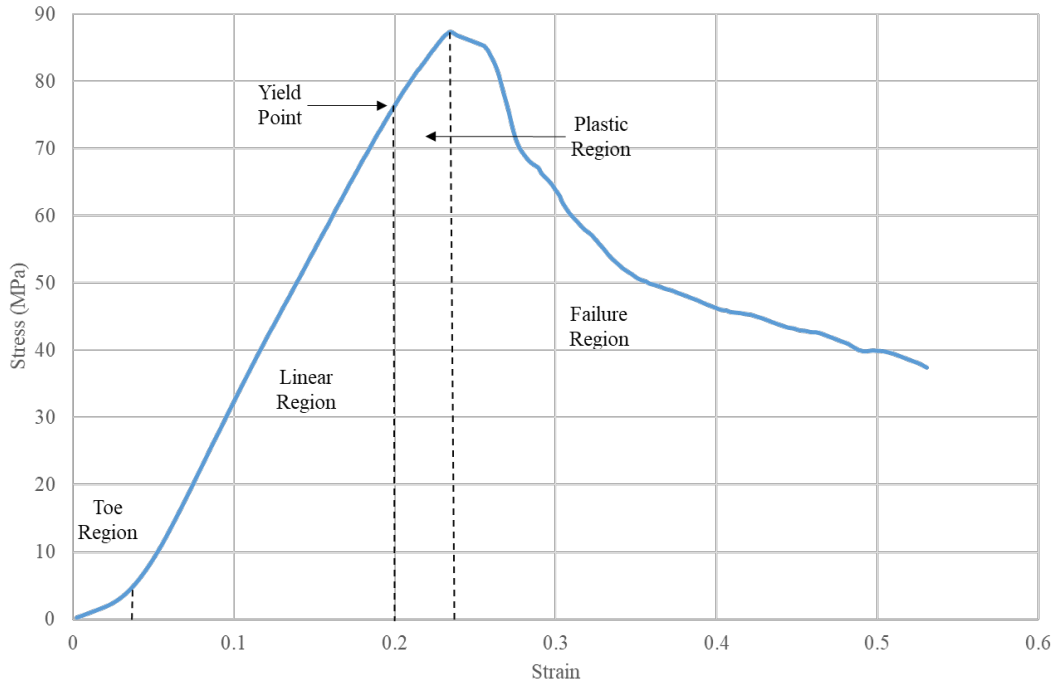

Note. Example of a stress-strain curve for tendons demonstrating four regions: the toe region, linear region, plastic region, and failure region.

The toe region is where the initial loading causes the uncrimping of collagen fibers prior to tendon elongation. Loading in the linear or elastic region exhibits constant elongation or strain as stress increases. In this region, strain is recoverable after stress is released. The slope of the elastic region provides Young's modulus of elasticity, a measure of material stiffness (James et al., 2008). The third region is the plastic region, which commences at the elastic region's yield point. The yield point is the point where the curve's slope changes, after which destructive

changes occur in tendons leading to a loss of elasticity. The final region is the failure region. At this point, several mechanisms could occur, including increasing elongation with decreasing load, unpredictable failure of collagen fibers, and tears that can result in rupture (Goodman & Choueka, 2005; James et al., 2008; K. & Saarakkal, 2011; Kirkendall & Garrett, 2007).

1.3 Fatigue Failure and Mechanical Testing of Human Tissue

Fatigue failure is the process by which materials fail when subjected to repeated stress, which consists of initiation and propagation of micro-failures due to repetitive or cyclic loading. The fatigue failure process has long been studied in non-biological materials (Gallagher & Schall Jr., 2017a); however, there is considerable evidence that this process applies to biological tissue (specifically musculoskeletal tissue) (Gallagher & Schall Jr., 2017a). Studies have also noted a link between mechanical loading and MSD risk (Andarawis-Puri & Flatow, 2011; Gallagher & Heberger, 2013; Gallagher & Schall Jr., 2017a). Specifically, an interaction between force and repetition has been identified which suggests a potential fatigue failure process. This relationship has been evaluated through the mechanical testing of both human (Schatzmann, 1998; Schechtman & Bader, 1994, 1997, 2002; Wren et al., 2003) and other mammalian tissue (Fung et al., 2009, 2010; Wang et al., 1995; Wang & Ker, 1995).

Mechanical testing of tissue refers to a variety of methods that have been used to better understand the mechanical properties of biological tissue. Typically, this involves placing a tissue sample between grips and or another type of fixture connected to an actuator that exposes a sample to some form of stress (tensile, fatigue, creep, compression, shear, etc.) for a specified period or testing to a specified parameter (e.g. max/min loads, extension, strain). In order to complete such tests, a wide variety of gripping fixtures have been used to secure testing samples. Scholze et al., 2018 however suggests that the large variety in fixture type can negatively impact

the accuracy and validity of study results, further suggesting that the validity issue is related to a lack of standardization. Material slippage is also noted as a potential source of error resulting from the use of different clamping systems.

There is a lack of both *in vitro/ex vivo* testing studying the mechanical properties of human tendons and a lack of standardization in performing such experiments. Specific tests include creep loading and evaluating the effects of sequential load ordering. Sequential load ordering is the concept of performing a repeating sequence of the same or different loading conditions (in combination) at set stress levels for a given duration or sequences.

1.4 Common Tendon Musculoskeletal Disorders and their Development

MSDs are injuries or disorders affecting the muscles, nerves, tendons, joints, cartilage, and spinal discs (da Costa & Vieira, 2009). As of 2018, the United States Bureau of Labor Statistics (BLS) noted that there were 272,780 days away from work (DAFW) from MSD cases, with the median DAFW being 12 days (BLS, 2021). According to the BLS, in 2020, there were 3,910 reported cases of CTS resulting in DAFW and 1,380 reported cases of tendonitis leading to DAFW (BLS, 2021). The development of MSDs can be impacted by a combination of physical and health-related risk factors that are not fully understood (Millar et al., 2021; Neviaser et al., 2012; Shepherd & Screen, 2013). Physical risk factors include high-force exertions, repetitive tasks, use of non-neutral postures, and exposure to whole-body or hand-arm vibration (Andarawis-Puri & Flatow, 2011; Gallagher & Schall, 2016; National Research Council and Institute of Medicine, 2001; Neviaser et al., 2012; NIOSH, 1997). In addition, risk factors may include personal characteristics such as age, sex, genetics, smoking, high body mass index (BMI), and comorbidities (da Costa & Vieira, 2009; Gallagher & Schall Jr., 2017a; Millar et al., 2021; Thornton & Hart, 2011). If injuries occur, these types of conditions and/or disorders can

place a large burden on both the worker (potential for poor quality of life, workplace disability) and employer (financial loss from training of new/replacement employee, loss of productivity, medical coverage for injured employee) (Bhattacharya, 2014).

1.4.1 Tendon-Related Musculoskeletal Disorders

A common term used to describe MSDs related to tendon degradation is tendinopathy. Common examples of tendinopathy include tendonitis (inflammation of tendons resulting from microtears that occur from overloading the tendon) and tendinosis (non-inflammatory degradation of tendon collagen as a response to repeated overuse) (Bass, 2012). The development of tendonitis begins with some damage to a tendon resulting in an inflammatory response. Tendon is less vascularized than muscle and bone, which leads to limited healing capability. As a result, tendons may not fully recover from incurred damage. Incurred damage could lead to non-inflammatory degradation of collagen, resulting in tendinosis. Specific tendinopathies include trigger finger, rotator cuff syndrome, medial epicondylitis (golfer's elbow), and lateral epicondylitis (tennis elbow) (Millar et al., 2021).

1.5 Distal Upper Extremity Ergonomic Risk Assessment Tools

Several observation-based risk assessment tools have been developed to aid practitioners in predicting injury risk for mono and/or multi-task jobs. Risk assessment tools include the Distal Upper Extremity Tool (DUET) (Gallagher et al., 2018), the Revised Strain Index (RSI) (Garg et al., 2017), and the American Conference of Governmental Industrial Hygienists (ACGIH) threshold limit value (TLV) for Hand Activity (ACGIH, 2018). Risk assessment tools such as DUET, RSI, and ACGIH TLV for Hand Activity use a combination of qualitative measures such as perceived exertions and quantitative measures such as number of repetitions for a given

task(s) throughout the workday. It has been documented through longitudinal studies that the RSI, and the ACGIH TLV for Hand Activity have demonstrated the ability to predict the risk of injury or development of an MSD for a given task or set of tasks (Garg et al., 2017; Yung et al., 2019). While a cross-sectional study conducted by Gallagher (2018), used DUET to demonstrate an association between estimated exertion level, number of repetitions and distal upper extremity outcomes (Gallagher et al., 2018). However, none of the aforementioned tools consider the effects of creep loading or the combined effects of creep and cyclic loading. Collecting such data could improve our understanding of the role of creep loading for future risk assessment tools.

1.6 Specific Aims

The research presented in this dissertation was developed to address three specific aims concerning research gaps in the current scientific literature regarding the *in vitro/ex vivo* mechanical properties of human tendons. The specific aims of this dissertation are as follows:

Aim 1. Determine the strain responses of flexor digitorum profundus and flexor digitorum superficialis tendons under cyclic loading at different stress levels.

Aim 2. Determine the effect of creep loading on the development of strain in flexor digitorum profundus and superficialis tendons at different stress levels.

Aim 3. Investigate the effect of combined creep and cyclic loading on the change in strain of flexor digitorum profundus and flexor digitorum superficialis tendons.

1.7 Organization of the Dissertation

This dissertation is organized into six chapters; this section provides a description of the topics to be discussed. Chapter 2 presents a literature review that will provide a background and introduce common themes that will be discussed throughout this dissertation. Chapter 2 also

discusses current testing methodologies that have been used for *in vitro* and *ex vivo* testing of tendons and the current challenges involved with this type of testing. Chapter 3 evaluates the ultimate tensile stress (UTS) of flexor digitorum profundus and flexor digitorum superficialis tendons and the fatigue life of flexor digitorum profundus and flexor digitorum superficialis tendons under cyclic loading at different levels of stress. Chapter 4 examines the effect of creep on the failure of flexor digitorum profundus and flexor digitorum superficialis at different stress levels. Chapter 5 investigates the effect of combined sequential creep loading and cyclic loading order on the failure of flexor digitorum profundus and flexor digitorum superficialis tendons. Chapter 6 discusses the key findings and limitations of the presented studies and provides a conceptual model of the effects of creep and cyclic loading on tendons. Recommendations for future research are also discussed in Chapter 6.

Chapter 2: *Ex Vivo/In Vitro* Loading of Human Tendon: A Literature Review of Recent Testing Methods

2.1 Introduction

Mechanical testing of tendons has been performed as early as the 1960s (Abrahams, 1967). In principle, performing a mechanical test is rather simple. A specimen is placed between clamps and/or a holder attached to an actuator and a load cell. From this point, a specimen can be exposed to different loading and/or environmental conditions. Loading conditions may include different modalities such as impact, cyclic, creep, tensile, compression, etc. Environmental conditions include temperature, emersion in a hydration solution, and testing inside or outside the original system. In science, the phrase *in vitro* refers to experiments conducted in a laboratory, often in a test tube or following the literal translation from Latin of "in glass." In contrast, *ex vivo* can refer to experiments conducted on tissue outside the living body or "out of the living." These terms have often been used interchangeably to describe tendon-testing experiments, but this should not be considered the proper practice as this could cause confusion.

The purpose of this review is to present common practices of *in vitro/ex vivo* testing techniques used in previous research examining the use of creep and cyclic loading in the testing of human tendons and provide notable findings. Methods described in this review include grip type, hydration method, loading modality, cross-sectional area measurement, and other considerations. Methods discussed in this review were found using the search strings described in the following section. Some methods were irrelevant to the loading used in this study. Thus, this review will not cover irrelevant aspects of different testing types. Examples of testing methods not discussed in detail by this review include examining the strength of different suture techniques on lacerated and/or ruptured tendons (Jahnke et al., 2019), the mechanical testing of

lacerated tendons (Erhard et al., 2002), and the mechanical testing of other tissue such as ligaments (Thornton et al., 2007; Thornton & Bailey, 2012). Due to the limited number of studies examining *in vitro*/*ex vivo* human tendon characteristics, some papers using mammalian tendons are included in this review.

2.2 Methods

Relevant articles from 1965 through 2021 were identified using three internet databases: Google Scholar, Medline, and Science Direct. Different combinations of search strings (Table 1) were used for the databases. The search strings included the Boolean logic operator 'AND' for all strings. Only peer-reviewed journals, research articles, short communications, and reviews written in English were used in this literature review. Searches excluded books, book chapters, abstracts, proceedings papers, and non-full text articles not in peer-reviewed journals. In addition, ten articles from a personal database of articles were initially included in this review. The selection process for the articles used in this review was conducted in a series of six phases. Phase 1 was the initial determination of the number of articles in the relevant search. At the time the search was performed, a total of 672 documents were derived from the three databases. During phase 2, material of the exclusion types mentioned above was removed, resulting in 641 remaining documents. A screening of duplicate articles was performed, which eliminated 189 articles. For example, the "creep loading" AND "of human tendons" in Medline generated five articles, all of which were duplicates of those generated using a different database. Article relevance was determined by the following criteria: 1) relevance to the subject matter of the review (*ex vivo* testing of human tendons), 2) full-text articles in peer-reviewed journals, and 3) written in English. Phase 3 involved screening articles based on title relevance. This screening removed two hundred and thirty articles, resulting in 222 remaining articles. Phase 4 was

screening based on the abstracts in which 109 articles were removed, resulting in 113 remaining articles. Phase 5 removed articles based on the article's relevance; 58 were removed, and 55 remained. Phase 6 added three articles that were found through a review of sources from the relevant articles. This review process is represented in Figure 3.

Table 1: Boolean Logic Terms

Search String	Search Term
1	‘cyclic loading’ AND ‘of human tendons’
2	‘creep loading’ AND ‘of human tendons’
3	‘residual strength’ AND ‘of human tendons’
4	‘residual strength’ AND ‘biomaterial’ AND ‘fatigue’

Figure 3: Search String Process

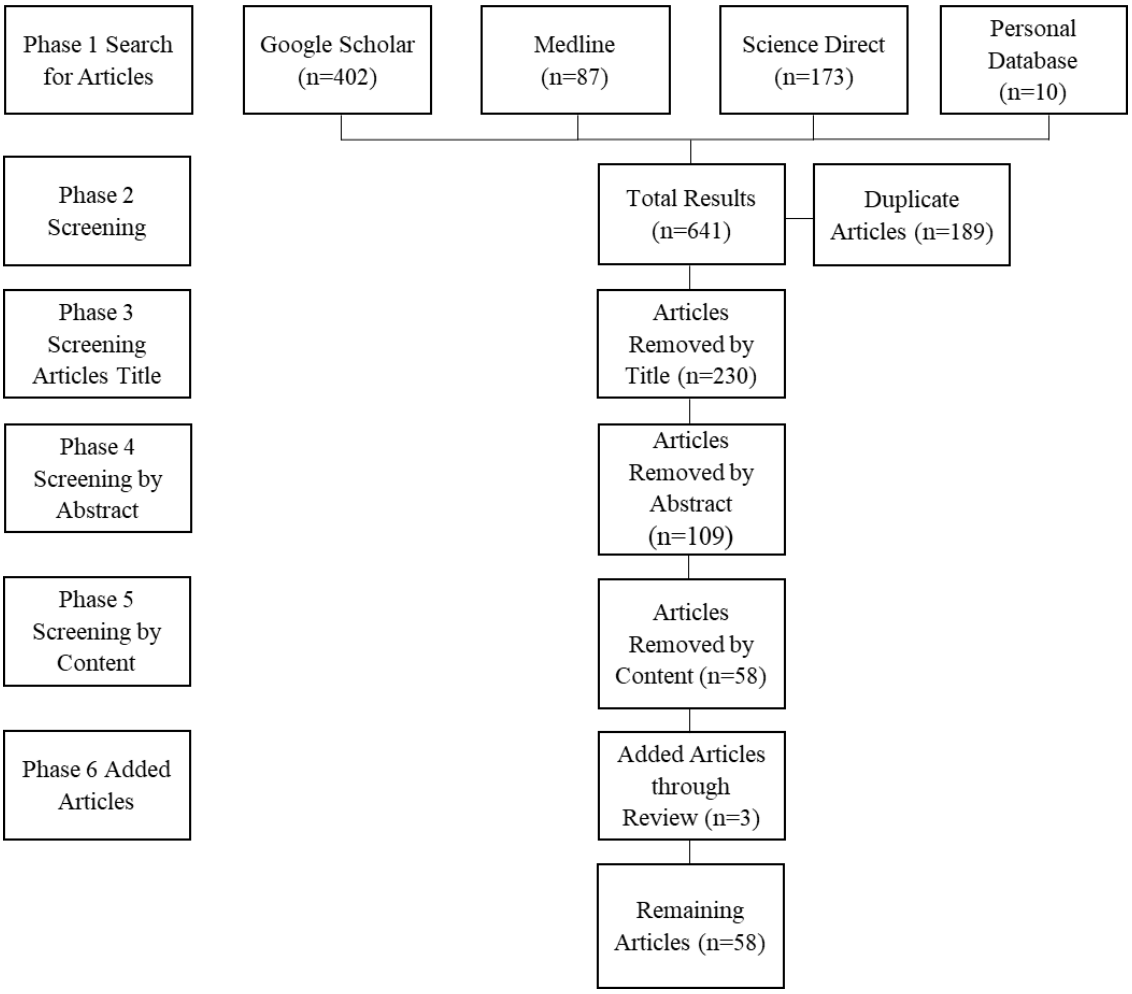

2.3 Results

The findings discussed in this section focus on considerations regarding the mechanical testing of tendons. Mechanical properties of human tendons, such as tensile strength, can vary between individuals and within the same individual performing a similar task (Komi et al., 1992). Similar variation was noted in adult mammalian tendons both in mass (0.04 - 545 kg) and UTS (40 - 144 MPa) (R. F. Ker et al., 2000). To account for variation, *ex vivo* tendon tensile test data have typically been normalized to an average UTS. For example, Schechtman and Bader 1994, Schechtman and Bader 1997, and Schechtman and Bader 2002 found that the UTS for freshly excised extensor hallucis longus (EHL) and extensor digitorum longus (EDL) tendons were around 100 MPa. Anatomically, both the EDL and EHL tendons are in close proximity (extensors of foot distal phalanges) and have similar functions. It is, therefore, plausible to assume that these tendons would have similar mechanical functions and viscoelastic properties. Thus, testing them at the same estimated level of nominal stress is logical.

Findings from *ex vivo* studies such as Wren et al., 2003 note the importance of the initial strain in predicting time and cycles to failure based on their data and failure model. The authors also suggest that tensile strain influences tendon development and functional adaptation. Wang & Ker, 1995 studied wallaby tail tendons and found that their results agree with the concept that damage accrued during tertiary creep has the most significant effect on the stiffness and strength of the specimen over time. The authors noted that during tertiary creep, the tendon acts as if the CSA of the intact specimen is being reduced; this is also known as necking. Although Wang & Ker, 1995 did not further discuss their observation in detail, it does suggest a potential insight on an aspect of mechanical testing of *ex vivo* tissue. As previously discussed, tendon is similar in composition and mechanical properties between species suggesting necking could be observed in

tendons of different species when exposed to *ex vivo* mechanical loading. Other notable findings include Fung et al., 2009 and Fung et al., 2010. In the study by Fung et al., 2009, the researchers performed a series of *ex vivo* fatigue tests on fresh rat flexor digitorum longus (FDL) tendons to quantify changes in the mechanical properties and corresponding changes to tendon structure at controlled load levels. Fatigue levels of low (6 - 7% strain), moderate (8.5 - 9.5% strain), and high (11 - 12% strain) were defined based on peak clamp-to-clamp strain. In the 2010 *in vivo* study, the researchers developed and tested an *in vivo* animal model for evaluating tendon response to fatigue loads at varying levels of damage based on the *ex vivo* results of the 2009 study. The researchers further tested their model using patellar tendons of anesthetized rats. The patellar tendons of the rats in the study were exposed to fatigue loading at different levels of failure strength based on results from the 2009 study. In both studies, the authors observed "kinked deformations" in rat patellar tendons. The kinks are ridge-like formations in the tendon fibers. They noticed these kinks transverse multiple fibers that started to form even at low levels of fatigue (6 - 7% strain based on grip-to-grip displacement). The authors suggest that the kinks result from early fatigue damage and contribute to the accumulation of damage demonstrated in Figure 4.

Figure 4: Microscopy of Rat Patellar Tendons

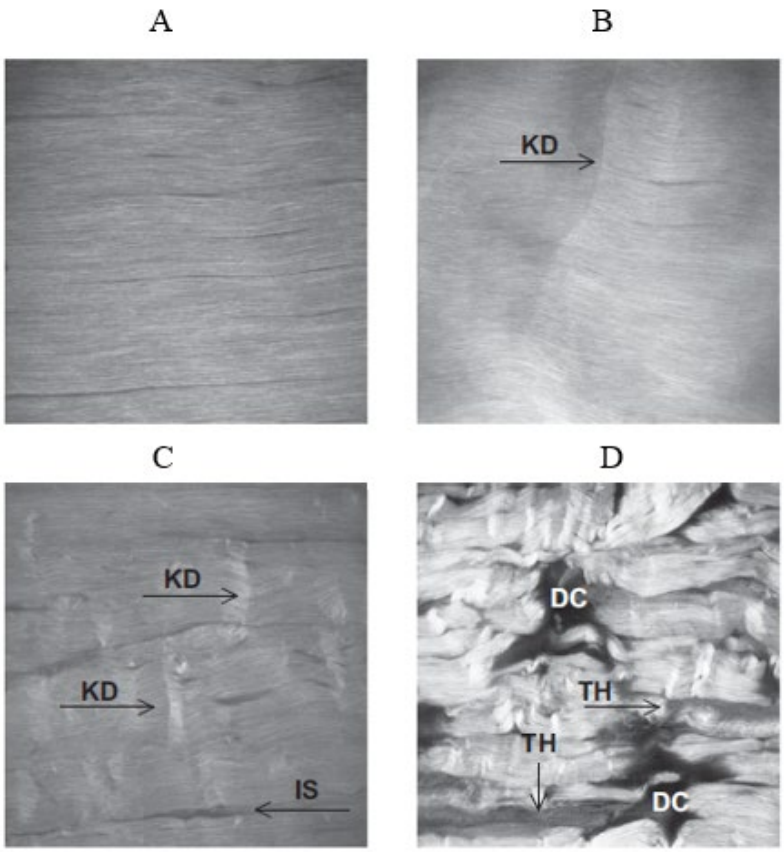

Note. (A) Control tendon image, no visible signs of damage. At low fatigue (B) isolated kinked fiber deformations (KD) spans multiple fibers. (C) Moderate fatigue, widening of interfiber space (IS) and appearance of increased kinking. (D) High fatigue decreased fiber alignment and further widening of interface space. Regions of low signal intensity suggest fiber thinning (TH) and more severely, matrix discontinuities (DC). FOV = 400mm. Figure reprinted from Fung, D. T., Wang, V. M., Andarawis-Puri, N., Basta-Pljakic, J., Li, Y., Laudier, D. M., Sun, H. B., Jepsen, K. J., Schaffler, M. B., & Flatow, E. L. (2010). Early response to tendon fatigue damage accumulation in a novel in vivo model. Journal of Biomechanics, 43(2), 274–279. Copyright [2009] by Elsevier.

The findings from both papers are consistent with Wren et al. (2003) regarding the importance of strain in the fatigue failure process. The authors provide further support that damage accumulation can, in part, result from repetitive loading in living tissues. The papers evaluated in this review support the idea that, similar to other viscoelastic materials, tendons incur damage via fatigue failure, highlighting the importance of this type of testing and the role fatigue failure plays in the development of tendon injury (Andarawis-Puri & Flatow, 2011; Fung et al., 2009, 2010; Gallagher & Schall Jr., 2017b; Neviaser et al., 2012; Parent et al., 2011; Shepherd & Screen, 2013).

2.3.1 Grip Type and Clamping Technique

There are a range of grip types, jaw faces, and clamping techniques that have been utilized in both creep and cyclic testing of human tendons and other mammalian musculoskeletal tissue. The terms “grips” and “clamps” have been used in the literature interchangeably. Grip and clamp generally refer to a mechanical device (hydraulic, pneumatic, self-tightening, cryogenic/freeze, wedge) that applies pressure as a clamping force to the specimens, which holds and stabilizes the specimen for testing. Depending on the type of grip, a range of jaw faces can also be selected. Examples are shown in Figure 2.3. Different designs and combinations of clamping technique, jaw faces, and grips mentioned above stem from the need to reduce specimen slippage, damage to the tissue caused by the physical clamping of the tissue, and the risk of the sample failing outside of the testing region (near clamping site or inside of jaw face).

Figure 5: Examples of Jaw Faces

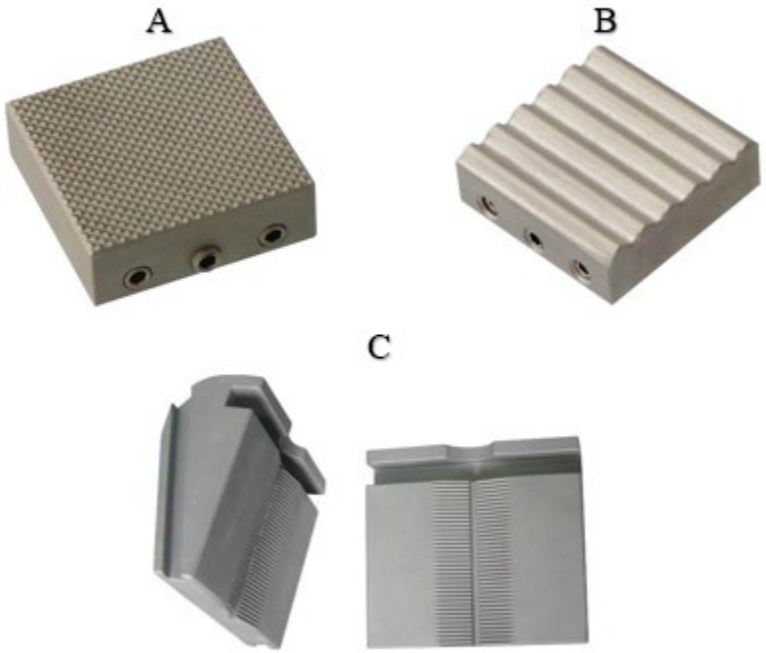

Note. (A) Pyramid or serrated jaw face. (B) Wave or serpentine jaw face. (C) V jaw face specifically for wedge grips. Images for the jaw faces procured from (Grip-Engineering Thümler GmbH, 2024)

Jiang et al. (2020) reviewed several clamping techniques for biological tissue and developed a clamping mechanism/device for fibrous membrane tissue such as rat abdominal wall tissue. Scholze et al. (2018; 2020) developed a set of 3D-printed clamps using hydraulic grips to hold tendons in place to prevent slippage and reduce the risk of the sample failing outside of the testing range. The most common grips types covered in this review for both human and animal tendon testing are freeze/cryogenic clamps (De Zee et al., 2000; Devkota & Weinhold, 2003; Hangody et al., 2016; Kiss et al., 2009; Schatzmann, 1998; Wren et al., 2003) and grips using a sandpaper technique (Ensey et al., 2009; Fung et al., 2009; Szczesny et al., 2018). Other used

grip types include self-tightening clamps (Abrahams, 1967; Schechtman & Bader, 1994, 1997, 2002), pneumatic and or hydraulic grips (Scholze et al., 2018), and custom grips (Chandrashekar et al., 2012; Ensey et al., 2009; Huang et al., 2011; Jiang et al., 2020; Kondratko-Mittnacht et al., 2015; Szczesny et al., 2018) or grips with other non-flat jaw faces (serpentine, wave, etc.) (Flick et al., 2006; KarisAllen & Veres, 2020; Peterson & Szczesny, 2020; Pike et al., 2000; Shepherd, Legerlotz, et al., 2014).

2.3.2 Hydration

Researchers testing tendons have also used a variety of hydration methods and solutions to better simulate the biological environment from which the tendons were dissected. Such methods include temperature-controlled hydration bath/system (Abrahams, 1967; Fung et al., 2009; KarisAllen & Veres, 2020; Pike et al., 2000; Szczesny et al., 2018; Wang et al., 1991; Wren et al., 2003), non-temperature controlled bath/system (Ensey et al., 2009; Kondratko-Mittnacht et al., 2015; Peterson & Szczesny, 2020; Shepherd, Legerlotz, et al., 2014; Shepherd, Riley, et al., 2014), spray methods (this method involves using a spray bottle and at regular intervals spraying the sample to avoid over hydration or dehydration) (Chandrashekar et al., 2012; Schechtman & Bader, 1994), wet gauze/paper technique (this method involves wrapping the specimen within a soaked gauze for the duration of the test) (Devkota & Weinhold, 2003; Herod & Veres, 2017; Schatzmann, 1998; Wang et al., 1995), and saline drip (Smith, 2019). This review did not find research directly comparing the different hydration techniques and their effects on tendon properties. Previous research has used a variety of hydration solutions, including phosphate-buffered saline (PBS), Ringer's solution, and paraffin wax. Evidence suggests that PBS can alter excised tendon properties (R. Ker, 2007). Support for this claim stems from an article referenced by (R. Ker, 2007) that examined rat tail tendons immersed in

two different hydration solutions for over 15 hours. The authors of this article suggest that PBS incubation caused fascial swelling resulting in a reduction in mechanical properties, which may limit the capacity to resist shear (Screen et al., 2005). Schechtman, 1995 noted that swelling occurred in the tendon when fully immersed in Ringer's solution, which increased measured CSA without increasing tensile strength, thus, reducing the calculated experienced stress at failure. These articles, however, do not discuss the use of 0.9% physiological saline as a hydration solution.

2.3.3 Loading Modalities

The articles discussed in this review indicate a lack of research studying creep, combination (sequence) loading, and the effects on human tendons. In contrast, cyclic and tensile loading has been more prevalent. Table 2.2 demonstrates the lack of creep testing results for human tendons in the current review. A plausible explanation for this is that research examining the effects of creep loading on excised human tendons has yet to be thoroughly examined. It is also plausible that the results were limited due to the specificity of the search strings. Along with creep, the results of the review indicate a lack of testing involving combinations of creep and cyclic loading and a lack of papers studying tendon residual strength.

Table 2: Testing Practices in Human Tendon Studies

Authors	Loading Type				Pre-Load Conditioning	Testing Temperature	Hydration Method (During Testing)	Grip Type	Tendon Tested	CSA Measurement Method
	Cyclic	Creep	In Combination	Tensile /Quasi Static						
Abrahams, 1967				✓		37°C	Ringer's Solution bath	Self-tightening	Achilles	Calculated with density and length
Chandrashker et al., 2012	✓					Room	Sprayed with Saline	Custom	Patellar	
Hangody et al., 2016				✓		Room		†	††	
Hohmann et al., 2019				✓	✓	Did not specify			Biceps	Measured Diameter instead
Schatzmann et al., 1998	✓				✓	Room		Cryogenic/freeze	Quadriceps	Calipers
Schechtman & Bader 1994	✓			✓		Room	Saline Drip	Self-tightening	EDL/EHL	Area micrometer
Schechtman & Bader 1997						Room	Saline Drip	Self-tightening	EDL	Area micrometer
Schechtman & Bader 2002	✓					Room	Saline Drip	Self-tightening	EDL	Area micrometer
Scholze et al., 2018	✓				✓	21°C	Soaked clamps in saline, pre-treated tendons, treated tendons every 20 mins	Hydraulic grips with 3D printed mount	FDP/FDS	
Smith 2019	✓					Room	Saline Drip	Wedge Grips with sandpaper	FDP/FDS	Method used by (R. F. Ker, 1981)
Wren et al., 2003	✓	✓				37°C	Phosphate buffered saline bath	Cryogenic/freeze	Achilles	High-frequency ultrasound

Note. (†) Several grip types were used: Premicron 3 surgical thread, general mounting clamp, cement fixation, wire mesh, Shi's modified freeze clamp. (††) Bone-patella tendon bone grafts, semitendinosus, gracilis, quadriceps tendon bone grafts, Achilles, and peroneus longus tendons

2.3.4 Cross-Sectional Area Measurement

CSA is a critical measure when it comes to analyzing stress. However, obtaining this measure is not always easy. Reasons for this include non-uniform material shape, tendon size, and drawbacks associated with certain measurement tools. Common measurement techniques include ultrasonography (Kruse et al., 2017; Wren et al., 2003), estimating CSA using an assumed density of 1,120kgm^{-3} (R. F. Ker, 1981; Smith, 2019; Wang et al., 1991, 1995; Wang & Ker, 1995), using an area micrometer (Schechtman & Bader, 1994), or using a caliper (Schatzmann, 1998). Other measurement techniques include the use of magnetic resonance imaging (MRI) (Kruse et al., 2017) and computed tomography (CT). Hayes et al. 2019 provide a literature review comparing current techniques for measuring CSA in soft tissue inside and outside the system.

A review by Hayes et al. 2019 classified measuring methods as involving contact, non-contact, destructive, and approximation. The authors also noted that these methods could be classified as either *ex vivo* or *in vivo* techniques. Hayes et al. 2019 do not define their measuring methods. The authors instead provide a description and examples of the different methods. Contact measuring refers to methods or techniques involving physically manipulating *ex vivo* specimens to measure them. Such methods discussed by Hayes et al. 2019 include area micrometry, 2D/3D ultrasound, and casting. A ruler, for example, is mentioned in the review but is not considered a contact method. A challenge with some contact methods results in the destruction of the specimen to measure the CSA, preventing further use of such methods, including using a planimeter or sectioning. Some destructive techniques prevent further specimen use (Hayes et al., 2019; Vergari et al., 2010).

Non-contact refers to methods that do not come into physical contact with the specimen during the measurement process. Non-contact approaches include CT, MRI, and laser micrometry. MRI has been shown to have conflicting results in accuracy and reliability (Hayes et al., 2019). However, CT may have limited clinical use due to difficulty differentiating soft tissues (Hayes et al., 2019). Estimation methods such as the gravimetric method (using length and volume) often assume uniform areas along the length. This assumption could negatively affect stress calculations for mechanical testing.

Hayes et al., 2019 mention the importance of reliability, repeatability, and reproducibility when selecting a measuring method due to their potential effects on comparing the results of different studies. They suggest that our ability to compare methods and techniques of *in vivo* tendon measurements is limited due to a lack of control of measurements. These measurements could enable us to compare measurements between different methods and studies. Although the authors discuss several types of measurement methods, the authors did not discuss different types of CT scanners such as volumetric, high resolution, micro, and the potential to measure excised tendon CSA.

2.3.5 Other Practical Considerations

Other areas of consideration when testing tissue include freeze-thaw cycles (Chang et al., 2014; Huang et al., 2011; Lee & Elliott, 2017; Quirk et al., 2018), donor search criterion and medical history, access to fresh human tissue samples, and testing machine specifics. Freeze-thaw cycles refer to the number of times samples are taken from a frozen state (commonly -20°C for human tendon testing) to testing temperature. It is well known that excised tissue will degrade faster than tissue inside a living system. Limiting the number of freeze-thaw cycles can help slow the tissue decomposition process prior to testing (Huang et al., 2011).

Access to fresh human tissue itself can be challenging, and donor restrictions may be necessary depending on the research goals. When studying tendon properties, it is advisable to avoid donors with any known history of endocrine diseases such as diabetes mellitus, any known bone or joint diseases, and/or a history of smoking (Schechtman & Bader, 1994). A reason for this recommendation is due to the common clinical understanding that smoking (nicotine) and comorbidities such as diabetes have been shown to impair healing response (Bishop et al., 2015; Gallagher & Barbe, 2022; Guo & DiPietro, 2010; Nichols et al., 2020; Santiago-Torres et al., 2015; Silverstein, 1992). The resulting impaired healing response could negatively affect tendon properties.

Reviews by Santiago-Torres et al., 2014, and Bishop et al., 2015 demonstrate the negative impacts of smoking on rotator cuff injuries, disease, and clinical outcomes after rotator cuff repair. Their findings suggest that smoking negatively affects tendon properties leading to an increased risk for rotator cuff injuries or disease (Bishop et al., 2015; Santiago-Torres et al., 2015). Both reviews do not discuss direct mechanical changes in tendon properties but provide support for overall impacts regarding healing and rotator cuff injuries. To investigate potential negative effects on tendon properties, Ichinose et al., 2010 performed a study with rats infused with different concentrations (low dose, high dose) of nicotine compared to a control group without nicotine exposure. Results from the study show that the maximum stresses and loads were higher for rats administered nicotine regardless of dose (low or high) when compared to the control group. The differences in maximum load and stress were not statistically significant for both nicotine groups. The results show that the difference in the elastic modulus of both nicotine dose groups were statistically significant compared to the control group (low dose vs. control

group: $p = 0.03$; high dose vs. control: $p = 0.04$). Based on their results, the authors suggest that the higher the modulus of elasticity, the higher the risk for tendon rupture.

Similarly, reviews by Guo & DiPietro, 2010, and Nichols et al., 2019 show the negative effects of diabetes mellitus on wound healing but do not discuss direct mechanical changes to tendon properties. However, previous rat tendon studies have sought to quantify such changes; research articles include work by Boivin et al., 2014 and Fox et al., 2011. Both articles found significant decreases in maximum/peak load and/or elastic modulus (Boivin et al., 2014; Fox et al., 2011). Neither paper provided an etiological explanation for their results. Future research could investigate the potential causes for the noted decreases in elastic modulus noted by both studies.

There are currently a variety of testing machine manufacturers on the market. Two commonly used testing machines include Instron (Instron Corporation, Norwood, MA, USA) and MTS (MTS Corporation, Eden Prairie, MN, USA). The machine manufacturer does not matter as much as the machine's capability to perform the required tests and collect the required data. For example, a quasi-static device could perform some tensile, shear, creep, and or compression tests. At the same time, dynamic testing devices could be used for cyclic fatigue and impact testing.

2.4 Discussion

This review provides an overview of past and recent research regarding the *ex vivo* mechanical testing of human tendons. It focuses on common testing methods/practices used in this prior research and their key findings. This review found significant variation in testing, indicating a lack of standardization in the *ex vivo* mechanical testing of human tendons, consistent with Scholze et al., 2018 and Jiang et al., 2020. This review did not find any scholarly

research in the literature evaluating *ex vivo* human tendon exposure to creep or sequence loading (use of varying loading modalities in a particular order), particularly for tendons of the hands and wrists (FDP/FDS). The only exception found is Wren et al. (2003) exposing the human Achilles tendon to creep loading.

Table 2 visually represents these gaps, common testing modalities (cyclic and tensile), and shared methodologies. Table 2 further demonstrates that there is no consistent set of methods when testing human tendons. Inconsistencies in testing include hydration methods, grip type, CSA measurement method, pre-conditioning (exposing tendons to a set number of cycles or a specific load before an actual test), and tendon(s) tested. The most consistent finding was performing tests at room temperature (Hangody et al., 2016; Schatzmann, 1998; Schechtman & Bader, 1994, 1997, 2002; Scholze et al., 2018; Smith, 2019). The blank spaces in the table represent either method not used in the experiment or not discussed by the researchers. Table 2 does not present plausible explanations for the variation in testing methods. Based on the papers discussed in this review, the author of this review believes that a plausible explanation for such varying testing methods is likely due to the need for maintaining sample viability before and during testing. Events that occur up to testing focus on maintaining the sample as much as possible to prevent degradation via decomposition through hydration and freezing. Maintaining sample viability in regard to mechanical testing requires the use of methods/techniques to prevent the following: sample slippage from the grips and tendon rupture at the grip site (area where sample is in contact with the edge of the jaw face) instead of within the region of interest.

Several articles discuss (directly or indirectly) the relationship between force and repetition interaction and the significant impact this interaction has on damage accumulation in a tendon. Fung et al., 2008, and Fung et al., 2010 show that damage can occur and visually appear

as kinks (fiber deformation) within the tendon at low fatigue levels, suggesting the importance of understanding damage accumulation even at low levels of fatigue. Evidence of similar kink development for tendons exposed to creep or sequence loading was not found.

2.4.1 Research Needs

The results of this review suggest there is still much that is unknown about the mechanical and viscoelastic properties of human tendons, indicating the need for future research. As mentioned in the previous section, this review indicates a lack of research regarding the *ex vivo* FDP/FDS human tendon to cyclic, creep, and sequence loading. The results of this review did not indicate if the order in which loading occurs has a significant effect on strain over time.

To address these gaps in the literature, the fatigue life and survival time of FDP/FDS tendons exposed to cyclic or creep loading will be evaluated. Then the potential effect of sequential load ordering on FDP/FDS tendon strain will be studied. Using a dynamic testing machine, a custom hydration bath filled with room temperature physiological saline (0.9%), 3D printed clamps (Scholze et al., 2018), and pneumatic grips. Protocols used by Schechtman, 1995 and Wren et al. (2003) set a strong foundation to develop methods for testing involving human tissue.

Chapter 3: *Ex Vivo* Fatigue of Human Flexor Digitorum Tendons at Four Levels of Ultimate Tensile Stress

3.1 Introduction

Tendons are exposed to concentric, eccentric, and isometric loads comprised of varying amounts of force on a daily basis. Exposure to such loads requires a flexible yet strong material built to withstand varying forces over a person's lifetime. Tendons have been compared to unidirectional fiber-reinforced composites (Schechtman & Bader, 2002; Shepherd & Screen, 2013). Like all composites, tendons will accrue damage over time. But, unlike composites, tendons have a (limited) healing capability enabling repair of some of the accrued damage. Studies have also demonstrated an interactive relationship between force and repetition related to an increased risk of tendon injury or damage (Andarawis-Puri & Flatow, 2011; Schechtman & Bader, 2002; Shepherd & Screen, 2013). This would suggest that tendons experience a fatigue failure process of damage accumulation when exposed to repetitive stress, similar to that experienced by other materials. Several lines of evidence support this fatigue failure hypothesis, including studies examining *ex vivo* testing of musculoskeletal tissues in both humans (Chandrashekar et al., 2012; Schatzmann, 1998; Schechtman & Bader, 1997; Wren et al., 2003) and animals (Barbe et al., 2013; Fung et al., 2010; Sun et al., 2010; Wang et al., 1995). In addition there is supported evidence in epidemiology (Gallagher & Heberger, 2013). Practical application of fatigue failure is demonstrated in validation studies of MSD exposure assessment tools that employ fatigue failure techniques (Bani Hani et al., 2021; Gallagher et al., 2017, 2018).

As discussed in section 2.3, tendons and other musculoskeletal tissues have viscoelastic properties such as hysteresis (the loading response of a system being dependent on the previous loads), as illustrated in Figure 3.1. In this example, the response of the tendon after the first cycle

(area in the curve) gradually increases as the load is applied and removed until failure is reached in the last cycle. The area under each curve in this figure represents a loss of energy in the material in the form of heat. Failure can be characterized by a rapid increase in strain with decreasing stress. If we consider tendons to behave like other composite materials, the first loop can be equated to a combination of strain hardening or "burn-in" and the removal of slack in the tendon leading to inflated strain values.

Figure 6: Hysteresis Loop Example for a Flexor Digitorum Tendon

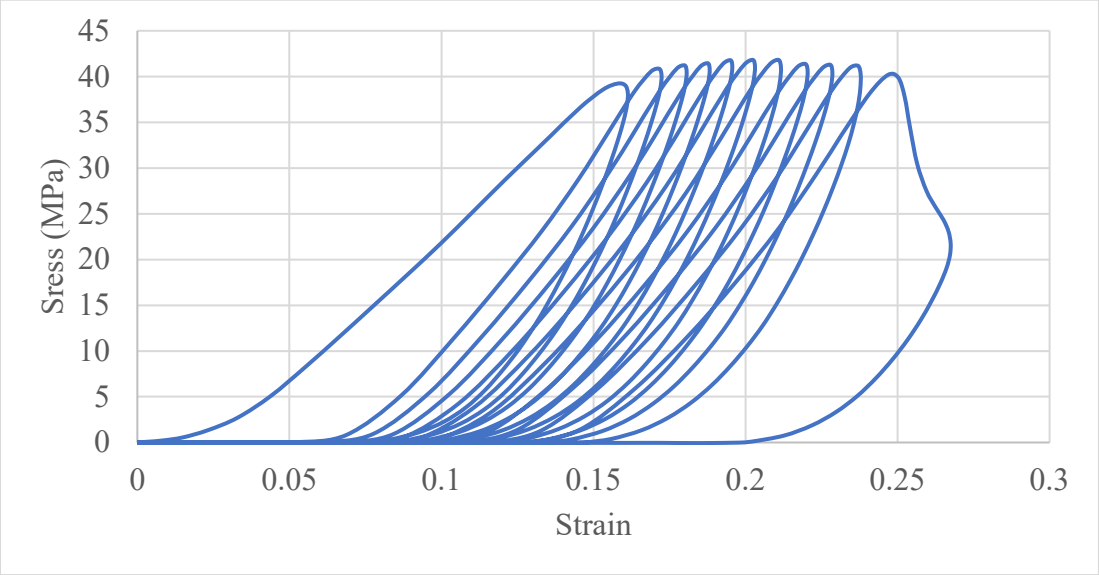

Note. The figure represents a typical example of a hysteresis loop for a tendon. This first loop (cycle) removes undue strain. The following nine cycles represent a steady state with the final cycle resulting in failure.

As discussed in the previous chapter, there is currently a limited number of articles studying *ex vivo* or *in vitro* testing of human tendons. This is particularly true for tendons of the hands and wrists. A lack of *ex vivo* tendon testing data makes the development of fatigue failure-

based risk assessment tools challenging especially for the distal upper extremities. The limited number of articles related to *ex vivo* testing of human tendon could be partially due to the challenges involved with this type of testing. For example, obtaining an accurate estimate for minimum cross-sectional area (CSA) is critical to deriving an estimate for the percentage of tendon ultimate tensile strength (UTS) and fatigue life as estimated in cycles to failure resulting from fatigue testing. The aims of the current study are (1) to assess the feasibility of using computed tomography (CT) to measure the minimum and average CSA of excised FDP/FDS tendon and (2) to evaluate the progression of strain in flexor digitorum profundus (FDP) and superficialis (FDS) tendons exposed to cyclic loading resulting from energy loss.

3.2 Materials and Methods

3.2.1 Tendon Preparation

A total of 32 fresh-frozen FDP/FDS tendons from four human donors were used in this study. Donor ages ranged from 48 - 75 years of age, with a mean of 64 ± 9.87 years. Donors were of various races, sexes (three females, one male), and body sizes, with a mean height of 1.65 ± 0.08 meters (65.3 inches) and a mean weight of 68.9 ± 18.37 kg (152 lbs.). More specifics on donor demographics are provided in Appendix A. Exclusion criteria for potential donors included known joint or bone disorders and a known history of endocrine diseases such as diabetes mellitus. One donor had a known history of smoking. Donors were provided by Science Care (Phoenix, AZ) and stored at -20 °C until dissection. After dissection, the excised flexor digitorum tendons were approximately 10 cm in length; tendons were centered within the flexor retinaculum such that (when excised) each tendon had about 5 cm in length on both proximal and distal ends. Tendons were measured using a ruler while in anatomical position prior to excision to ensure consistency. Excised tendons were immediately placed in self-sealing plastic bags that

were folded to prevent the tendon from rotating or sliding within the bag and then stored at -20 °C prior to imaging. Twenty-seven randomly selected extensor digitorum tendons were excised for use in setup of the testing equipment and preliminary testing to test clamp-tendon adhesion while submerged in saline following a similar protocol as mentioned above. The extensor digitorum tendons were not used as a part of this study. All FDP and FDS tendons were weighed at the time of dissection using a ME303E Precision Balance (METTLLER TOLEDO MeGreifensee, Switzerland).

3.2.2 CT Imaging Setup and Filtering

A GE LightSpeed VCT 64 volumetric computerized tomography (CT) scanner (GE Healthcare, Chicago, IL) was used to scan all tendons prior to testing. Twelve custom trays were used to hold tendons in place during scanning. The trays were designed with channels to individually hold each tendon in place during scanning, as shown in Figure 3.2. The trays used were assigned to specific donors to maintain consistency. As shown in Figure 3.2, the tendons were placed following the same pattern of distal end to proximal FDP followed by FDS. Extensor digitorum tendons from donors were placed in separate trays from the left and right hands to reduce the risk of confusing tendons. The CT scanner settings and tendon placement were consistent with medical CT imaging practices; specifically, trays were placed in the scanner as if a human were lying on the table. To fit the trays on the scanner bed, the 12 trays were divided into two stacks of three, and two rounds of scans (i.e., two donors per scan) were performed. The stacked order was set as right hand on top, followed by left hand, then extensors. Reflective markers specific to CT scanning were used to mark the location of the proximal end of the tendons within the images (for both FDP and FDS tendons). The scanner took a total of 1017 images, with the scan type being a full helical. The slice intervals were 2.5 mm with a field

of view (FOV) diameter of 10 cm. Blank images were removed. Further image filtering was used to determine the actual length of the tendon that would be within the 30 mm grip-to-grip distance used by the mechanical testing device. Through a simple calculation, the total required images that would be needed to analyze was 12. The number of images included in the scan was increased by 10 - 11 images to ensure that the minimum CSA was accounted for within the testing region, as it is difficult to precisely position the tendon to have the minimum be in the center of the testing region.

Figure 7: Donor Tendon Placement

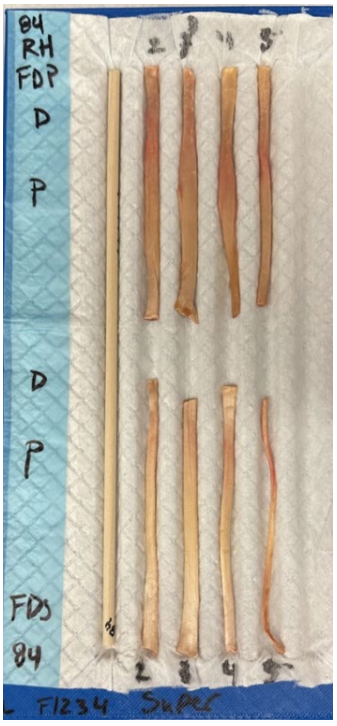

Note. Tendon placement was by donor, hand, and tendon. This tray contains all FDP/FDS tendons for the right hand of a donor. Tendons were placed in the channels from the distal (D) to the proximal (P) end.

3.2.4 Cross-Sectional Area Measurement

To automate the acquisition of tendon features across digits and z-planes, a custom ImageJ (Schneider et al., 2012) macro code using the Fiji package (Schindelin et al., 2012) that identified and extracted the CSA (alongside other morphometric features) was developed. The macro first imported a 16-bit image of tendons graphically organized according to digits from a sequence of CT scans. The dynamic range of the images was then adjusted using a fixed set of minimum and maximum values, which brightened the image to reveal the entirety of the imaged tendon. A set of pre-drawn regions of interest (ROI) that were customized to the respective imaging plate was called and copied the tendons from the channel and pasted them onto a newly generated blank image of the same dimensions. This step subtracted the background plate from the image leaving only a grid of the tendons themselves. The image was then binarized using a set of threshold values, which classified pixels as black or white, and assigned values to the determined thresholds where black was zero and white was one. The binarized image was then run through the extended particle analyzer in ImageJ which extracted all contiguous white pixels as objects and represented them as ROIs. The ROIs were filtered using a set of morphometric gates for features such as CSA and circularity. Gates were determined according to typical tendon morphology. This macro would perform this analysis for each image sequence in the z-plane. CSA measurements derived from our automated analysis were calibrated using an imaged wooden dowel rod of known diameter (3/16 inches) in each image along with comparisons to manually drawn and measured ROIs. Figures 8 and 9 demonstrate before and after running the code where the ROIs and thresholds have been determined. The dowel rod of row A in both figures was used as the 'ruler' to set the threshold values. This resulted in estimated CSAs ± 1% mm^2 of the dowel rods CSA (~17.82 mm^2). The average CSA of the dowel was calculated by

taking multiple diameter measurements along the length of the dowel using a digital caliper then calculated using the equation $A=\pi r^2$.

Figure 8: Image from CT scans

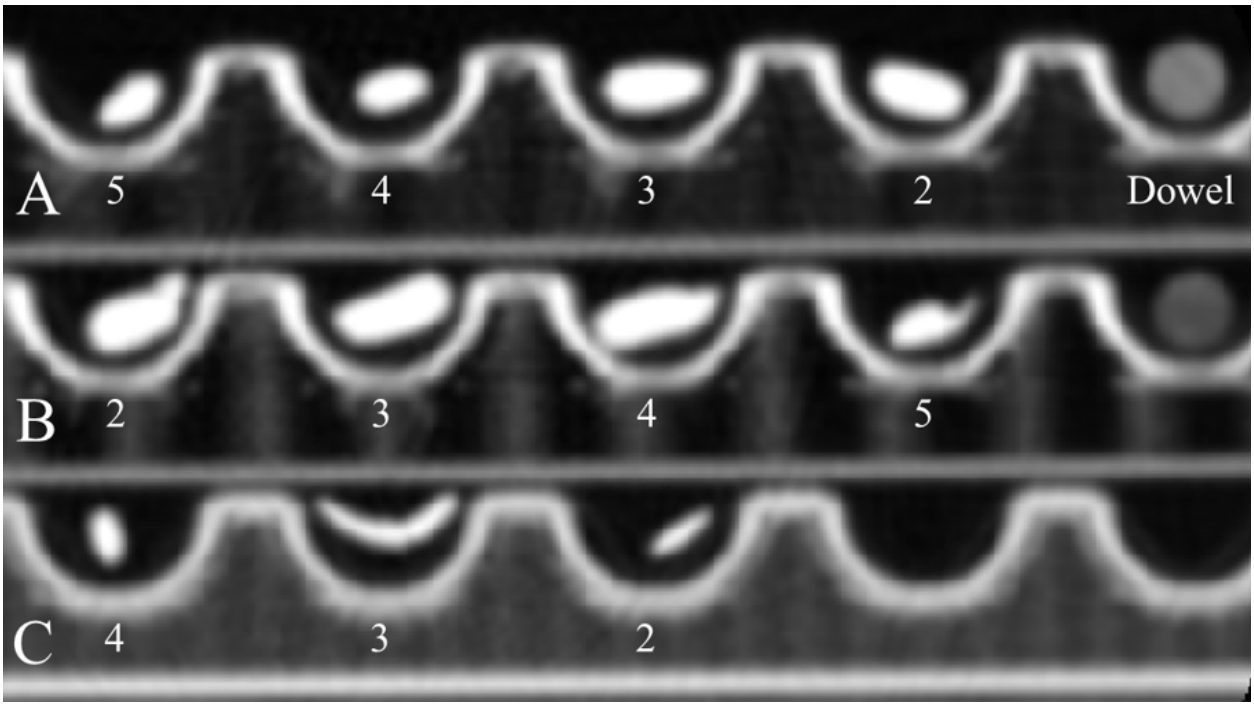

Note. Image from CT scans of the top row is the right hand (A), the second row is the left hand (B), and the right EDL. The trays used are also visible in the scan.

Figure 9: CT Scan Image with ROIs

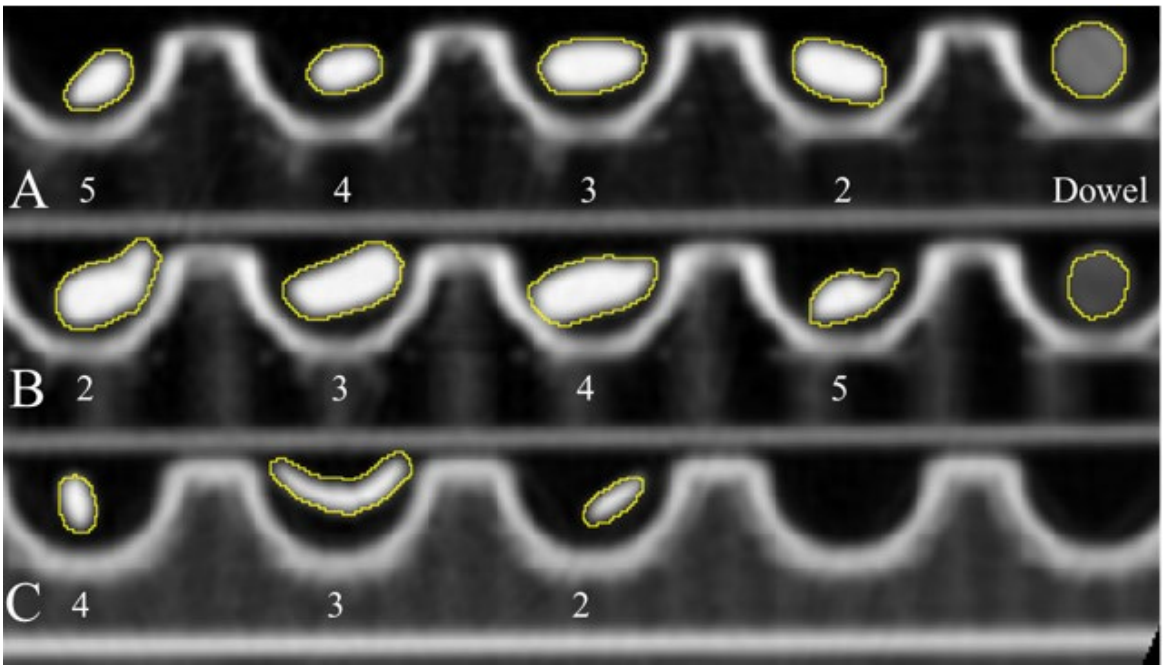

Note. Represents the same image as Figure 8 after running code with identified ROIs. The wooden dowel rod in row A was used as the estimate of minimum CSA.

To check the CT scan estimates of CSA, two other non-destructive approaches were used. The first approach used an assumed density for tendon of 1120 kg/m^3 following the method used by R. F. Ker (1981). Using this approach, calculating an average CSA along the length is straightforward, requiring only the length and mass of the specimen. For example, if a tendon is 0.1109 m long and weighs 0.00173 kg with an assumed density, the associate average CSA would be 13.98 mm^2, as shown in the worked example below in Example 1.

$$\left(\frac{0.00173\ kg}{\left(1120\ \frac{kg}{m^3}(0.1109\ m)\right)}\right)1{,}000{,}000 = 13.98\ mm^2 \qquad \text{(Example 1)}$$

The second approach used a volumetric method of measuring displacement. In this approach, a standard 250 mL ± 1mL graduated cylinder was used to measure the displacement volume of tendons used in the tensile test. This was later switched with a standard 100 mL ± 1mL graduated cylinder for the tendons used in the cyclic tests to improve measurement resolution. To ensure consistency, tendons measured with the standard 250 mL graduated cylinder were not used in this analysis. Both cylinders were filled with 0.9% saline to measure the volume displacement for each tendon. A non-invasive holder made of wire was used to suspend each tendon in the graduated cylinder. A tendon submerged in the 100 mL cylinder is demonstrated by Figure 10. The displacement of the wire was measured to be 1 mL. This value was subtracted from the displacement from when the tendon is added to the holder. The volume of saline was checked before each tendon was measured to account for any potential losses of saline from transferring tendons in and out of the cylinder.

Figure 10: Submerged Tendon Example

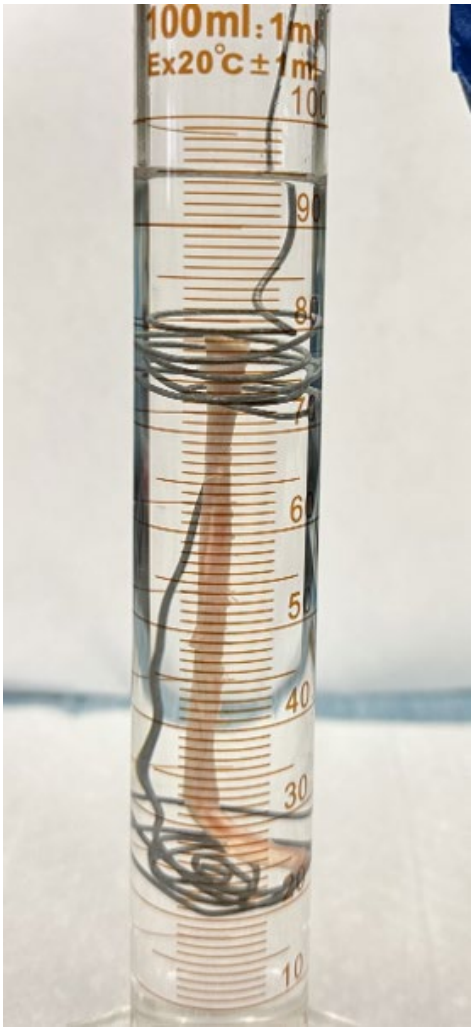

Note. The holder used was made from bent wire.

3.2.4 3D Printed Parts

Several 3D parts were printed for this experiment using either polylactic acid (PLA) or thermoplastic polyurethane (TPU). Parts included 10 custom (12 in x 7 in x .393701 in) trays with 10 channels (10 in x 0.19685), printed using a Stratasys F370 printer (Stratasys, Eden Prairie, MN). Custom 3D printed clamps were also printed using PLA while clamp arms were printed out of TPU using a Dremel Digilab 3D45 printer (Dremel, Mt. Prospect, IL). All 3D parts (excluding the trays) followed design and printing specification requirements from Scholze (2018, 2020), except for the length of the clamp arms which were changed from 40 mm to 30 mm to match the grip-to-grip clamp distance for this experiment. The clamps were designed with pyramidal structures on both sides that interlock when compressed as shown in Figure 11. The clamp arms were designed to hold the clamps at the desired grip-to-grip distance and aid with specimen placement within the grips and were removed prior to testing. Figure 12 depicts tendon placement within the clamps and arm before testing. In order to ensure that clamps did not arbitrarily cut or damage the tendon, the build plate side of the clamps are faced away from the testing region. The non-build plate sides were lightly sanded to remove any sharp edges.

Figure 11: Internal Clamp Pyramidal Structure

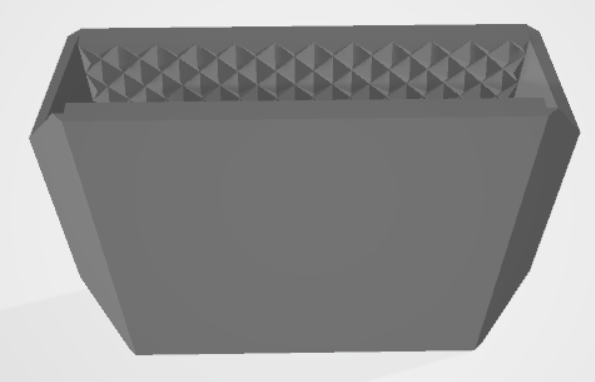

Note. Clamps developed by (Scholze et al., 2018, 2020), used pyramidal structures inside to evenly distribute tissue surface area.

Figure 12: Tendon Clamp Setup

Note. Clamp tendon setup example with TPU holder.

3.2.5 General Testing Conditions

Tests were completed using an INSTRON 5948 micro-tester (INSTRON, Norwood, MA) having a ± 0.5% load measurement accuracy. The micro-tester was affixed with a 2 kN load cell, custom hydration bath, and 1.2 kN pneumatic grips with pyramid jaw faces (Grip-Engineering, GmbH Thümler, Nürnberg, Germany). Cyclic tests were performed using load control settings to ensure that the actuation rate would be consistent. Tests were set to finish within 16 hours, after which data would become censored and used to test residual strength. All tests were set to not exceed 800 N to reduce the risk of damaging the micro tester. The grip-to-grip distance for all tests was set to 30 mm following similar research protocols (Schechtman & Bader, 1994, 1997, 2002; Scholze et al., 2018, 2020; Smith, 2019). A 2 N preload was applied to all tendons to remove any additional slack from tendon placement prior to testing.

3.2.6 Tensile Testing

Sixteen quasi-randomly selected FDP/FDS tendons were used for this test to ensure that all donors would have an equal distribution of tendons. Tendons were tested to failure at a rate of 1% strain/sec following the methods used by (Schechtman & Bader, 1994, 1997, 2002; Smith, 2019) using a sampling rate of 0.1 s. The data collected from this testing was used to calculate the different levels of UTS that would be used for the cyclic loading tests. Ultimate strain was calculated starting from when the tendon reached 2 MPa (beginning of linear region) to account for any remaining slack in the tendon using Formula 1.

$$\varepsilon = \frac{\Delta L}{L_0} \qquad \text{(Formula 1)}$$

Where ε refers to the strain, ΔL refers to change in length (L - L_0), and L_0 refers to initial length.

3.2.7 Cyclic Loading

Sixteen randomly selected FDP/FDS tendons (four from each donor) used for this test were cycled at 1 Hz to failure or 16 hrs. For this testing, a load (N) value is required to calculate the load rate (N/s) that would be needed to travel at 1 Hz. The tendons used for this study were tested at 20, 40, 60, and 80% of the average UTS for each donor, each tested at 1 Hz. Table 3 shows the expected stresses based on the average UTS for each donor. These values were used for this study to calculate the corresponding load and load rate using the minimum CSA for each individual tendon tested as shown in Table 4. The sampling rate for the cyclic tests was set on a decreasing scale from 25 - 10 Hz corresponding with the decreasing percent UTS. As shown in Table 5, this was necessary for one main reason. The results from preliminary EDL tests showed that the working memory of the computer used with the micro-tester did not have the memory capacity for sampling rates of 25 Hz for the 16-hour test duration. To account for sampling longer tests, decreasing rates were used, knowing that tendons tested at lower levels of expected UTS would take longer to fail than tendons tested at higher levels. This allowed for maximizing data collection while decreasing the risk of data loss from a system crash. Values such as strain and area under the curve (work) were calculated after data collection. Strain was calculated using Formula 1 while the work experienced per cycle was calculated using Simpson's integration (Weisstein, 2024).

Table 3: Load Rate Calculations

Donor	Type*	Digit	Study #	% of UTS	Min CSA (mm^2)	Max Load (N)	Load Rate (N/s) at 1 Hz
1	LFDS	3	20	20	13.43	87.56	175.11
1	RFPD	5	30	40	8.58	111.93	223.87
1	RFPD	4	38	60	10.38	202.97	405.95
1	RFDS	2	32	80	7.71	120.27	240.54
2	LFDS	3	61	20	10.99	64.55	129.10
2	LFPD	2	53	40	15.07	177.06	354.12
2	LFPD	4	25	60	8.20	144.56	289.12
2	RFPD	5	47	80	7.59	178.40	356.80
3	RFPD	4	24	20	10.26	47.20	94.40
3	RFDS	5	40	40	2.14	19.65	39.30
3	LFPD	3	17	60	9.35	128.97	257.94
3	LFDS	2	43	80	7.48	137.57	275.13
4	LFPD	5	36	20	8.20	32.00	64.01
4	RFDS	4	55	40	12.89	100.62	201.24
4	LFPD	3	34	60	19.91	233.10	466.19
4	RFPD	2	31	80	17.28	269.71	539.43

Note. * Left flexor digitorum profundus (LFDP), Right flexor digitorum profundus (RFDP), Left flexor digitorum superficialis (LFDS), Right flexor digitorum superficialis (RFDS).

Table 4: Expected Stress for Each Donor

Donor	% Avg of UTS	Expected Stress (MPa)
1	20	6.52
	40	13.04
	60	19.56
	80	26.08
3	20	4.60
	40	9.20
	60	13.80
	80	18.40
2	20	5.88
	40	11.75
	60	17.63
	80	23.50
4	20	3.90
	40	7.80
	60	11.71
	80	15.61

Note. The table presents values for the expected stress for each donor based on a percent of the average UTS specific to each donor. The expected stresses were used to calculate the load and load rate.

Table 5: Sampling Rate

% of UTS	Sampling Rate (Hz)
20	10
40	15
60	20
80	25

Note. The table presents the sampling rate that corresponds with each test level used in this study.

3.2.8 Data Analysis

Means, standard deviations (SD), and 95% confidence intervals (CIs) were calculated for each measurement technique. A one-way analysis of variance (ANOVA) was performed to determine if statistically significant variation exists between the different measurement techniques in determining the average CSA of FDP/FDS tendons. A Type I error rate of 0.05 was used for this analysis. A Tukey's test was used for pairwise comparisons to assess significant differences between measurement methods. This analysis was performed using Minitab® software (version 21.4.3, LLC, USA). To determine practical significance, the effect sizes for each statistically significant different pair was calculated.

3.3 Results

3.3.1 CSA Measurement Analysis

The average and standard deviation of the average CSA across all tendons and methods were as follows: CT: 11.83 ± 4.67 mm^2, Volumetric: 9.68 ± 5.00 mm^2, and Ker: 9.07 ± 3.82 mm^2 (Table 6). A physical representation of the information provided in Table 5 is shown in Figure 13. The full data set of all the average CSAs from each method for each tendon can be found in Appendix A. Results of the one-way ANOVA (Table 3.5) suggested a statistically significant difference between at least one of the measurement methods ($p = 0.013$). A post-hoc Tukey HSD test indicated a statistically significant difference between the CT and Ker approaches. Results of Tukey's test also found that the pairs volumetric-CT, and Ker-volumetric are not statistically significantly different. The results of Tukey's HSD test are shown in Table 8. The CT-Ker pair difference was determined to be practically significant, with a Cohen's d of 0.65 with a 95% CI of (0.21, 1.08) indicating a medium effect size.

Table 6: Cross-Sectional Area Measurement Results

Method	n	Mean CSA ± Standard Deviation (mm^2)	95% CI
CT	44	11.83 ± 4.67	(10.48, 13.18)
Volumetric	44	9.68 ± 5.00	(8.33, 11.03)
Ker	44	9.07 ± 3.82	(7.72, 10.42)

Figure 13: Box Plot of Average CSA by Method

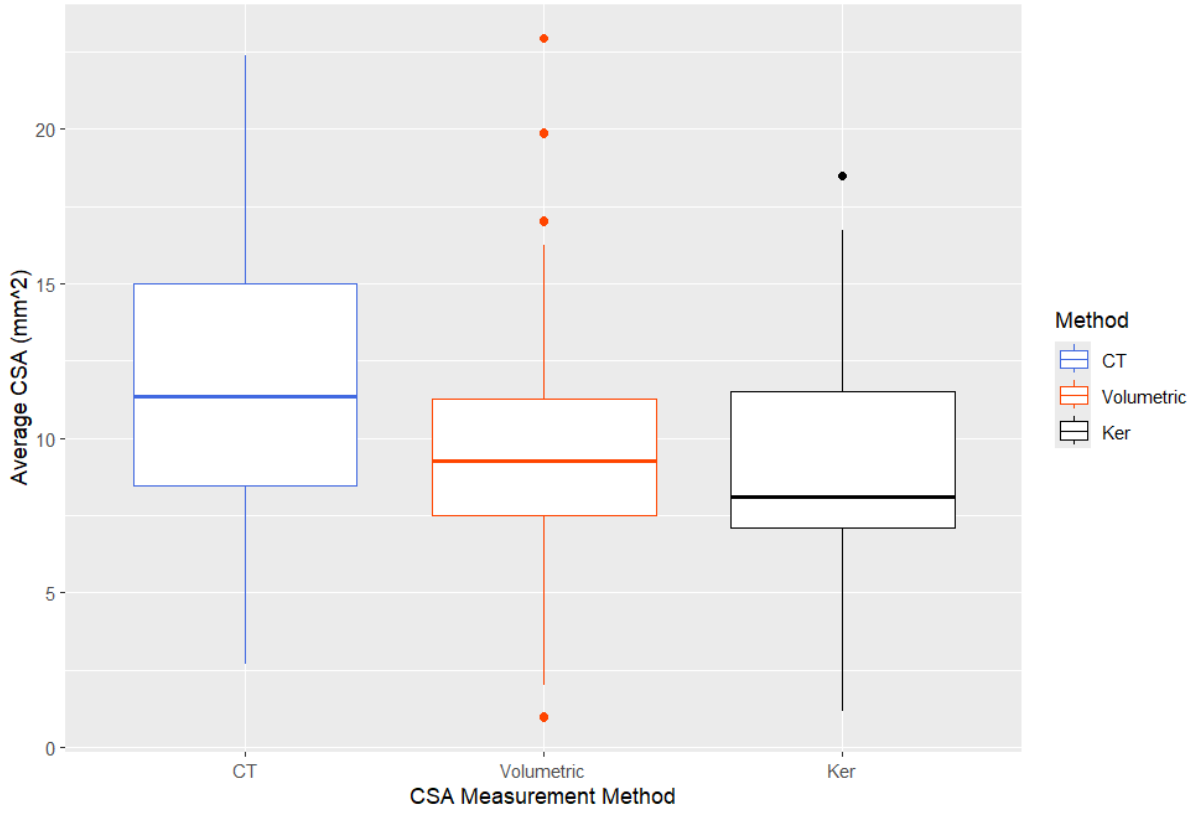

Note. The figure depicts data presented in Table 6.

Table 7: Analysis of Variance

Source	DF	Adj SS	Adj MS	F-Value	P-Value
Method	2	184.9	92.46	4.51	0.013
Error	129	2642.0	20.48		
Total	131	2826.9			

Note. Results of the one-way ANOVA suggest on average, at least one of the measurement methods is statistically significantly different from the others.

Table 8: Tukey Pairwise Comparisons

Method	n	Mean	Grouping	
CT	44	11.83	A	
Volumetric	44	9.68	A	B
Ker	44	9.07		B

Note. Means that do not share a letter are significantly different. Indicating that there is a statistically significant difference between CT and Ker, but not between CT and Volumetric or Volumetric versus Ker.

3.3.2 Tensile Testing

The UTS across donor-sampled tendons ranged from 13.6 to 62.39 MPa. Ultimate strain or strain at failure ranged from 10 to 19%. The results can be viewed in Tables 9 and 10. Table 9 provides the means and standard deviations for each donor and Table 10 provides the results of the UTS tests for all 16 tendons tested.

Table 9: Ultimate Tensile Strength Test Results by Donor

Donor	Mean ± Standard Deviation			
	Max Load (N)	**Min CSA (mm^2)**	**UTS (MPa)**	**Ultimate Strain**
1	225.72 ± 79.21	8.65 ± 4.88	34.16 ± 16.63	13 ± 1%
2	248.69 ± 25.51	8.56 ± 1.88	30.02 ± 4.88	14 ± 1%
3	253.02 ± 30.19	11.35 ± 2.62	23.00 ± 4.10	15 ± 2%
4	277.59 ± 6.68	15.09 ± 4.35	19.51 ± 4.45	13 ± 2%

Note. The table shows the means and standard deviations for each donor. The results used to calculate the values are presented in Table 10.

Table 10: Ultimate Tensile Strength Test Results

Donor	Study #	Type	Digit	Max Load (N)	Min CSA (mm^2)	UTS (MPa)	Ultimate Strain
1	1	RFPD	2	295.08	9.80	30.10	0.12
1	2	RFDS	5	92.82	1.49	62.39	0.16
1	3	LFPD	3	274.88	12.25	22.45	0.13
1	4	LFDS	2	240.10	11.06	21.70	0.13
2	5	RFPD	2	290.72	11.02	26.37	0.15
2	6	RFDS	4	243.72	8.01	30.42	0.14
2	7	LFPD	3	238.09	9.35	25.48	0.13
2	8	LFDS	2	222.23	5.87	37.83	0.16
3	9	RFPD	2	211.50	7.90	26.78	0.14
3	10	RFDS	3	242.95	13.16	18.46	0.13
3	11	LFPD	4	294.48	10.76	27.37	0.19
3	12	LFDS	3	263.15	13.58	19.38	0.15
4	13	RFPD	5	273.32	11.37	24.04	0.15
4	14	RFDS	3	272.81	20.07	13.60	0.10
4	15	LFPD	4	292.59	17.40	16.82	0.15
4	16	LFDS	4	271.65	11.52	23.58	0.13

Note. The data table shows the results of the ultimate tensile tests by donor.

3.3.3 Cyclic Loading

Of the 16 tendons tested, two tendons tested at 20% UTS survived the 16-hour testing period. Thus, the data became censored and not included in the current analysis. One outlier was also removed after performing an outlier test at 80% UTS. The average times to failure at the four levels of %UTS ranged from (0.34 - 10.28 hrs.) with average strains at failure of (15 - 18%) and average work per cycle of (0.007 - 0.07 J). Table 11 provides a summary of the results of the fatigue tests by each level of %UTS. The average work per cycle and cycles to failure are shown in Figure 14. The data presented in Figure 14 indicates that for this data a power model provides the best fit. The model suggesting the best fit was:

$$y = 0.054x^{-7^{-5x}} \qquad \text{(Model 1)}$$

Where *y* refers to the average work experienced per cycle and *x* refers to the number of cycles to failure, suggesting that the relationship between average work per cycle and cycles to failure is nonlinear.

Table 11: Summary Results for Fatigue Tests

% of UTS	n	Mean ± Standard Deviation					
		Max Load at Failure (N)	**Max Stress at Failure (MPa)**	**Time to Failure (hrs.)**	**Completed Cycles to Failure**	**Failure Strain**	**Average Work per Cycle (J)**
20	2	216.02 ± 32.89	18.15 ± 4.51	10.28 ± 3.73	19460 ± 8159	16 ± 3%	0.007 ± 0.004
40	4	208.38 ± 62.21	27.70 ± 12.14	1.88 ± 2.70	3189 ± 4690	15 ± 4%	0.04 ± 0.02
60	4	264.85 ± 59.03	23.38 ± 3.88	1.53 ± 2.34	3238 ± 5067	18 ± 4%	0.07 ± 0.01
80	3	287.30 ± 71.67	29.18 ± 9.65	0.34 ± 0.14	660 ± 507	16 ± 3%	0.07 ± 0.03

Note. The table shows the mean and standard deviation results for all tendons that failed.

Figure 14: Inelastic Work vs. Cycles to Failure

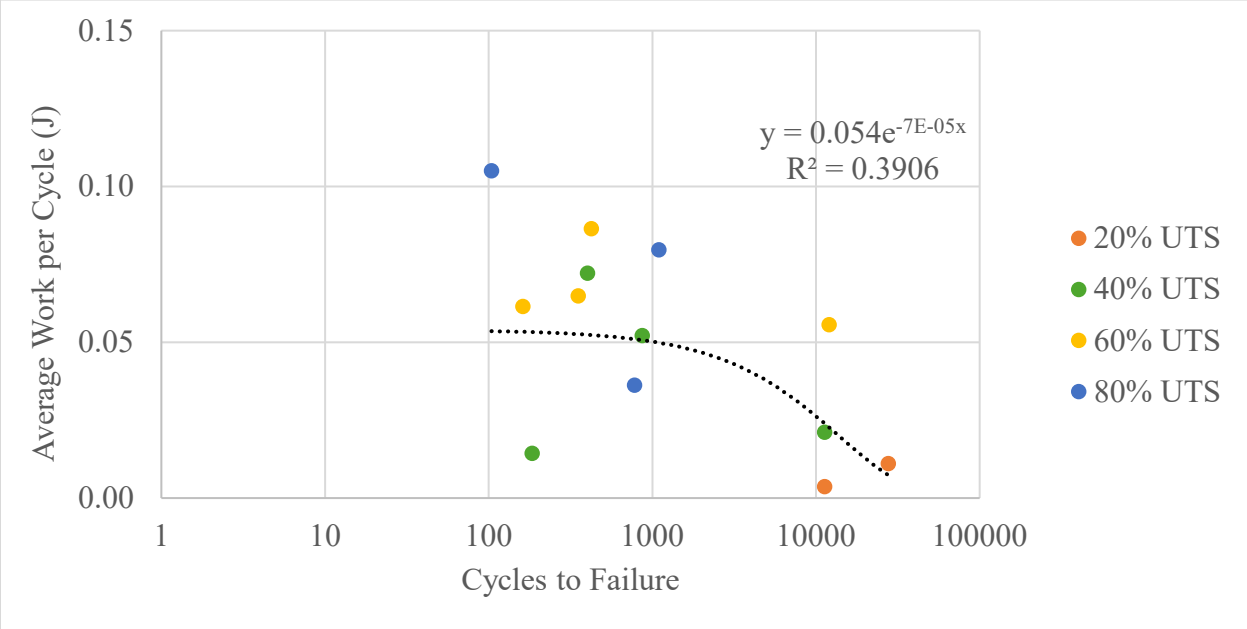

Note. The figure represents the average work per cycle in joules with the corresponding cycles to failure.

The effects of fatigue loading can also be shown using a method commonly used in another viscoelastic material, solder, as seen in Figure 15. The figure is an example of one of the tendons tested at 80% UTS showing the progression of inelastic work as the number of cycles increases. This progression is similar to that of soldering which includes three regions (Abueed et al., 2022). The first region is strain hardening, followed by the steady-state region, and then tear initiation and propagation.

Figure 15: Inelastic Work vs. Number of Cycles

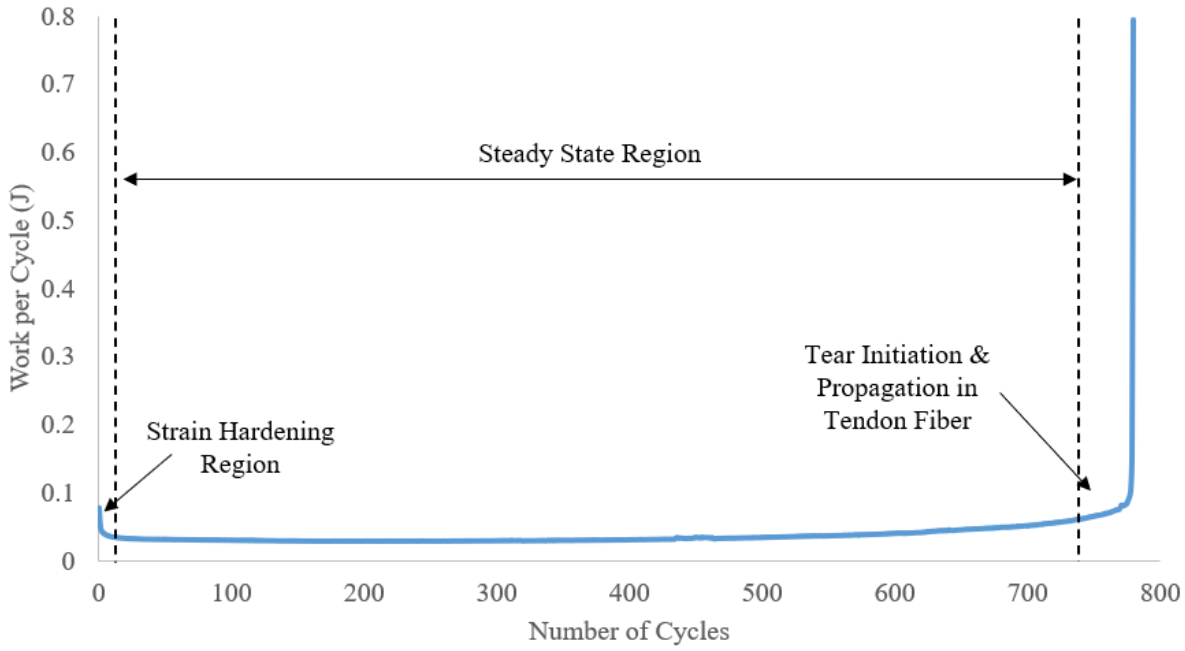

Note. This figure demonstrates the inelastic work of an FDP/FDS tendon test at 26 MPa (80% of donor UTS) vs. the number of cycles to failure. The figure also indicates three different regions: strain hardening, steady state, and tear initiation and propagation.

3.4 Discussion

Results of this study suggest that CT may be useful in estimating the average CSA of excised FDP/FDS tendon when compared to Ker's method of assumed density method but not volumetric measurement. The usefulness of CT when compared to Ker's method of assumed density is supported by the effect size of the CT-Ker pair was found to have a medium effect, suggesting the presence of a meaningful difference between the two methods. The range of the confidence interval suggests that while the average effect size is medium, the true effect could vary; more data may reduce the CI range. However, obtaining a minimum CSA is still preferred

but not possible to assess with assumed density or volumetric methods. The Ker and volumetric methods have an inherent limitation in measuring CSA. Both methods assume that tendon is uniform across the length which makes accounting for tendon morphology impossible. The inability to account for natural tendon morphology can result in increased error (over estimation of average CSA) (Hayes et al., 2019). It is not yet clear the effectiveness of CT to assess minimum CSA of excised FDP/FDS tendon based on the methods used in this study. To the knowledge of the author, no study exists using CT to estimate CSA of excised FDP/FDS tendons using the methods described in the current chapter.

Regardless of %UTS or the amount of energy lost, the strains at the failure of 10 to 19% for FDP/FDS were consistent with known literature (Schechtman & Bader, 1997; Smith, 2019; Wren et al., 2001, 2003). However, when compared to the ultimate strength at 1% s^{-1} of leg tendons such as extensor digitorum longus (99.9 ± 12.2 MPa), hallucis longus (87.1 ± 12.5 MPa) (Schechtman & Bader, 1997), and Achilles (71 ± 17 MPa) (Wren et al., 2001), values for FDP/FDS were less (13 - 62 MPa). Plausible explanations for this may stem from the *in vivo* fatigue quality or the ability to resist time-dependent failure (Pike et al., 2000) of tendon. The size of the tendon may play a factor in this as well (leg tendons vs hand and wrist). The energy loss per cycle ranged from 0.007 - 0.07 J. These values slightly differ from the average work per cycle reported by Smith, 2019 (0.07 - 0.13 J). Plausible reasons for the difference stem from the methods of both studies. Smith (2019) evaluated the effect of the duty cycle on the fatigue of FDP/FDS tendons. This led to the use of different loading patterns, which could affect energy loss, while the current study used the same loading pattern for all tests. Another plausible reason could be the effect of two tendons that failed at 20% UTS. These two tendons lost less energy compared to the other tested tendons, which affected the ranges shown in the results section.

3.5 Limitations

The results of this experiment are subject to certain limitations. One donor had a known history of smoking which may have affected the overall strength of the tendons of that specific donor. An inherent limitation of *ex vivo* tissues testing is grip/clamp to sample adhesion. The current study used clamps developed by Scholze (2018, 2020) designed to reduce the impact of potential specimen slipping. However, that does not mean some slipping may have occurred, effecting results. The author of the current study found that none of the tendons failed mid-substance (center of 30 mm grip-to-grip distance). The lack of specimen mid-substance failures may be due to the tendons submerged in a hydration bath during testing or the area of the minimum CSA being near the clamp site. The author did not notice failure within or at the clamp site for any specimen tested. The INSTRON 5948 micro-tester was not initially designed to test large viscoelastic samples such as tendons using load control. As a result of this, the consistency of the peak loads of each cycle may have been affected. Due to the sample size within each donor (one tendon per donor for each level of %UTS) other forms of analysis to determine potential effects on time to failure such as Cox regression were not able to be performed.

3.6 Conclusion

The aims of this study were: (1) to determine the feasibility of using CT to estimate CSA of excised FDP/FDS tendons when compared to other non-destructive methods, and (2) evaluate the progression of strain in excised FDP/FDS tendons exposed to cyclic loading resulting from energy loss. It can be concluded from this study that if a CT is not available to measure minimum CSA, using the volumetric method can be effective in determining the average CSA of human FDP/FDS tendon. Results of this experiment suggest strain at failure appears to be independent of energy loss (work experienced).

Chapter 4: Viscoelastic Creep *Ex Vivo* Testing of Flexor Digitorum Profundus and Superficialis Tendons

4.1 Introduction

Creep is the tendency a material has to deform over time when exposed to constant stress. This concept has been applied to the testing of many different materials including polymers, metals, concrete, tendon, and more recently ligaments (Thornton & Bailey, 2012; Wren et al., 2003). In the case of viscoelastic materials, creep is referred to as viscoelastic creep. Viscoelastic creep occurs when viscoelastic materials experience a time-dependent increase in strain (deformation) when exposed to constant stress. Creep curves divide into five phases, beginning with a period of initial extension. The period of initial extension can also be referred to as instantaneous deformation or the ramp-up. Initial extension is a brief period where a material may experience changes in extension before reaching the testing load. However, this section of displacement can vary depending on the experimental setup and material. Primary creep is the first phase in which the rate of deformation decreases over time. Secondary or steady-state creep is the phase where the strain rate is held constant. This continues until signs of tertiary creep begin; at this point, the amount of strain experienced accelerates resulting in failure. Figure 16 demonstrates the regions of a creep curve.

Figure 16: General Creep Curve for Tendon

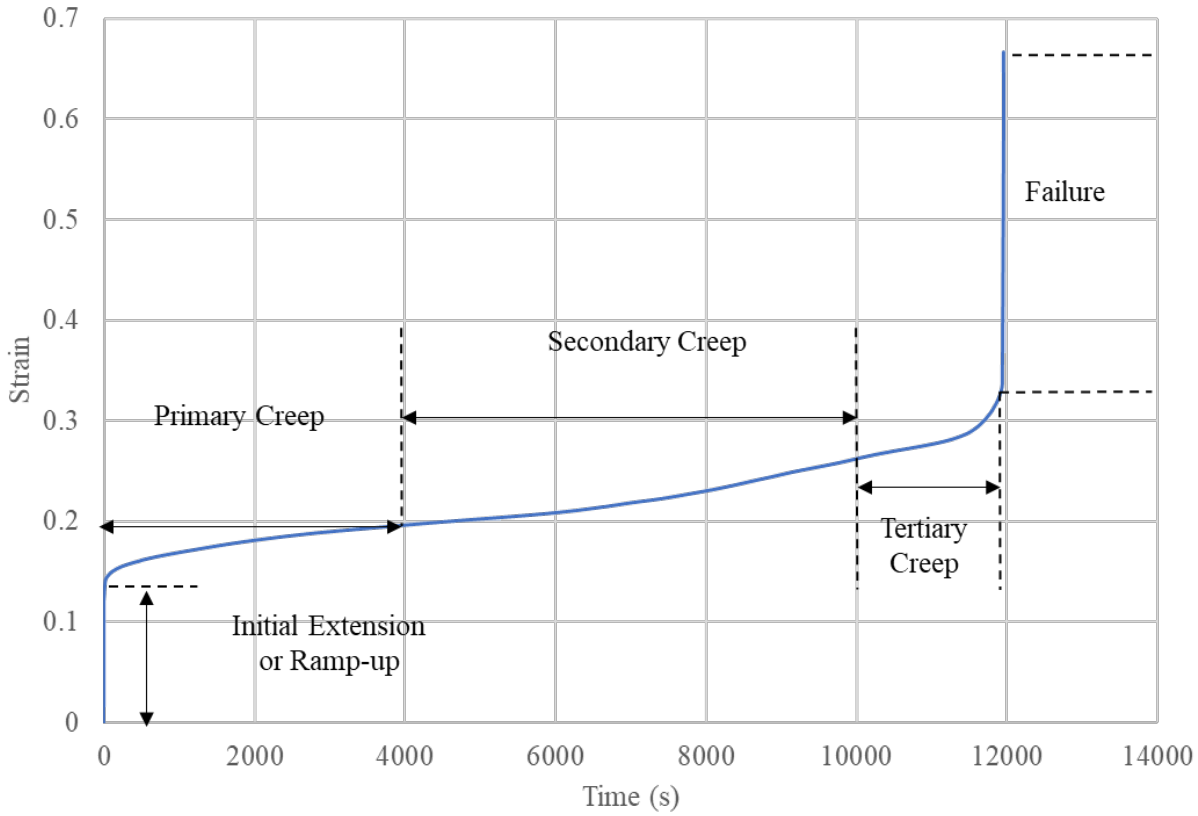

Note. Example of a strain-time curve for tendons demonstrating five phases: initial extension/ramp-up, primary creep, secondary creep, tertiary, creep, and failure region.

As indicated in chapter two, there is a lack of literature assessing the effects of *ex vivo* creep loading of human tendons particularly for tendons of the distal upper extremities. The most recent papers evaluating *ex vivo* creep loading of tendon include Wren (2003), and Wang & Ker, (1995). Wren (2003) examined time dependent changes in the tendon modulus and in energy dissipation of the human Achilles tendon. Wren (2003) found as applied stress increases, time and cycles to failure decreased exponentially. Wren (2003) also found a decreased secant modulus and increased energy loss over time with cyclic loading. Wang & Ker, (1995) sought to

develop a creep theory and model times to failure as a function of nominal stress using wallaby tail tendons. To address the lack of literature regarding exposing human tendon to *ex vivo* creep loading, the current study sought to determine the effects of creep loading on excised human FDP/FDS tendons. Results from the current study could further inform researchers and clinicians that creep loading contributes to the development of strain in tendon.

4.2 Methods

4.2.1 Creep Loading

This study shares the same methods for CSA measurement, general testing parameters, and tensile tests used in Chapter 3, except for a difference in sampling rate. The sampling rate parameters used in the current study was every 0.02 mm change in extension, instead of varying sampling rates of 10 - 25 Hz as described in Chapter 3. Like Chapter 3, the current study used 16 randomly selected FDP/FDS tendons (four from each donor). Selected tendons were then randomly assigned to creep loading at a level of average UTS (20, 40, 60, or 80%), based on the results of the tensile test in the previous chapter. All tendons were preloaded to 2 N before the test began to remove slack resulting from tendon placement. All tests had a 1 - 2 s ramp-up (i.e., period of time required for the testing apparatus to reach the target load (expected maximum load)) following the methods of (Wren et al., 2003). Similarly to Wren (2003), strain resulting from exposure to creep loading (strain occurring during dwell) was calculated using Formula 1 from the point at which the target load was reached. The ramp-up rate and the expected maximum load for each tendon tested are provided in Table 12. Once the target load was reached, a constant load was applied until rupture or until 16 hrs. of loading. Failure was characterized by rapidly increasing strain with decreasing stress (Schechtman, 1995). It was expected that many tendons would survive the 16-hr. creep test period. To account for this

likelihood, predictive models using an average strain rate (% strain per second) for each tendon were developed to predict the time to failure. The calculation for strain rate in this study assumed that the progression of strain was consistent and linear until failure. For example, a tendon takes five seconds to reach a target load of 100 N. The test ended after 10 hrs. reaching 10% strain. An average strain rate was calculated from when the target load was reached to the end of the test as shown in Example 2. For this example, the average strain rate is 0.00278 %/s.

$$\left(\frac{0.10}{(36000\ s - 5\ s)}\right) \times 100\% \ = 0.00278\ \%/s \qquad \text{(Example 2)}$$

In this case, tendons would reach strains between 15 - 20%. This is based on the averages for the strain at failure from the previous chapter. Times required to reach different levels of *in vivo* strain (1.3, 5, and 8%) (Cutts et al., 1991; Kubo et al., 2014) associated with levels of maximum voluntary contraction were also predicted.

Table 12: Load and Ramp-Up Rate Calculations

Donor	Type	Digit	Study #	% of UTS	Min CSA (mm^2)	Max Load (N)	Ramp-Up Rate (N/s)
1	RFPD	3	51	20	10.19	66.41	132.83
1	LFPD	2	63	40	11.52	150.24	300.48
1	LFDS	5	41	60	2.59	50.74	101.49
1	RFDS	4	44	80	9.84	256.70	513.40
2	LFDS	4	27	20	8.32	48.86	97.72
2	RFDS	2	60	40	6.41	75.31	150.61
2	LFPD	5	35	60	8.47	149.27	298.53
2	RFDS	3	46	80	9.73	228.61	457.22
3	LFPD	5	23	20	7.17	32.99	65.98
3	RFDS	4	39	40	8.47	77.91	155.81
3	LFPD	2	21	60	9.46	130.55	261.09
3	RFPD	3	42	80	7.82	143.88	287.77
4	RFPD	4	18	20	11.14	43.46	86.93
4	LFDS	5	54	40	4.08	31.85	63.71
4	LFDS	2	29	60	11.86	138.88	277.75
4	RFPD	3	19	80	14.92	232.80	465.60

Note. The max load refers to the expected target load for each tendon to reach based on the average %UTS for each donor and the minimum CSA for each specific tendon. The ramp-up column is the load per second used for each tendon to reach the maximum load.

4.3 Results

Of the 16 tendons tested, 10 survived the 16-hr testing period. The average strains of the 10 tendons that survived the 16-hr tests ranged from 0.7 - 4.0%. Two tendons tested at 80% UTS failed with strains of 21% and 40%. Tables 13 and 14 provide a summary of the results of the creep tests at each level of %UTS. Table 13 presents data for tendons that survived the test while Table 14 presents data for the two tendons that failed. The full dataset for these results is provided in Appendix B. Figure 17 presents the data from Appendix B showing the strains either

at failure or after 16-hrs of testing. Figure 18 presents a stress-strain curve example of one of the tendons that reached failure and identifies different regions of the curve.

Table 13: Summary Results for Censored Creep Tests

% of UTS	n	Mean ± Standard Deviation				
		Max Load Experienced (N)	Max Stress Experienced (MPa)	Completed Time (hrs.)	Average Strain Rate (%/s)	Strain
20	3	54.99 ± 14.02	5.82 ± 1.13	16	0.000015 ± 0.000003	1 ± 0.2%
40	2	98.89 ± 61.43	11.55 ± 2.37	16	0.000023 ± 0.000009	1 ± 1%
60	3	125.62 ± 3.03	19.60 ± 3.17	16	0.000026 ± 0.000002	1 ± 0.1%
80	2	206.09 ± 47.29	18.65 ± 1.66	16	0.000051 ± 0.00003	8 ± 3%

Note. Table presents summary creep data for tendons that survived the 16 hr. tests.

Table 14: Summary Results for Creep Tests Resulting in Failure

% of UTS	n	Mean ± Standard Deviation				
		Max Load at Failure (N)	Max Stress at Failure (MPa)	Time to Failure (hrs.)	Average Strain Rate (%/s)	Failure Strain
80	2	264.70 ± 0.06	27.04 ± 0.001	5.88 ± 4.82	0.0034 ± 0.002	31 ± 9%

Note. Table presents summary creep data for the tendons that failed.

Figure 17: Strain vs. Time Plot

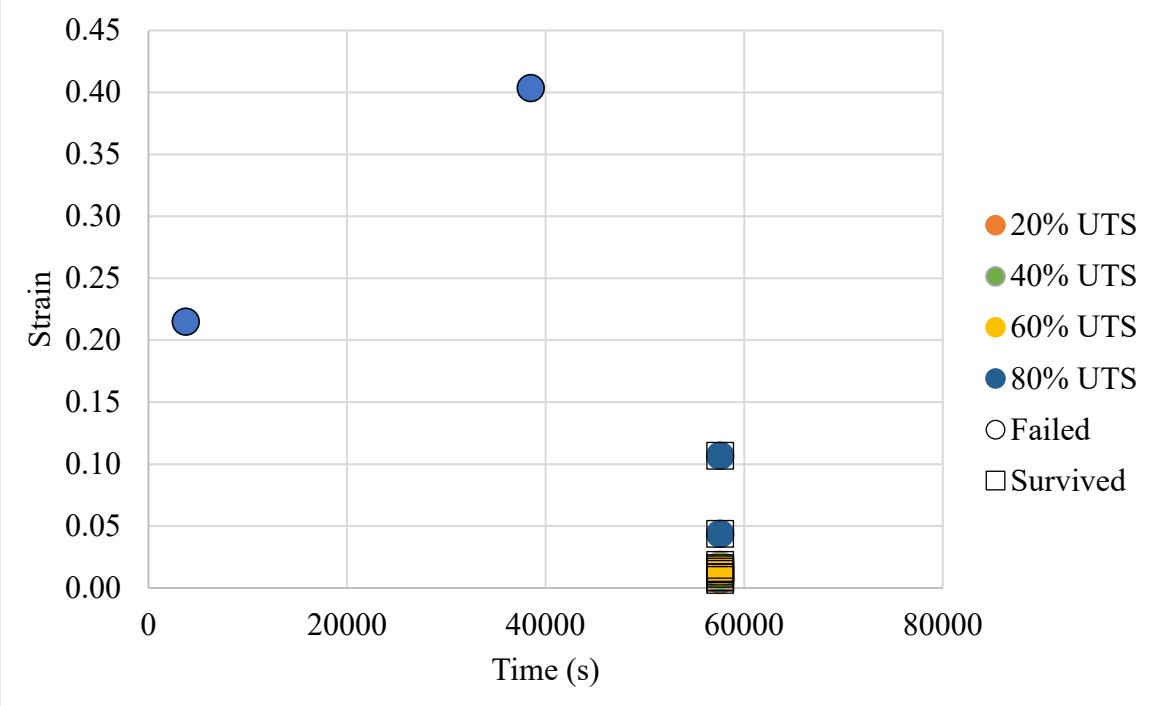

Note. Figure shows results of creep tests for each % of UTS and if the tendon failed during the test.

Figure 18: Stress vs. Strain Plot Example

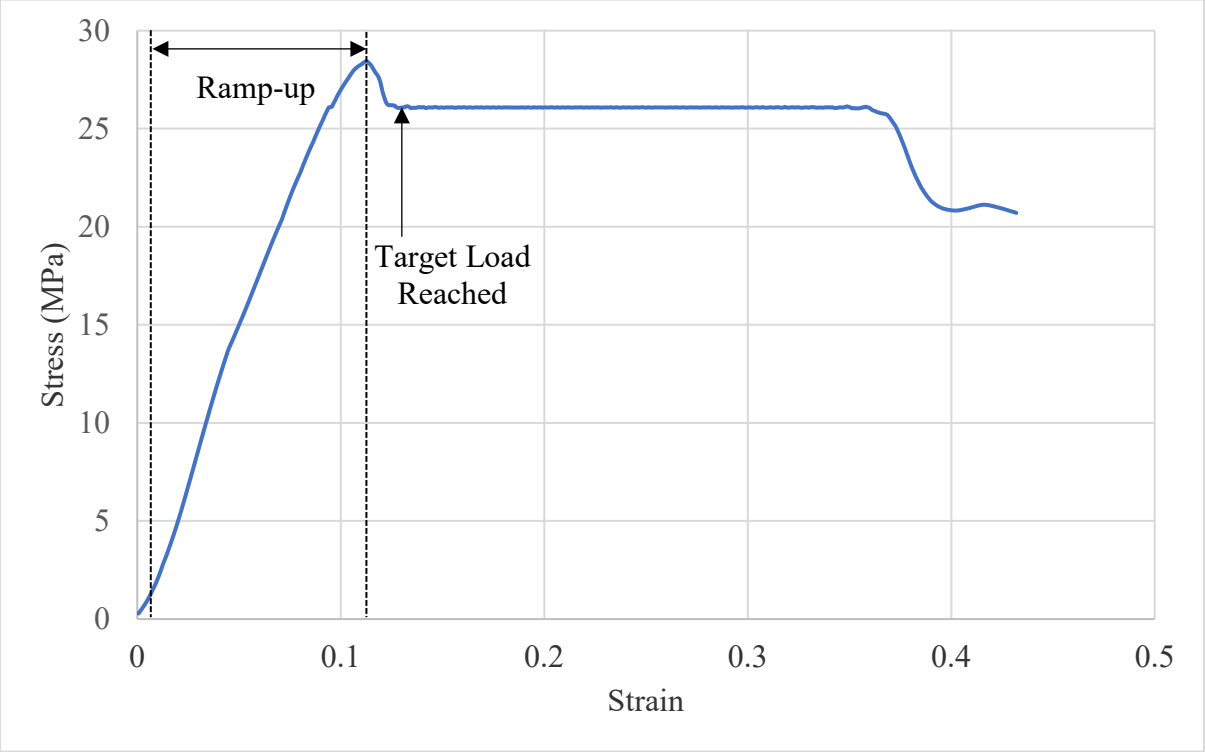

Note. This figure represents the stress strain data for one of the tendons that reached failure.

4.3.1 Predictive Models Results

Total predicted times to failure range from (58 - 393 hrs.) assuming the strains to failure (on average) range from 15 - 18% as shown in Table 15. Table 15 also includes the average strain rates for each tendon used in the prediction models. These results assume the progression of strain is linear until close to failure. The data presented in Table 15 indicates that for these data, a linear model provides the best fit. The model shown in Figure 19 suggests the best fit was with an $R^2 = 52.0\%$:

$$y = -1 \times 10^6 x + 1 \times 10^6 \qquad \text{(Model 1)}$$

Where *y* refers to the predicted time to failure in seconds and *x* refers to the %UTS.

Table 15: Predicted Times to Failure Based on Estimated Average Strain at Failure

Donor	Study #	% of UTS	Strain at 16 (hrs.)	Average Strain Rate (%/s)	Total Predicted Time to Failure (hrs.)	Average Strain at Failure*
4	18	20	0.0088	0.000015	290.22	0.16
3	23	20	0.0065	0.000011	393.55	0.16
1	51	20	0.011	0.000020	225.09	0.16
4	54	40	0.008	0.000014	291.57	0.15
1	63	40	0.019	0.000032	128.99	0.15
3	21	60	0.013	0.000023	219.15	0.18
2	35	60	0.015	0.000026	191.96	0.18
1	41	60	0.016	0.000028	160.27	0.16
4	19	80	0.04	0.000076	58.61	0.16
3	42	80	0.11	0.000026	167.89	0.16

Note. *Refers to the average strain at failure generated from the results of Chapter 3 for varying levels of %UTS.

Figure 19: Predicted Time to Failure

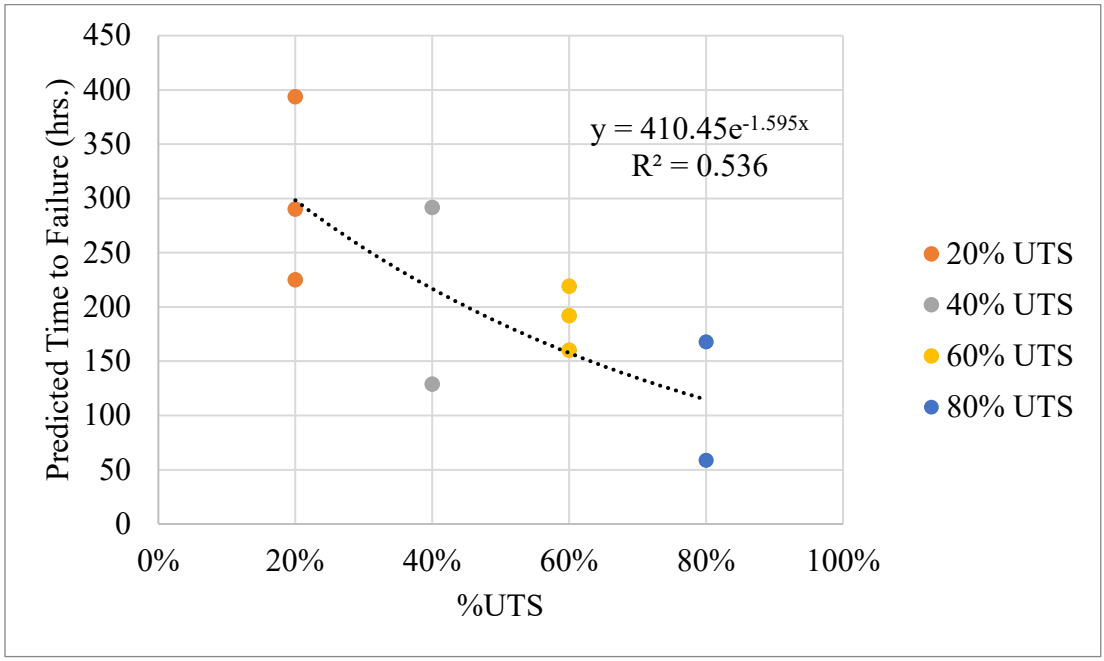

The six tendons that did not fail, however, reached 1.3% strain during the 16-hr test with only one of the six tendons reaching 5% then 8% strain. Tested times to reach 1.3% strain range from (0.02 - 16 hrs.), with predicted times of (18 - 31 hrs.) to reach the same level of strain. To reach 5% strain, the predicted times range from (43 - 122 hrs.) and (68 - 196 hrs.) to reach 8%. Figures 20, 21, and 22 graphically present the predicted times to reach the target strains (1.3, 5, and 8%). All three figures indicate that progression of strain as result of creep loading is linear.

Table 16: Actual and Predicted Times to Different Levels of Strain

Donor	Study #	% of UTS	Time to 1.3% Strain (hrs.)	Time to 5% Strain (hrs.)	Time to 8% Strain (hrs.)
4	18	20	23.58*	90.69*	145.11*
3	23	20	31.98*	122.99*	196.78*
1	51	20	18.29*	70.34*	112.54*
4	54	40	25.27*	97.19*	155.50*
1	63	40	0.24	43.00*	68.79*
3	21	60	16.00	60.88*	97.40*
2	35	60	6.45	53.32*	85.31*
1	41	60	6.52	50.08*	80.13*
4	19	80	0.02	52.47*	83.95*
3	42	80	5.41	18.32	29.31

Note. *Represents predicted times to reach specific levels of strain.

Figure 20: Regression Estimates for Time to 1.3% Strain in Human Flexor Digitorum Tendons

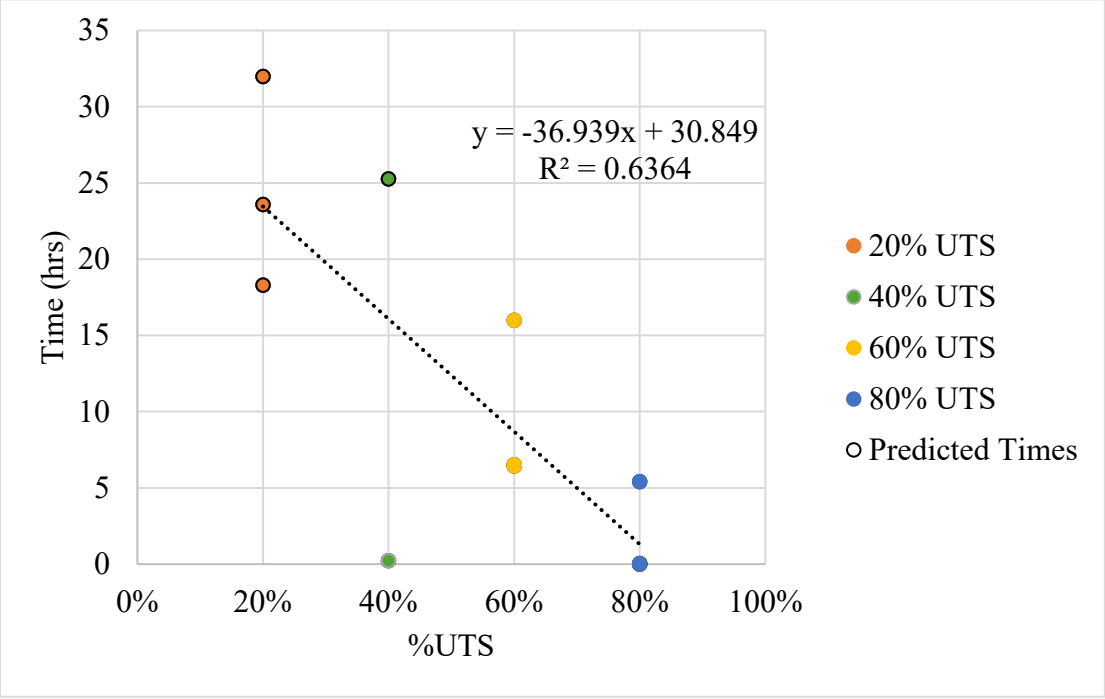

Figure 21: Regression Estimates for Time to 5% Strain in Human Flexor Digitorum Tendons

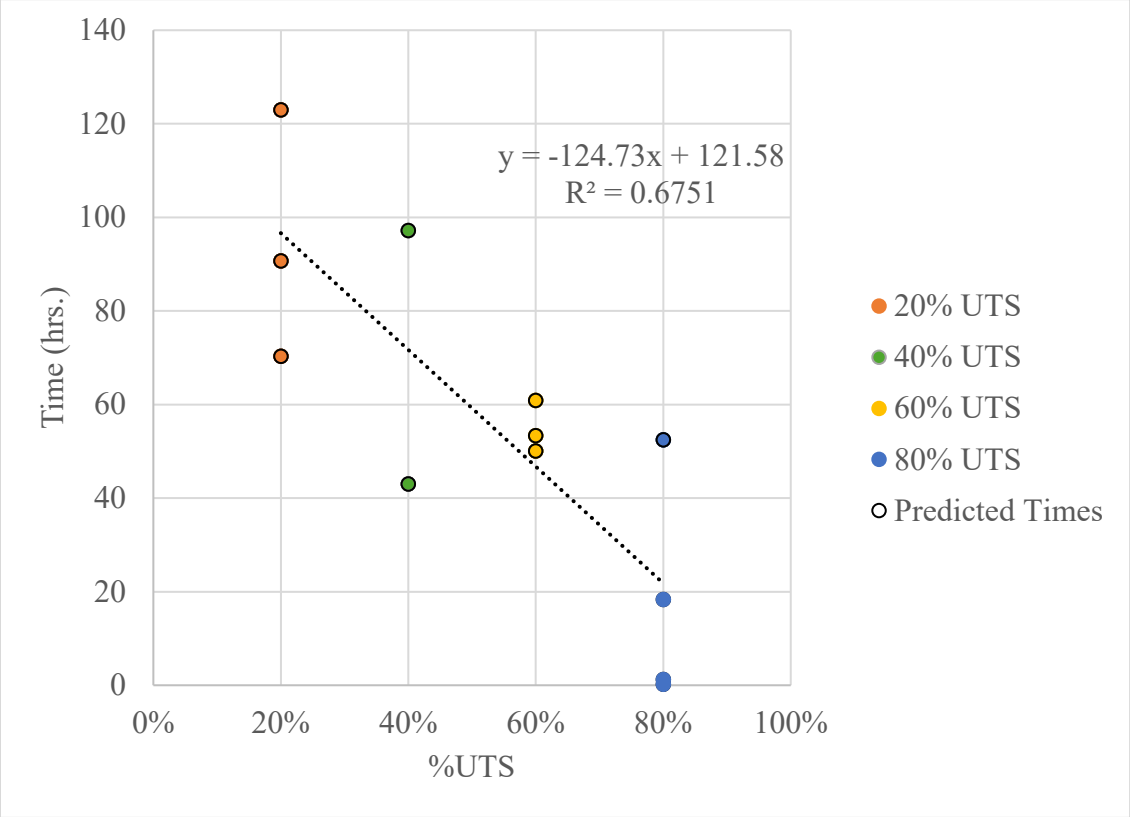

Figure 22: Regression Estimates for Time to 8% Strain in Human Flexor Digitorum Tendons

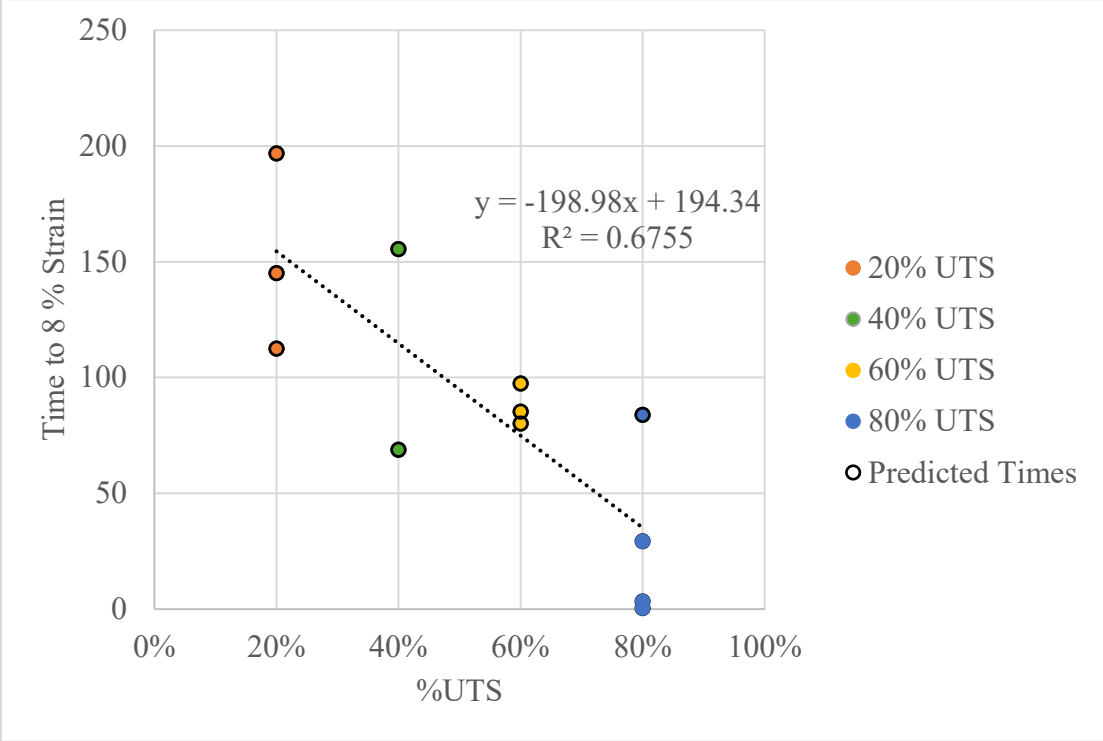

4.4 Discussion

Time to failure for tendons used in this study differed from the only other study found evaluating human tendons (Wren et al., 2003). Wren (2003) exposed human Achilles to creep loading. There are several reasons for the differences in time to failure including experimental design. First, Wren (2003) tested Achilles tendon, not FDP/FDS tendons. Second, the Achilles tendons tested by Wren (2003) were exposed to varying levels of nominal stress (35 - 75 MPa) rather than testing different levels of %UTS. Making direct comparisons is not possible since the %UTS was unknown for the varying levels of nominal stress. For example, an Achilles tendon tested at 75 MPa could be 95% of a particular tendon's UTS or it could also be any other

percentage (Wren et al., 2003). Wren (2003) also did not find a significant difference between applied stress and time to failure. This contradicts the findings of this study where %UTS was associated to time to failure. It is possible that findings from Wren (2003) regarding applied stress is a result of how the Achilles tendons were tested (not normalizing to an average %UTS) but also other factors such as within and between donor variation (Schechtman, 1995; Smith, 2019; Wren et al., 2003). The present study controlled for within donor variation by normalizing the average UTS to each donor. Controlling for within donor variation could also have a potential impact on the calculated stress experienced thereby impacting the times to failure. The strains at failure of the two tendons that failed are generally higher than what would be expected (21 and 40%); however, these levels are still within what has been reported in the literature (Smith, 2019; Wren et al., 2003). These authors reported a tendon reaching up to 50% strain.

4.5 Limitations

This study used the same donors and similar testing methods to that of Chapter 3, and thus will be subject to similar limitations. A difference between the current chapter and Chapter 3 is the sampling rate, with a sampling rate of every 0.02 mm. Therefore, if little deformation occurred then fewer data points were sampled. The limited sampled data led to the decision to use an average strain rate. Using an average strain rate assumes the average change in strain is linear until close to failure. The current study also assumes that all predicted times to failure start from when the target load is reached.

4.6 Conclusions

The aim of the current study was to determine the effect of creep on the failure of FDP/FDS tendons at varying stress levels. Results of this experiment suggest strain at failure appears to be dependent on the constant load applied and the time exposed to that load. This study was not able to determine the amount of physical damage accumulated from the loading process. The predictions made during this study were based on values associated with *in vivo* MVCs suggesting that after these levels of strains are reached, it would be possible for tendon to become damaged.

Chapter 5 Determination of Load Transition Effects on *Ex Vivo* Human Flexor Digitorum Profundus and Superficialis Tendon

5.1 Introduction

Tendons, like other musculoskeletal tissues, experience both cyclic loading and creep loading on a daily basis. Both loading modalities can affect the deformation and damage development of tissues (Gallagher & Huangfu, 2019). However, there is a lack of research regarding the response of human musculoskeletal tissues to combined cyclic and creep loading (NORA, 2018). In order to address this gap in the literature, Gallagher & Huangfu (2019) presented a method of evaluating the combined effect of creep and cyclic loading known as creep-fatigue. To evaluate the creep-fatigue interaction, Gallagher & Huangfu (2019) used the creep-fatigue life equation (Equation 1) from the American Society of Mechanical Engineers code (Wright et al., 2016).

$$\sum_j \left(\frac{n}{N_d}\right)_j + \sum_k \left(\frac{\Delta t}{T_d}\right)_k \leq D \qquad \text{(Equation 1)}$$

Where n and N_d refer to the number of cycles and the number of cycles to failure of cycle type j; Δt and T_d refer to the creep loading time (dwell) and the time to failure at stress level k; D is the combined damage fraction of both sections where failure would be reached when $D = 1$.

In their proceedings paper, Gallagher & Huangfu (2019) note that they were not able to find data combining creep and fatigue data in musculoskeletal tissue. This is also consistent with the results of the literature review presented in Chapter 2. Accordingly, the purpose of this study was to perform *ex vivo* combined creep and fatigue loading on human tendons to evaluate the

development of strain over time associated with transitioning between both load modalities and to determine the significance of a load order effect (load sequence). For the purposes of this study, the phrase 'load sequence' simply refers to the prescribed order in which a material is exposed to a load modality (i.e., loading regimen initiated with creep versus cyclic). The term 'load modality' may be interchangeable with 'load phase' or the instances in which a tendon is loaded.

5.2 Methods

5.2.1 Tendon Preparation

A total of 82 randomly selected fresh-frozen flexor digitorum profundus (FDP) and superficialis (FDS) tendons from 10 human donors were used in this study. Donor ages ranged from 30 - 77 (mean of 55). Donors were of various races, sex (6 female, 4 male), and BMI with a mean height of 1.66 meters (65.5 in.) and a mean weight of 73.7 kg (162.5 lbs.). More specifics on donor demographics can be found in Appendix C. This experiment uses the same exclusion criterion as Chapters 3 and 4. Donors were provided by Science Care (Phoenix, AZ) and stored at -20 °C until dissection. At the time of dissection, excised tendon length was approximately equal to 8 cm, with the flexor retinaculum being centered along the removed tendon so that ~4 cm remained on the proximal and distal end of the tendons. Tendons were measured while in anatomical position prior to excision to preserve consistency. Excised tendons were immediately placed in self-sealing plastic bags that were folded to prevent the tendon from rotating or sliding within the bag, then stored at -20 °C before imaging was performed.

5.2.2 CT Imaging Setup and Filtering

A GE LightSpeed VCT 64 (GE Healthcare, Chicago, IL) was used to scan the tendons prior to testing. To hold the tendons in place during scanning, 10 custom trays were used. The trays were designed with channels to individually hold each tendon in place during scanning as demonstrated by Figure 5.1. The trays used were assigned to specific donors to maintain uniformity. All tendons were placed following the same pattern of distal end to proximal of the tendon. Placement started with the FDP tendons followed by FDS. Extensor digitorum tendons from donors were placed in the two most center channels of the trays. The CT scanner settings and tendon placement were consistent with normal medical CT imaging techniques, meaning trays were placed in the scanner as if a human was laying on the table. To fit the trays on the scanner bed, the 10 trays were divided into three stacks, consisting of three trays, three trays, and four trays. The stack order was randomly assigned and maintained the previously mentioned orientation. Figure 5.2 provides an example CT image of one of the stacks which consisted of three trays. Reflective markers common to CT scanning were used to mark the starting locations of the tendons within the images. A full helical scan was performed resulting in a total of 1523 images. The slice intervals were 0.625 mm apart. All blank images were removed. Further image filtering was used to determine the actual length of the tendon that would fit the 30 mm grip-to-grip distance of the clamps. The total required images analyzed was 50.

Figure 23: 3D printed tray with donor tendon sample placement

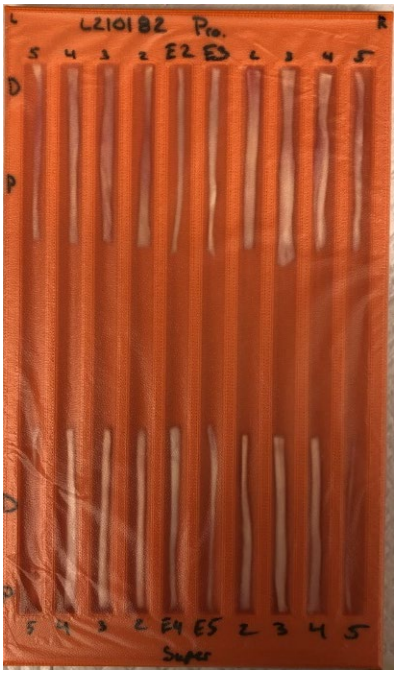

Note. Figure shows donor tendon placement within the tray that was used for scanning.

Figure 24: Example image of a CT scan for a stack of three trays

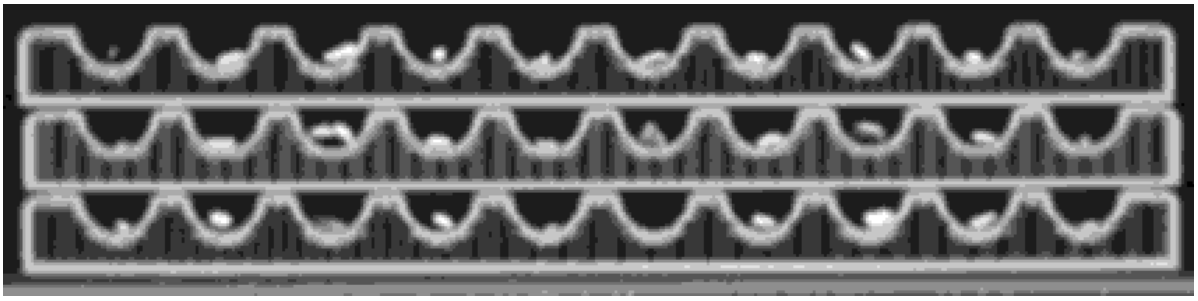

Note. The tray position of EDL tendons followed digit order: (left hand 5-4-3-2 and right hand 2-3-4-5).

5.2.3 Cross-Sectional Area (CSA) Measurement

Tendon CSA quantification was performed unsupervised in ImageJ (Schneider et al., 2012) through a custom computer program using the Fiji package (Schindelin et al., 2012). This program identified transverse sections of tendon tissue scanned via CT and calculated the cross-sectional area. This image was loaded into the program where a machine-learning classifier first identified the bounds of each individual tray and created a region of interest (ROI). An ROI can be used to select a specific region in the image. This ROI was used to select the tray and center it onto a new image to account for variation in tray placement. Once centered, pre-set ROIs were retrieved, and the image was scanned in x and y dimensions to find the edges of the tray. The exact location of the tray was then used to select individual channels containing a single scanned tendon via the pre-set ROIs (which matched the dimensions of each of the channels). Subtracting the tray from the image was important for ensuring tendon detection and CSA calculation were not confounded. Once all of the individual channel images were selected, the program cut and embedded the selections into a new image. Due to small variations in image acquisition, the placement of ROIs was not always perfect and sometimes included minor elements of the tray. To extract solely the tendon, this image was run through a classifier program that was trained to segregate tendons from confounding tray pieces. The classifier output was then used to generate novel individual tendon ROIs. Once all background was subtracted, the image was thresholded (classified pixels as black or white) and binarized (assigned values to threshold where black was zero and white was one). A particle analysis algorithm systematically scanned all rows in the tray, measuring all contiguous white pixels (tendon tissue) and outputting the area along with other morphometric measurements. The result of this procedure thus delivered highly accurate

and referenceable data for each tendon. Furthermore, the program was able to batch process hundreds of images, enabling high-throughput measurements of thousands of tendon sections.

5.2.4 General Testing Parameters

All tests were completed using the same testing equipment described in the previous chapters. All tests were performed using load control settings to ensure that the actuation rate would be consistent. Like the previous chapters, all tests were set to not exceed 800 N to reduce risk of damaging the micro tester. The grip-to-grip distance for all tests was 30 mm, following similar research protocols that used a consistent grip-to-grip distance (Schechtman & Bader, 1997; Scholze et al., 2018; Smith, 2019; Wren et al., 2003).

5.2.5 Tensile Testing

Eleven randomly selected FDP/FDS tendons were used for this test. Tendons were tested to failure at a rate of 1 mm/s using a sampling rate of 0.02 s. This procedure was used to allow an accurate assessment of the different levels of UTS that would be used for each test. Strain was calculated from when tendons reached 2 MPa; this was done to account excessive tendon slack.

5.2.6 Combined Creep and Cyclic Loading

Seventy-one randomly selected FDP/FDS tendons were used for this study. Tendons were tested to failure or were censored at a load rate determined by the minimum CSA of each specific tendon at specified levels of the average UTS (25% and 55%) using a frequency of 1 Hz. Stress estimates were calculated using the average UTS of 49.38 MPa from the prior UTS tests. The specific values for expected stress were 12.35 and 27.16 MPa, respectively. These values were then used to calculate the expected maximum load and load rate using the minimum CSA of each tendon tested, the values of which can be found in Appendix C. The duration for each

test was set to 1,000,000 s (~12 days) to ensure sufficient time for each tendon to rupture. Due to the extended duration, and to ensure consistent sampling among tested tendons, the sampling rate was set to sample every 20 s for all combined loading tests. Tendons were randomly selected to be initially exposed to either cyclic loading or creep loading, which was followed by the opposite loading condition on an alternating basis. Loading conditions were set based on time, and one complete sequence took about four minutes to complete. For example, a complete sequence consists of a one-minute exposure to cyclic loading, one-minute of recovery, one-minute of creep loading, followed by another minute of rest. Specifically, if a tendon was set to start with cyclic loading at 25% UTS, after exposure to 30 cycles (one minute), the grip-to-grip distance returns to 30 mm for a 60 s rest/recovery period similar to that of De Zee et al. (2000). The tendon would then be exposed to creep loading with a dwell time of 60 s. After dwell, the grip-to-grip distance returns to the 30 mm starting position for a rest period of 60 s before starting the next 30 cycles. This process continued until failure. The level of UTS and the load order was randomly assigned to the tendon before the test began and this sequence of loading continued for the duration of each test. Figure 25 provides a simplified depiction of the loading pattern to demonstrate a sequence.

Figure 25: Combined Loading Example Stress vs. Time

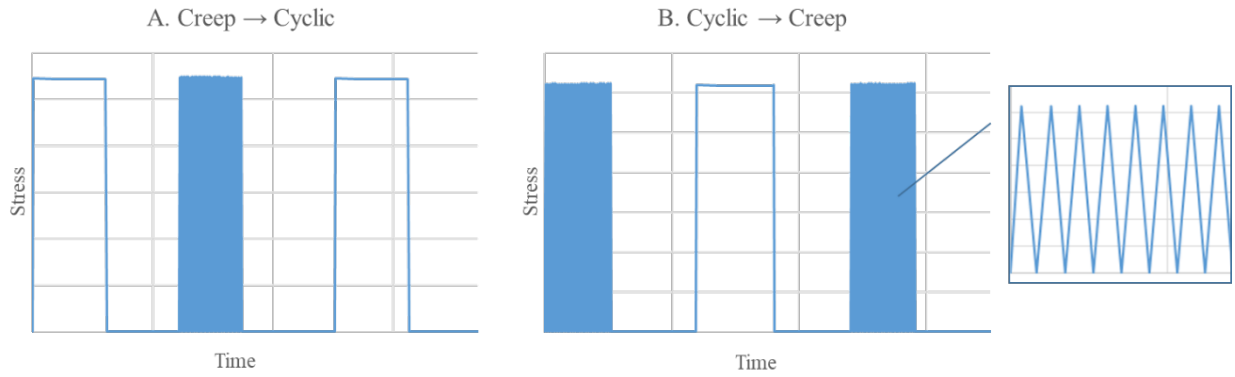

Note. This figure demonstrates a load sequence with stress over time if the first load modality was creep (A) or cyclic (B). The box to the right of Figure 25 is a zoomed in version to show what the loading cycles looked like.

5.2.7 Data Processing and Statistical Analysis

To evaluate the effects of combined loading on the changes in strain, strain was calculated for all tests either from the point at which the target load was reached (for creep exposures) or after the peak strain of the first cycle (for cyclic exposures), depending on which loading modality started first. This accounted for excessive displacement caused by the initial ramp-up as well as potential slack in the tendon from tendon placement within the grips. The raw sequence data was then processed and filtered for analysis. Data processing consisted of filtering out rest periods, ramp-ups, and the return to the starting load. The data used for the analysis after filtering consisted of the peak strain at the end of each load modality of the sequence and the corresponding time. This equates to the peak strain at every 30^{th} cycle and the peak strain at the end of each dwell phase. In addition, the values at time zero and one row of data after failure were included to be used as dummy rows for the analysis. A linear mixed effect model with a

nested design was developed and tested (represented by Model 2) which accounted for within donor variation. These types of models have been used in longitudinal studies especially for repeated measures and unbalanced designs (Brown, 2021; Schober & Vetter, 2018).

$$Y_{ij} = \beta_0 + \beta_1 L_{j(i)} + \beta_2 S_{j(i)} + u_{0j} + \varepsilon_{ij} \qquad \text{Model 2}$$

Where:

i = Donor number

j = Tendon sample number

$Y_{j(i)}$ = Change in strain ($\Delta\varepsilon$) when transitioning from Creep → Cyclic or Cyclic → Creep

$L_{j(i)}$ = The assigned level of %UTS

$S_{j(i)}$ = Load sequence (Transitioning from Creep → Cyclic = 1 or Cyclic → Creep = 0)

$T_{j(i)}$ = Time between transitions (ΔT), seconds

$u_{0(i)}$ = Random effect: tendon within donor

ε_{ji} = Random Error

Analysis was conducted using R (R Core Team, 2023), RStudio 2023.09.1+494 (Rstudio Team, 2023), and the lme4 package (Bates et al., 2015). The code calculated strain and time differences for each tendon tested over time, providing the changes in strain and the time difference that corresponded to that change. The use of the dummy rows was crucial to calculating the strain and time differences to ensure the first and last rows of data from the tests were included. Code used to calculate the strain and time differences and the subsequent analysis is included in Appendix C. Practical significance of the changes in strain was determined by calculating Cohen's d effect sizes for within tendon differences at both levels of %UTS.

5.3 Results

5.3.1 Tensile Testing

The calculated mean UTS for the tested FDS/FDS tendons was 49.38 MPa with a standard deviation of 20.91 MPa. The average ultimate strain or strain at failure was 14 ± 3%. The results of the tensile test can be viewed in Table 5.1. The load rates for this experiment were calculated using the average CSA and average UTS.

Table 17: Ultimate Strength Test Results

Donor	Study #	Type	Digit	Max Load (N)	Min CSA (mm^2)	UTS (MPa)	Ultimate Strain
7	1	LFDP	3	377.37	8.31	45.42	0.14
2	2	RFDP	5	290.16	3.32	87.31	0.23
8	3	RFDS	3	357.74	11.26	31.76	0.12
10	4	LFDP	3	338.62	8.68	39.02	0.12
2	5	LFDS	5	72.34	1.48	48.98	0.12
7	6	RFDS	4	312.50	9.05	34.54	0.14
10	7	LFDP	4	81.18	5.72	14.18	0.08
5	8	RFDS	2	303.86	6.83	44.48	0.14
1	9	RFDS	5	143.17	2.40	59.65	0.13
8	10	RFDP	2	344.23	6.65	51.79	0.15
9	11	LFDS	3	349.56	4.06	86.06	0.11
Mean ± Standard Deviation				**270.06 ± 108.69**	**6.15 ± 2.93**	**49.38 ± 20.91**	**14 ± 3%**

5.3.2 Combined Creep and Cyclic Loading

Of the 71 tested tendons, three survived their tests, two lasting five days and one 10 days, respectively. All three were stopped for the sake of time, and the results censored (not included in analysis). A strain summary table for surviving tendons was included in Appendix C. Thirty tendons were removed from the analysis for any of the following reasons: tested tendons did not

survive the ramp-up, did not complete a full sequence, were inadvertently tested using incorrect settings, failure at the clamp site, tendon slipped from the grips during testing, or due to a mechanical error with the actuator of micro tester.

Regardless of load sequence or %UTS level, the average strain at failure for all tendons tested was 10 ± 4% which is consistent with strain failure of tendons in the current literature (Schechtman & Bader, 1997; Wren et al., 2003). Average failure times for all tested tendons regardless of load sequence or %UTS ranged from (1.16 - 29.53 hrs.). Table 18 presents the average times and strains at failure. Average strains at failure are depicted in Figure 26 as a box and whisker plot. Examples of each load sequence are included in Appendix C. Appendix C also contains a version of Table 18 that includes the values of tendons that did not complete a full sequence. These examples show the increases in strain over time resulting in failure. The examples also show that testing at 25% UTS resulted in considerably longer times to failure (on average six times longer) than testing at 55% UTS. The results show that, on average, tendon failed sooner when the sequence starts with creep. One tendon tested at 25% UTS where the sequence starts with cyclic was removed as an outlier with a strain at failure of 22% (lower bound 3.9%, upper bound 16% strain).

Table 18: Table of Average Strain by Load Sequence and %UTS

Transition	**n**	**% of UTS**	**Average ± Standard Deviation**	
			Strain at Failure	**Time to Failure (hrs.)**
Cyclic → Creep	7	25	10 ± 2%	29.53 ± 29.24
Creep → Cyclic	7	25	12 ± 2%	26.24 ± 33.04
Cyclic → Creep	12	55	11 ± 3%	8.3 ± 19.15
Creep → Cyclic	11	55	10 ± 4%	1.16 ± 0.64

Note. The order column indicates the repeated loading modality for the tests of which failure occurred.

Figure 26: Strain at Failure Plot by Load Transition

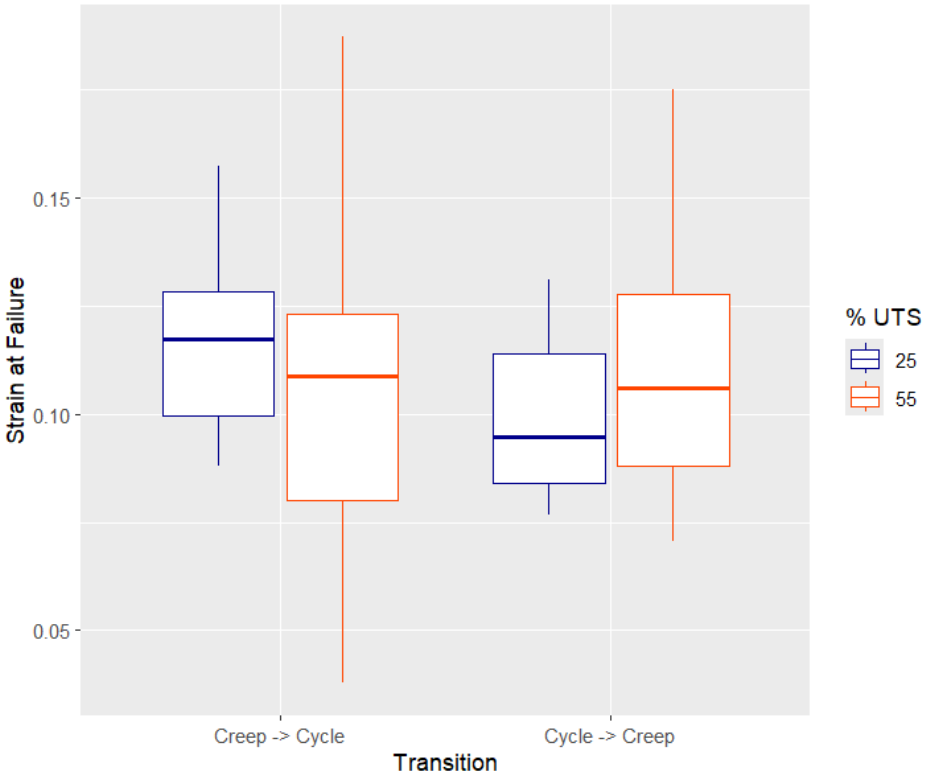

Note. Boxplot of data shown in Table 18.

Average strain rates during 'steady state' (after the first completed phase of a given sequence to the completed phase before failure) for either phase ranged between (0.003 - 0.018 %/s) were also analyzed. This is demonstrated in Table 19 where the average strain rates for each loading condition are presented. These averages are calculated from the average strain rate of each phase. For example, the first 'Creep' average from Table 19 was calculated from the average strain rate for each creep phase of each tendon where the load sequence starts with creep. To further elaborate, 11 tendons were tested at 55% UTS where the sequence started with creep. Each tendon experienced 'x' number of creep phases. An average creep phase strain rate was calculated for each tendon then a total average was calculated.

Table 19: Average Strain Rates

Average Strain Rate ± Standard Deviation			
55% UTS Creep → Cyclic		**55% UTS Cyclic → Creep**	
Creep	0.010 ± 0.002 %/s	Creep	0.018 ±0.022 %/s
Cyclic	0.010 ± 0.002 %/s	Cyclic	0.011 ± 0.009 %/s
25% UTS Creep → Cyclic		**25% UTS Cyclic → Creep**	
Creep	0.008 ± 0.002 %/s	Creep	0.006 ± 0.002 %/s
Cyclic	0.005 ± 0.002 %/s	Cyclic	0.003 ± 0.002 %/s

5.3.3 Statistical Analysis

Results of the model shown in Table 20 indicate that a statistically significant interaction effect exists between %UTS and the time spent in each phase ($p < 0.001$). This presence of an interaction effect will most likely mask the main effects, and thus require the use of a simple main effects analysis.

Table 20: Summary Table of Model Output

	Strain Difference		
Predictors	*Estimates*	*95% CI*	*p*
(Intercept)	-0.000458	(-0.004872, 0.003956)	0.839
Transition: Cycle → Creep	-0.003486	(-0.003628, -0.003345)	**<0.001**
Load (%UTS)	0.009067	(0.003442, 0.014693)	**0.002**
Change in Time per Transition	0.000041	(0.000033, 0.000048)	**<0.001**
Load (%UTS) * Change in Time per Transition	-0.000036	(-0.000049, -0.000022)	**<0.001**
ICC	0.90		
Marginal R^2 / Conditional R^2	0.136 / 0.911		

Note. The output from model shows that all variables in the model are statistically significant ($p < 0.001$).

Results of the simple main effect analysis shown in Tables 21 and 22 indicate for this study regardless of %UTS there is a statistically significant difference in the change of strain when transitioning between both loading phases ($p < 0.001$). For 55% UTS, the model estimates that per transition (transitioning from cyclic to creep) the change in strain will on average be 0.34% less strain than when transitioning from creep to cyclic. The overall Cohen's d effect size for 55% UTS is 0.57 with 95% CI (0.50, 0.64) suggesting a medium effect. For 25% UTS the change in strain will on average be 0.40% less strain than when transitioning from creep to cyclic. The Cohen's d effect size for 25% UTS is 2.55 with 95% CI (2.50, 2.60) suggesting a large effect. The Cohen's d effect sizes for the combined loading tests are shown in Figure 27. Two tendons tested at 55% UTS following the cyclic to creep sequence only completed one full sequence, which does not allow for Cohen's d effect sizes to be calculated. For tendons that completed more than one sequence, 52.4% of the tendons tested at 55% UTS suggest a large effect size $|d| \geq 0.8$, and 78.6% of the tendons tested at 25% UTS suggest a large effect size $|d| \geq 0.8$ or greater. Medium effect sizes of 14.3 and 19% respectively with the remainders suggest either small or negligible effect sizes.

Both models are designed to account for tendon (random effect) within donor (fixed effect) variation. Model effectiveness is represented by the interclass correlation coefficient (ICC) which captures the percentage of variation among donors and tendons relative to variation within tendons. Meanwhile, the conditional R-squared indicates that variation of the dependent variable (change in strain) is explained by the independent variables. The values for each model are as follows (ICC = 0.79, conditional-R^2 = 79.1%) for the 55% UTS model and (ICC = 0.18, conditional-R^2 = 57.7%) for the 25% UTS model. Results suggest that the 55% UTS model better accounts for tendon within donor variation when compared to 25% UTS model. However,

in the case of the marginal R-squared which indicates the variation explained by the fixed effect (between donor variation), the 55% UTS model has a lower value than the 25% UTS model (marginal-R^2 = 2.2, 57.7%).

Table 21: Summary of Simple Main Effects Analysis 55% UTS

55% UTS	**Change in Strain**		
Predictors	*Estimates*	*95% CI*	*p*
(Intercept)	0.008916	(0.004666, 0.013166)	**<0.001**
Transition: Cycle → Creep	-0.003430	(-0.003800, -0.003060)	**<0.001**
ICC	0.79		
Marginal R^2 / Conditional R^2	0.022 / 0.791		

Table 22: Summary of Simple Main Effects Analysis 25% UTS

25% UTS	**Change in Strain**		
Predictors	*Estimates*	*95% CI*	*p*
(Intercept)	0.002575	(0.002150, 0.003021)	**<0.001**
Transition: Cycle → Creep	-0.004007	(-0.004064, -0.003950)	**<0.001**
ICC	0.18		
Marginal R^2 / Conditional R^2	0.577 / 0.654		

Note. The increase of the Marginal R^2 compared to tendons tested at 55% UTS results from initial tendon randomization where two donors account for six out of 14 tendons tested at 25% UTS.

Figure 27 Cohen's d Effect Sizes of Creep → Cyclic to Cyclic → Creep Transition

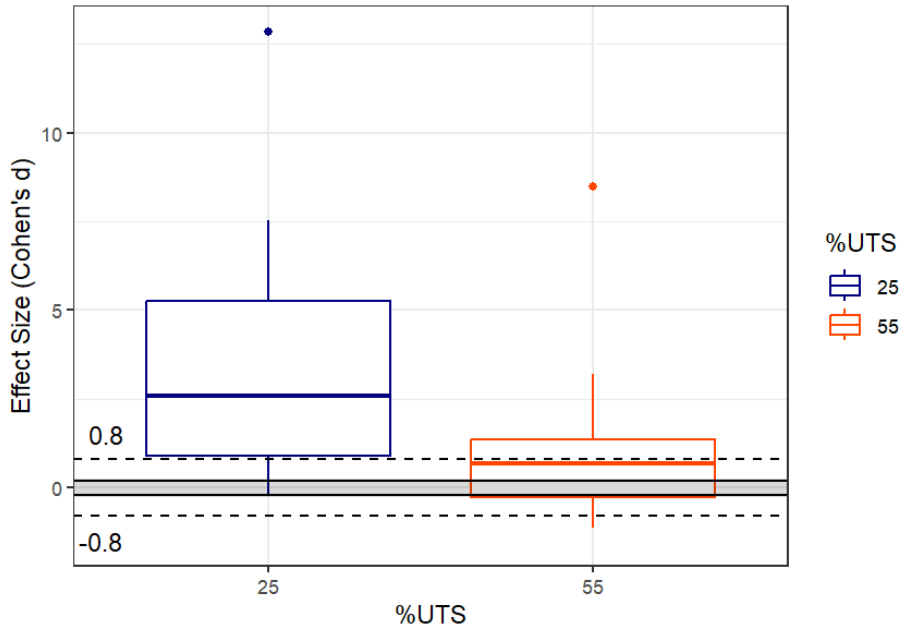

Note. Figure represents a box plot of Cohen's d effect sizes for the changes in strain at both tested levels of %UTS. Large effect size are values above and below the dashed lines $|d| \geq 0.8$. The small effect $|d| \leq 0.2$ is indicated by the shaded gray shaded region.

5.4 Discussion

It is generally understood that materials that are exposed to cyclic loads incur more strain and thus more damage than those subjected to creep loads. However, results from this study found that on average, regardless of %UTS, transitioning from a creep load to a cyclic load resulted in a larger change in strain ($\Delta\varepsilon$) than transitioning from a cyclic load to a creep load. The results of this study do not suggest that creep loading damaged the tested tendons more than cyclic loading. The average change in strain when changing from one modality to the next is on average slightly greater (by approximately 0.3% - 0.4% strain) when transitioning from creep to

cyclic loading. The results are supported by a medium Cohen's d effect size for tendons tested at 55% UTS and a large Cohen's d effect size for tendons tested at 25% UTS indicating the changes in strain resulting from transitions between creep and cyclic loading are practically relevant. Possible reasons for the difference between the effects sizes include that the tendons loaded at 55% UTS tendons are exposed to both higher loads and faster rates of loading resulting in shorter times to failure. Shorter time to failure results in less available data for computing an effect size. It may be possible that tendons tested at higher levels of %UTS reach a 'ceiling' or steady state in regard to the changes in strain until failure. However, further research at more varied levels of %UTS would be required to provide evidence for or against this hypothesis.

Potential reasons for the differences observed in $\Delta\varepsilon$ include that cyclic loading may be more damaging to the tendon than creep loading. This effect could also be influenced by the ramp-up rate used to reach the target load having a more significant effect than previously considered. This observation is supported by tendons that did not survive that ramp-up or the number of tendons that did not complete a full sequence. When starting with creep load, five tendons survived the creep phase but did not complete 30 cycles of cyclic loading. It was also observed that most of the tendons tested failed during a cyclic loading phase, indicating the possible significant effect that cyclic loading has on musculoskeletal tissue. Results of this study found that tendons on average fail sooner when exposed to high levels of ultimate stress, which is consistent with our current understanding of tendon material properties (Schechtman, 1995; Smith, 2019; Wren et al., 2003). Results of this study found UTS for human hand flexor digitorum tendons to be around 49.38 ± 20.91 MPa. This is consistent with the findings from (Smith, 2019) 41.17 ± 10.01 MPa. These are less than the UTS of reported leg tendon (extensor

digitorum longus/hallucis longus 99.9 ± 12.2 MPa and 87 ± 12.5 MPa (Schechtman & Bader, 1997) and 71 ± 17 MPa for Achilles tendon (Wren et al., 2001).

5.4.1 Limitations

The main limitations of this study stem from the CSA measurement and the subsequent calculations. To fit all tendons from one donor in one tray to be scanned, the diameter of the field of view (DFOV) of the CT was set to its maximum of approximately 22 cm, compared to Chapters Three and Four where the DFOV was approximately 10 cm. The DFOV can impact the pixel density which directly affects the CSA estimation. It is not possible to determine if the minimum CSA is over or underestimated. However, in general, the smaller the tendon is, the harder it will be to obtain accurate estimate with the VCT scanner used in this study, which greatly affects the values used to calculate the UTS. The original intent was for the micro tester to be programed to complete 60 cycles at a load rate of 1 Hz. However, the micro tester could not reach a frequency of 1 Hz with the current loading configuration. A frequency of 0.5 Hz was achievable. Therefore, the time required to reach 30 cycles was approximately 1 minute, which was the same as the target time for the creep phases. While the original intent was to cycle the tendons more quickly (i.e., at 1 Hz, for a total of 60 cycles), the tendons instead were exposed to 30 cycles for approximately 1 minute. There is no current precedent regarding combined loading (i.e., alternating cyclical and creep loading) for tendon testing. Therefore, although the intent was to cycle the tendons for 60 cycles between 1-minute creep loads, they were instead cycled 30 times. All tests were conducted in a consistent manner with the same loading configuration settings. Ultimately, there is no reason to believe that the data are any more or less valid for 30 loading cycles rather than 60.

5.5 Conclusions

This study aimed to determine the significance of a load sequence effect on human FDP/FDS tendon when balanced for time. The progression of strain when transitioning between different load modalities posed an interesting and challenging question to investigate with the collected data. The main objective of the current study changed to evaluate the development of strain over time as load modalities changed. The results indirectly suggest a load order effect; however, this question requires further investigation. The results of the current study do not suggest that exposure to creep loading causes more damage to FDP/FDS tendon; however, transitioning from creep to cyclic loading results in larger differences on average than transitioning from cyclic to creep. The results do suggest that creep loading affects the development of strain in FDP/FDS tendon in the context of combined loading.

Chapter 6: Conclusions

6.1 Introduction

This work explored the *ex vivo* viscoelastic properties of human hand and wrist flexor tendons by evaluating the evolution of strain using different loading modalities (cyclic, creep, and combined cyclic-creep loading) to inform future development of risk assessment models based on fatigue failure. This chapter will discuss the key findings and limitations presented in each of the studies and discuss some key principles/practical considerations related to testing tendon. This chapter will also discuss recommendations for future research.

6.2 Summary of Key Findings

In the completion of these studies the following conclusions can be made:

- Strains at failure appear to be consistent with known literature suggesting that human tendon, regardless of anatomical location, applied stress, and load exposure, fail at similar levels of strain typically between (8 - 20%) (Schechtman, 1995; Smith, 2019; Wren et al., 2003).
- In the case of fatigue loading, strains at failure did not appear to depend on energy loss: meaning more work did not correspond to higher levels of strain at failure. The tendons tested in this work showed a similar pattern of inelastic work per cycle to that of soldering. This observation provides further support suggesting that tendon follows similar failure mechanisms to other viscoelastic materials.
- Computed Tomography (CT) may be a viable method of estimating the minimum CSA of excised tendon. If one does not have access to such a scanner, using the volumetric method for estimating an average CSA may render similar results to that of CT.

However, it is recommended that a high precision graduated cylinder be used to measure FDP/FDS tendon.

- In the case of creep loading, results of Chapter 4 found that predicted time to failure assuming the progression of strain is dependent upon the applied stress and the time exposed to that applied stress.
- The clamps developed by (Scholze et al., 2018) demonstrated to be an effective clamping method of clamping tendon. Out of 160 tendons across three studies, only two tendons were found to show visible signs of slipping with only one tendon failing at the clamp site, suggesting the effectiveness of the designed clamps to prevent slipping and damaging tendon at the clamp site.
- The results of the third study found that when transitioning between load modalities, transitions of creep to cyclic loading resulted in larger changes in strain. This does not suggest that creep loading caused more damage than cyclic. This suggests that creep loading contributes to the development of damage in tendon.

6.3 Dissertation Limitations

6.3.1 Common Limitations of *Ex Vivo* Testing

Studies conducted in the completion of this dissertation have several limitations related to *ex vivo* testing tendon testing, common limitations to be considered include:

- Healing: To the knowledge of the author, no *ex vivo* study has been truly able to account for healing. Though attempts have been made to account for it by assuming a healing rate of 1% per day (Schechtman, 1995), the studies comprising this dissertation did not.

- Necking: The phenomenon known as necking or local decreases in CSA over time as result of exposure to tensile loading, is known to occur in many other non-biological materials, and tendon is no different. Necking was observed in tendon during these studies' completion, but it was impossible to measure the CSA while the tendon was in the bath.
- Grip Adhesion: Grip specimen adhesion is also a commonly discussed challenge, as the specimen can either slip out from the clamps or the force concentration of the grips acting on the specimen can tear/damage tendon at the clamp site.
- CSA Estimation: As discussed in earlier chapters, the CSA is a crucial measure required for stress calculations. It is imperative that the most accurate measure of CSA possible is taken. However, obtaining an accurate measure for tendon poses a significant challenge when tendon has varying morphology and non-uniformity (irregular shape along length).
- Donor Acquisition: Donors with specific restrictions are often either difficult to acquire or take considerable time to do so. As a result, researchers may choose to use animals which are more accessible in research. However, animal models may be close to what can be observed in humans, but animal models are not human models and may not be as effective.
- Donor Variability: Previous chapters have demonstrated the significant variability between donors and the potential effects the variability can have on subsequent analysis, highlighting the importance of controlling for between and within donor variability. Controlling for such variability by means such as normalizing to %UTS enables comparisons to be made between different tendons and donors. Within donor

normalization can become a challenge in some cases due to a lack of multiple tendons, such as two Achilles tendons per donor.

- Donor Personal/Medical History: Certain medical conditions (e.g., diabetes mellitus, endocrine disease, and known bone and joint diseases) and personal history (e.g., smoking status) that affect the musculoskeletal system and thus tissue properties should be avoided; however, due to donor scarcity, selecting for certain parameters may not be possible. In *ex vivo* testing, most donors are typically older than the general working population (above 65 years old). It is not currently possible to account for personal histories to determine the amount of damage tissues received in life.
- *In/Ex Vivo* Differences: It is understood that significant differences exist between *in vivo* and *ex vivo* tissue properties. For example, Schechtman (1997) suggested tendon could fail after four months of normal walking *in vivo* using the model he developed. However, his *in vitro* model does not consider *in vivo* processes. To the knowledge of the author, literature does not exist directly comparing *in*/*ex vivo* differences in human tendon.

6.3.2 Dissertation Specific Limitations

The studies comprising this dissertation have shared and specific limitations. All three studies used an Instron Micro Tester. The Micro Tester was not designed to test large viscoelastic samples such as FDP/FDS tendon using load control. In the case of cyclic loading, using load control led to significant overshooting during cyclic test (Chapter 3), potentially leading to much higher percentages of UTS than expected, particularly for relatively low loads (i.e., 20% of UTS). The third study uses a different diameter size for the field of view (~22 cm) for the CT scanner than the first two studies (~9.6 cm) which may have impacted the accuracy of

the minimum CSA estimates used for the UTS calculations. The first two studies included a dowel rod with known dimensions to use as a ruler. Though the CT scanner was able to produce an estimate of CSA to be ± 1% of the dowel rod CSA, tendons with a CSA smaller than that of the dowel may have higher estimation error rates. All three studies used the same GE VCT scanner for estimating CSA. As a result, the smaller the tendon, the more difficult it is to obtain accurate estimates for CSA due to pixel density (number of pixels within a defined area). Conversely, it appears that with this scanner, the larger the tendon, the more accurate the estimate becomes with respect to the comparator dowel. A single dowel rod from one of the scans was used for all scaling. The same comparator dowel was not included in each scan. Tendons were separated from the scanning trays by low-density pads. In some cases, the pads appear to have absorbed some moisture from tendons, thereby potentially obscuring the boundary of the tendon. The tendon-pad boundary can be manually corrected within the ImageJ software on an individual basis.

6.4 General Research Recommendations

To address the limitations described in Section 6.3.2, recommendations for future research are described.

- Testing Apparatus: To address machine overshoot, it may be possible to use estimates of peak loads (and their corresponding percentages of UTS) rather than the nominal, "target" UTS specified for a given test. Using peak loads may introduce some complications, but could shed light on the fatigue failure process, particularly when loads vary significantly from those intended. If possible, use a testing machine that is able to dynamically test larger viscoelastic samples at high loads with a frequency of at least 1 Hz. Using one of the largest tendons as an example (min CSA of 21.93 mm^2), testing this

tendon at 1 Hz would require a load rate of 684.71 N/s to reach an expected target load of 342.35 N within 0.5 seconds.

- CSA Estimation: A higher resolution scanner may be more effective for estimating CSA of excised FDP/FDS tendons. Machining a "ruler" from a non-metallic, high-density plastic could increase the accuracy of tendon estimation. The "ruler" device should be included in every scan and or every tray. It might also be possible to integrate the ruler device into the scanning trays themselves. Scanning the ruler every time would also facilitate quick visual confirmation of each and every scan. Future studies should explore other non-absorbent materials to separate tendons from the trays.

6.5 Future Research

There are several areas of research that can stem from this dissertation. Immediate research based on results from Chapter 5 include the determination of a load order effect on the development of strain in FDP/FDS tendon and evaluating the effects of rest periods on the development of strain over time. Other areas of research that would require more data include further investigation of tendon properties, fatigue-failure based research, and strain.

- Tendon Properties: Current *ex vivo* research of FDP/FDS tendons assumes that both tendon types have similar ultimate strengths and properties, increasing the overall "N" of tendons that can be tested. Currently, it is assumed that tendons are similar in strength (normalized by cross sectional area) across digit/individual fingers, hands (dominant and non-dominant), and tendon type (FDP/FDS). Future research should test each assumption and compare within and between donors. Typically, FDP/FDS are tested from areas that run through the carpal tunnel; however, if the full length of FDP/FDS tendon is consistent

in ultimate strength (myotendinous junction to osteotendinous junction), the total "N" for both tendon types from each donor could be increased by creating multiple samples per tendon.

As discussed in earlier chapters, it is understood that both smoking and diabetes mellitus can affect tendon properties; however, it is not known by how much. Performing a case-control study comparing the ultimate strength of donors who smoke and/or have diabetes mellitus against a control group could help inform risk assessment models. In a similar fashion, vibration exposure is another factor that could be considered to determine the effects on tendon ultimate strength.

- Fatigue Failure Related Research: Future research could pursue the development of S-N and creep time to failure curve for the FDP/FDS tendons using the minimum CSA at multiple levels of UTS. Failure curve data could be used to develop a creep fatigue model to improve our understanding of damage development in FDS/FDP tendon. Knowledge from this type of research could be further expanded to include more complex loading patterns that could better simulate manual manufacturing tasks (variable amplitude loading and other variable loading conditions).

Strain is not currently accounted for in current ergonomic assessment tools but could be added given more research in the following area.

- Functional Strain Limit: What level of strain results in significant reduction or loss of function? Answering this question could require a combination of *in vivo* and *ex vivo* studies. Studies similar to that of (Cutts et al., 1991; Houghton et al., 2023; Kubo et al., 2014) could be conducted to determine *in vivo* strains associated with varying levels of

maximum voluntary contraction when exposed to cyclic loading, creep loading, and static loading. *In vivo* measurement could also be made with varying degrees of flexion and/or extension. Improving our understanding of the capabilities/properties of human tendon could enable the development of risk assessment tools that are able to better predict the reduction or loss of function and subsequent risk of permanent injury. This would be analogous to temporary threshold shifts in hearing. Temporary functional loss could be indicative of future injury.

References

Abrahams, M. (1967). Mechanical behaviour of tendonIn vitro: A preliminary report. *Medical & Biological Engineering*, *5*(5), 433–443. https://doi.org/10.1007/BF02479137

Abueed, M., Al Athamneh, R., Tanash, M., & Hamasha, S. (2022). The Reliability of SAC305 Individual Solder Joints during Creep–Fatigue Conditions at Room Temperature. *Crystals*, *12*(9), 1306. https://doi.org/10.3390/cryst12091306

Andarawis-Puri, N., & Flatow, E. L. (2011). Tendon fatigue in response to mechanical loading. *Journal of Musculoskeletal & Neuronal Interactions*, *11*(2), 106–114.

Bani Hani, D., Huangfu, R., Sesek, R., Schall, M. C., Davis, G. A., & Gallagher, S. (2021). Development and validation of a cumulative exposure shoulder risk assessment tool based on fatigue failure theory. *Ergonomics*, *64*(1), 39–54. https://doi.org/10.1080/00140139.2020.1811399

Barbe, M. F., Gallagher, S., Massicotte, V. S., Tytell, M., Popoff, S. N., & Barr-Gillespie, A. E. (2013). The interaction of force and repetition on musculoskeletal and neural tissue responses and sensorimotor behavior in a rat model of work-related musculoskeletal disorders. *BMC Musculoskeletal Disorders*, *14*(1), 303. https://doi.org/10.1186/1471-2474-14-303

Bass, E. (2012). Tendinopathy: Why the Difference Between Tendinitis and Tendinosis Matters. *International Journal of Therapeutic Massage & Bodywork: Research, Education, & Practice*, *5*(1), 14–17. https://doi.org/10.3822/ijtmb.v5i1.153

Bhattacharya, A. (2014). Costs of occupational musculoskeletal disorders (MSDs) in the United States. *International Journal of Industrial Ergonomics*, *44*(3), 448–454. https://doi.org/10.1016/j.ergon.2014.01.008

Bishop, J. Y., Santiago-Torres, J. E., Rimmke, N., & Flanigan, D. C. (2015). Smoking Predisposes to Rotator Cuff Pathology and Shoulder Dysfunction: A Systematic Review. *Arthroscopy: The Journal of Arthroscopic & Related Surgery*, *31*(8), 1598–1605. https://doi.org/10.1016/j.arthro.2015.01.026

Boivin, G. P., Elenes, E. Y., Schultze, A. K., Chodavarapu, H., Hunter, S. A., & Elased, K. M. (2014). Biomechanical properties and histology of db/db diabetic mouse Achilles tendon. *Muscles, Ligaments and Tendons Journal*, *4*(3), 280–284.

Brown, V. A. (2021). An Introduction to Linear Mixed-Effects Modeling in R. *Advances in Methods and Practices in Psychological Science*, *4*(1), 251524592096035. https://doi.org/10.1177/2515245920960351

Chandrashekar, N., Slauterbeck, J., & Hashemi, J. (2012). Effects of cyclic loading on the tensile properties of human patellar tendon. *The Knee*, *19*(1), 65–68. https://doi.org/10.1016/j.knee.2010.11.014

Chang, E. Y., Bae, W. C., Statum, S., Du, J., & Chung, C. B. (2014). Effects of repetitive freeze–thawing cycles on T2 and T2* of the Achilles tendon. *European Journal of Radiology*, *83*(2), 349–353. https://doi.org/10.1016/j.ejrad.2013.10.014

Cutts, A., Alexander, R. M., & Ker, R. F. (1991). Ratios of cross-sectional areas of muscles and their tendons in a healthy human forearm. *Journal of Anatomy*, *176*, 133–137.

da Costa, B. R., & Vieira, E. R. (2009). Risk factors for work-related musculoskeletal disorders: A systematic review of recent longitudinal studies. *American Journal of Industrial Medicine*, *53*(3), 285–323. https://doi.org/10.1002/ajim.20750

De Zee, M., Bojsen-Møller, F., & Voigt, M. (2000). Dynamic viscoelastic behavior of lower extremity tendons during simulated running. *Journal of Applied Physiology*, *89*(4), 1352–1359. https://doi.org/10.1152/jappl.2000.89.4.1352

Devkota, A. C., & Weinhold, P. S. (2003). Mechanical response of tendon subsequent to ramp loading to varying strain limits. *Clinical Biomechanics*, *18*(10), 969–974. https://doi.org/10.1016/S0268-0033(03)00168-2

Ensey, J. S., Hollander, M. S., Wu, J. Z., Kashon, M. L., Baker, B. B., & Cutlip, R. G. (2009). Response of tibialis anterior tendon to a chronic exposure of stretch-shortening cycles: Age effects. *BioMedical Engineering OnLine*, *8*(1), 12. https://doi.org/10.1186/1475-925X-8-12

Erhard, L., Zobitz, M. E., Zhao, C., Amadio, P. C., & An, K.-N. (2002). *Treatment of Partial Lacerations in Flexor Tendons by Trimming: A Biomechanical in Virto Study*. *84*(6), 1006–1012.

Flick, J., Devkota, A., Tsuzaki, M., Almekinders, L., & Weinhold, P. (2006). Cyclic loading alters biomechanical properties and secretion of PGE2 and NO from tendon explants. *Clinical Biomechanics*, *21*(1), 99–106. https://doi.org/10.1016/j.clinbiomech.2005.08.008

Fox, A. J. S., Bedi, A., Deng, X.-H., Ying, L., Harris, P. E., Warren, R. F., & Rodeo, S. A. (2011). Diabetes mellitus alters the mechanical properties of the native tendon in an experimental rat model: DIABETES MELLITUS ALTERS THE MECHANICAL PROPERTIES OF THE NATIVE TENDON. *Journal of Orthopaedic Research*, *29*(6), 880–885. https://doi.org/10.1002/jor.21327

Fung, D. T., Wang, V. M., Andarawis-Puri, N., Basta-Pljakic, J., Li, Y., Laudier, D. M., Sun, H. B., Jepsen, K. J., Schaffler, M. B., & Flatow, E. L. (2010). Early response to tendon

fatigue damage accumulation in a novel in vivo model. *Journal of Biomechanics*, *43*(2), 274–279. https://doi.org/10.1016/j.jbiomech.2009.08.039

Fung, D. T., Wang, V. M., Laudier, D. M., Shine, J. H., Basta-Pljakic, J., Jepsen, K. J., Schaffler, M. B., & Flatow, E. L. (2009). Subrupture tendon fatigue damage. *Journal of Orthopaedic Research*, *27*(2), 264–273. https://doi.org/10.1002/jor.20722

Gallagher, S., & Barbe, M. F. (2022). The impaired healing hypothesis: A mechanism by which psychosocial stress and personal characteristics increase MSD risk? *Ergonomics*, *65*(4), 573–586. https://doi.org/10.1080/00140139.2021.1974103

Gallagher, S., & Heberger, J. R. (2013). Examining the Interaction of Force and Repetition on Musculoskeletal Disorder Risk: A Systematic Literature Review. *Human Factors: The Journal of the Human Factors and Ergonomics Society*, *55*(1), 108–124. https://doi.org/10.1177/0018720812449648

Gallagher, S., & Huangfu, R. (2019). An example of modeling the combined effects of creep and fatigue loading in musculoskeletal tissue. *Proceedings of the Human Factors and Ergonomics Society Annual Meeting*, *63*(1), 1114–1116. https://doi.org/10.1177/1071181319631242

Gallagher, S., & Schall Jr., M. C. (2017a). Musculoskeletal disorders as a fatigue failure process: Evidence, implications and research needs. *Ergonomics*, *60*(2), 255–269. https://doi.org/10.1080/00140139.2016.1208848

Gallagher, S., & Schall Jr., M. C. (2017b). Musculoskeletal disorders as a fatigue failure process: Evidence, implications and research needs. *Ergonomics*, *60*(2), 255–269. https://doi.org/10.1080/00140139.2016.1208848

Gallagher, S., & Schall, M. (2016). The Biomechanical Relevance of Stress Range and Mean Stress in the Analysis of Variable Loading on Musculoskeletal Tissues. *Proceedings of the Human Factors and Ergonomics Society Annual Meeting*, *60*(1), 987–991. https://doi.org/10.1177/1541931213601228

Gallagher, S., Schall, M. C., Sesek, R. F., & Huangfu, R. (2018). An Upper Extremity Risk Assessment Tool Based on Material Fatigue Failure Theory: The Distal Upper Extremity Tool (DUET). *Human Factors: The Journal of the Human Factors and Ergonomics Society*, *60*(8), 1146–1162. https://doi.org/10.1177/0018720818789319

Gallagher, S., Sesek, R. F., Schall, M. C., & Huangfu, R. (2017). Development and validation of an easy-to-use risk assessment tool for cumulative low back loading: The Lifting Fatigue Failure Tool (LiFFT). *Applied Ergonomics*, *63*, 142–150. https://doi.org/10.1016/j.apergo.2017.04.016

Garg, A., Moore, J. S., & Kapellusch, J. M. (2017). The Revised Strain Index: An improved upper extremity exposure assessment model. *Ergonomics*, *60*(7), 912–922. https://doi.org/10.1080/00140139.2016.1237678

Goodman, H. J., & Choueka, J. (2005). Biomechanics of the Flexor Tendons. *Hand Clinics*, *21*(2), 129–149. https://doi.org/10.1016/j.hcl.2004.11.002

Grip-Engineering Thümler GmbH. (2024). https://grip.de/

Guo, S., & DiPietro, L. A. (2010). Factors Affecting Wound Healing. *Journal of Dental Research*, *89*(3), 219–229. https://doi.org/10.1177/0022034509359125

Hangody, G., Pánics, G., Szebényi, G., Kiss, R., Hangody, L., & Pap, K. (2016). Pitfalls during biomechanical testing—Evaluation of different fixation methods for measuring tendons

endurance properties. *Acta Physiologica Hungarica*, *103*(1), 86–93. https://doi.org/10.1556/036.103.2016.1.8

Hayes, A., Easton, K., Devanaboyina, P. T., Wu, J.-P., Kirk, T. B., & Lloyd, D. (2019). A review of methods to measure tendon dimensions. *Journal of Orthopaedic Surgery and Research*, *14*(1), 18. https://doi.org/10.1186/s13018-018-1056-y

Herod, T. W., & Veres, S. P. (2017). Development of overuse tendinopathy: A new descriptive model for the initiation of tendon damage during cyclic loading: INITIATION OF TENDON FATIGUE DAMAGE. *Journal of Orthopaedic Research*. https://doi.org/10.1002/jor.23629

Houghton, F. C., Huff, R. D., Earl, C. C., Ghajar-Rahimi, E., Dogra, I., Darling, A. J., Damen, F. W., Zhou, G., Yu, D., Goergen, C. J., Harris-Adamson, C., & O'Connell, G. D. (2023). Relating in-vivo Strain of the Flexor Digitorum Superficialis Tendon with Grip Force. *Proceedings of the Human Factors and Ergonomics Society Annual Meeting*, *67*(1), 873–876. https://doi.org/10.1177/21695067231193681

Huang, H., Zhang, J., Sun, K., Zhang, X., & Tian, S. (2011). Effects of repetitive multiple freeze–thaw cycles on the biomechanical properties of human flexor digitorum superficialis and flexor pollicis longus tendons. *Clinical Biomechanics*, *26*(4), 419–423. https://doi.org/10.1016/j.clinbiomech.2010.12.006

Jahnke, A., Gernandt, M., Hudel, H., Ahmed, G. A., Rickert, M., Fonseca Ulloa, C. A., & Stolz, D. (2019). Biomechanical testing of various suture techniques for Achilles tendon repair with and without augmentation by using synthetic polyester grafts. *Journal of Biomechanics*, *93*, 132–139. https://doi.org/10.1016/j.jbiomech.2019.06.021

James, R., Kesturu, G., Balian, G., & Chhabra, A. B. (2008). Tendon: Biology, Biomechanics, Repair, Growth Factors, and Evolving Treatment Options. *The Journal of Hand Surgery*, *33*(1), 102–112. https://doi.org/10.1016/j.jhsa.2007.09.007

Jiang, M., Lawson, Z. T., Erel, V., Pervere, S., Nan, T., Robbins, A. B., Feed, A. D., & Moreno, M. R. (2020). Clamping soft biologic tissues for uniaxial tensile testing: A brief survey of current methods and development of a novel clamping mechanism. *Journal of the Mechanical Behavior of Biomedical Materials*, *103*, 103503. https://doi.org/10.1016/j.jmbbm.2019.103503

K., R., & Saarakkal, S. (2011). Biomechanics and Modeling of Skeletal Soft Tissues. In V. Klika (Ed.), *Theoretical Biomechanics*. InTech. https://doi.org/10.5772/19975

Kannus, P. (2000). Structure of the tendon connective tissue: Tendon connective tissue structure. *Scandinavian Journal of Medicine & Science in Sports*, *10*(6), 312–320. https://doi.org/10.1034/j.1600-0838.2000.010006312.x

KarisAllen, J. J., & Veres, S. P. (2020). Effect of testing temperature on the nanostructural response of tendon to tensile mechanical overload. *Journal of Biomechanics*, *104*, 109720. https://doi.org/10.1016/j.jbiomech.2020.109720

Ker, R. (2007). Mechanics of tendon, from an engineering perspective. *International Journal of Fatigue*, *29*(6), 1001–1009. https://doi.org/10.1016/j.ijfatigue.2006.09.020

Ker, R. F. (1981a). Dynamic Tensile Properties of the Plantaris Tendon of Sheep. *Journal of Experimental Biology*, *93*(1), 283–302. https://doi.org/10.1242/jeb.93.1.283

Ker, R. F. (1981b). Dynamic tensile properties of the plantaris tendon of sheep (Ovis aries). *Journal of Experimental Biology*, *93*(1), 283–302. https://doi.org/10.1242/jeb.93.1.283

Ker, R. F. (2002). The implications of the adaptable fatigue quality of tendons for their construction, repair and function. *Comparative Biochemistry and Physiology Part A: Molecular & Integrative Physiology*, *133*(4), 987–1000. https://doi.org/10.1016/S1095-6433(02)00171-X

Ker, R. F., Wang, X. T., & Pike, A. V. (2000). Fatigue quality of mammalian tendons. *Journal of Experimental Biology*, *203*(8), 1317–1327. https://doi.org/10.1242/jeb.203.8.1317

Kirkendall, D. T., & Garrett, W. E. (2007). Function and biomechanics of tendons. *Scandinavian Journal of Medicine & Science in Sports*, *7*(2), 62–66. https://doi.org/10.1111/j.1600-0838.1997.tb00120.x

Kiss, M.-O., Hagemeister, N., Levasseur, A., Fernandes, J., Lussier, B., & Petit, Y. (2009). A low-cost thermoelectrically cooled tissue clamp for in vitro cyclic loading and load-to-failure testing of muscles and tendons. *Medical Engineering & Physics*, *31*(9), 1182–1186. https://doi.org/10.1016/j.medengphy.2009.06.008

Komi, P. V., Fukashiro, S., & Järvinen, M. (1992). Biomechanical Loading of Achilles Tendon During Normal Locomotion. *Clinics in Sports Medicine*, *11*(3), 521–531. https://doi.org/10.1016/S0278-5919(20)30506-8

Kondratko-Mittnacht, J., Duenwald-Kuehl, S., Lakes, R., & Vanderby, R. (2015). Shear load transfer in high and low stress tendons. *Journal of the Mechanical Behavior of Biomedical Materials*, *45*, 109–120. https://doi.org/10.1016/j.jmbbm.2015.01.021

Kruse, A., Stafilidis, S., & Tilp, M. (2017). Ultrasound and magnetic resonance imaging are not interchangeable to assess the Achilles tendon cross-sectional-area. *European Journal of Applied Physiology*, *117*(1), 73–82. https://doi.org/10.1007/s00421-016-3500-1

Kubo, K., Teshima, T., Ikebukuro, T., Hirose, N., & Tsunoda, N. (2014). Tendon properties and muscle architecture for knee extensors and plantar flexors in boys and men. *Clinical Biomechanics*, *29*(5), 506–511. https://doi.org/10.1016/j.clinbiomech.2014.04.001

Lee, A. H., & Elliott, D. M. (2017). Freezing does not alter multiscale tendon mechanics and damage mechanisms in tension: Effects of freezing on multiscale tendon mechanics. *Annals of the New York Academy of Sciences*, *1409*(1), 85–94. https://doi.org/10.1111/nyas.13460

Millar, N. L., Silbernagel, K. G., Thorborg, K., Kirwan, P. D., Galatz, L. M., Abrams, G. D., Murrell, G. A. C., McInnes, I. B., & Rodeo, S. A. (2021). Tendinopathy. *Nature Reviews Disease Primers*, *7*(1), 1. https://doi.org/10.1038/s41572-020-00234-1

Miller, S. A., & Freivalds, A. (1995). A stress-strength interference model for predicting CTD probabilities. *International Journal of Industrial Ergonomics*, *15*(6), 447–457. https://doi.org/10.1016/0169-8141(94)00063-9

National Research Council and Institute of Medicine. (2001). *Musculoskeletal Disorders and the Workplace: Low Back and Upper Extremities* (p. 10032). National Academies Press. https://doi.org/10.17226/10032

Neviaser, A., Andarawis-Puri, N., & Flatow, E. (2012). Basic mechanisms of tendon fatigue damage. *Journal of Shoulder and Elbow Surgery*, *21*(2), 158–163. https://doi.org/10.1016/j.jse.2011.11.014

Nichols, A. E. C., Oh, I., & Loiselle, A. E. (2020). Effects of Type II Diabetes Mellitus on Tendon Homeostasis and Healing. *Journal of Orthopaedic Research*, *38*(1), 13–22. https://doi.org/10.1002/jor.24388

NIOSH. (1997). *Musculoskeletal Disorders and Workplace Factors: A Critical Review of Epidemiologic Evidence for Work-Related Musculoskeletal Disorders of the Neck, Upper Extremity, and Low Back* (DHHS (NIOSH) Publication No. 97B141). U.S. Department of Health and Human Services Public Health Service Centers for Disease Control and Prevention National Institute for Occupational Safety and Health. https://www.cdc.gov/niosh/docs/97-141/default.html

Parent, G., Huppé, N., & Langelier, E. (2011). Low Stress Tendon Fatigue is a Relatively Rapid Process in the Context of Overuse Injuries. *Annals of Biomedical Engineering*, *39*(5), 1535–1545. https://doi.org/10.1007/s10439-011-0254-0

Peterson, B. E., & Szczesny, S. E. (2020). Dependence of tendon multiscale mechanics on sample gauge length is consistent with discontinuous collagen fibrils. *Acta Biomaterialia*, *117*, 302–309. https://doi.org/10.1016/j.actbio.2020.09.046

Pike, A. V., Ker, R. F., & Alexander, R. M. (2000). The development of fatigue quality in high- and low-stressed tendons of sheep (Ovis aries). *The Journal of Experimental Biology*, *203*(Pt 14), 2187–2193.

Quirk, N. P., Lopez De Padilla, C., De La Vega, R. E., Coenen, M. J., Tovar, A., Evans, C. H., & Müller, S. A. (2018). Effects of freeze-thaw on the biomechanical and structural properties of the rat Achilles tendon. *Journal of Biomechanics*, *81*, 52–57. https://doi.org/10.1016/j.jbiomech.2018.09.012

Santiago-Torres, J., Flanigan, D. C., Butler, R. B., & Bishop, J. Y. (2015). The Effect of Smoking on Rotator Cuff and Glenoid Labrum Surgery: A Systematic Review. *The American Journal of Sports Medicine*, *43*(3), 745–751. https://doi.org/10.1177/0363546514533776

Schatzmann, L. (1998). Effect of cyclic preconditioning on the tensile properties of human quadriceps tendons and patellar ligaments. *Knee Surgery, Sports Traumatology, Arthroscopy*, *6*(0), S56–S61. https://doi.org/10.1007/s001670050224

Schechtman, H. (1995). *Mechanical Characterisation of Fatigue Failure in Human Tendons*. University of London.

Schechtman, H., & Bader, D. L. (1994). Dynamic Characterization of Human Tendons. *Proceedings of the Institution of Mechanical Engineers, Part H: Journal of Engineering in Medicine*, *208*(4), 241–248. https://doi.org/10.1243/PIME_PROC_1994_208_294_02

Schechtman, H., & Bader, D. L. (1997). In vitro fatigue of human tendons. *Journal of Biomechanics*, *30*(8), 829–835. https://doi.org/10.1016/S0021-9290(97)00033-X

Schechtman, H., & Bader, D. L. (2002). Fatigue damage of human tendons. *Journal of Biomechanics*, *35*(3), 347–353. https://doi.org/10.1016/S0021-9290(01)00177-4

Schindelin, J., Arganda-Carreras, I., Frise, E., Kaynig, V., Longair, M., Pietzsch, T., Preibisch, S., Rueden, C., Saalfeld, S., Schmid, B., Tinevez, J.-Y., White, D. J., Hartenstein, V., Eliceiri, K., Tomancak, P., & Cardona, A. (2012). Fiji: An open-source platform for biological-image analysis. *Nature Methods*, *9*(7), 676–682. https://doi.org/10.1038/nmeth.2019

Schneider, C. A., Rasband, W. S., & Eliceiri, K. W. (2012). NIH Image to ImageJ: 25 years of image analysis. *Nature Methods*, *9*(7), 671–675. https://doi.org/10.1038/nmeth.2089

Schober, P., & Vetter, T. R. (2018). Repeated Measures Designs and Analysis of Longitudinal Data: If at First You Do Not Succeed—Try, Try Again. *Anesthesia & Analgesia*, *127*(2), 569–575. https://doi.org/10.1213/ANE.0000000000003511

Scholze, M., Safavi, S., Li, K. C., Ondruschka, B., Werner, M., Zwirner, J., & Hammer, N. (2020). Standardized tensile testing of soft tissue using a 3D printed clamping system. *HardwareX*, *8*, e00159. https://doi.org/10.1016/j.ohx.2020.e00159

Scholze, M., Singh, A., Lozano, P. F., Ondruschka, B., Ramezani, M., Werner, M., & Hammer, N. (2018). Utilization of 3D printing technology to facilitate and standardize soft tissue testing. *Scientific Reports*, *8*(1), 11340. https://doi.org/10.1038/s41598-018-29583-4

Screen, H. R. C., Shelton, J. C., Chhaya, V. H., Kayser, M. V., Bader, D. L., & Lee, D. A. (2005). The Influence of Noncollagenous Matrix Components on the Micromechanical Environment of Tendon Fascicles. *Annals of Biomedical Engineering*, *33*(8), 1090–1099. https://doi.org/10.1007/s10439-005-5777-9

Shepherd, J. H., Legerlotz, K., Demirci, T., Klemt, C., Riley, G. P., & Screen, H. R. (2014). Functionally distinct tendon fascicles exhibit different creep and stress relaxation behaviour. *Proceedings of the Institution of Mechanical Engineers, Part H: Journal of Engineering in Medicine*, *228*(1), 49–59. https://doi.org/10.1177/0954411913509977

Shepherd, J. H., Riley, G. P., & Screen, H. R. C. (2014). Early stage fatigue damage occurs in bovine tendon fascicles in the absence of changes in mechanics at either the gross or micro-structural level. *Journal of the Mechanical Behavior of Biomedical Materials*, *38*, 163–172. https://doi.org/10.1016/j.jmbbm.2014.06.005

Shepherd, J. H., & Screen, H. R. C. (2013). Fatigue loading of tendon. *International Journal of Experimental Pathology*, *94*(4), 260–270. https://doi.org/10.1111/iep.12037

Silverstein, P. (1992). Smoking and wound healing. *The American Journal of Medicine*, *93*(1), S22–S24. https://doi.org/10.1016/0002-9343(92)90623-J

Smith, N. (2019). *In Vitro Tensile Fatigue of Human Flexor Digitorum Profundus and Superficialis Tendons*. Auburn University.

Sun, H. B., Andarawis-Puri, N., Li, Y., Fung, D. T., Lee, J. Y., Wang, V. M., Basta-Pljakic, J., Leong, D. J., Sereysky, J. B., Ros, S. J., Klug, R. A., Braman, J., Schaffler, M. B., Jepsen, K. J., & Flatow, E. L. (2010). Cycle-dependent matrix remodeling gene expression response in fatigue-loaded rat patellar tendons. *Journal of Orthopaedic Research*, *28*(10), 1380–1386. https://doi.org/10.1002/jor.21132

Szczesny, S. E., Aeppli, C., David, A., & Mauck, R. L. (2018). Fatigue loading of tendon results in collagen kinking and denaturation but does not change local tissue mechanics. *Journal of Biomechanics*, *71*, 251–256. https://doi.org/10.1016/j.jbiomech.2018.02.014

Thornton, G. M., & Bailey, S. J. (2012). Repetitive loading damages healing ligaments more than sustained loading demonstrated by reduction in modulus and residual strength. *Journal of Biomechanics*, *45*(15), 2589–2594. https://doi.org/10.1016/j.jbiomech.2012.08.013

Thornton, G. M., & Hart, D. A. (2011). The interface of mechanical loading and biological variables as they pertain to the development of tendinosis. *Journal of Musculoskeletal & Neuronal Interactions*, *11*(2), 94–105.

Thornton, G. M., Schwab, T. D., & Oxland, T. R. (2007). Cyclic loading causes faster rupture and strain rate than static loading in medial collateral ligament at high stress. *Clinical Biomechanics*, *22*(8), 932–940. https://doi.org/10.1016/j.clinbiomech.2007.05.004

Vergari, C., Pourcelot, P., Holden, L., Ravary-Plumioën, B., Laugier, P., Mitton, D., & Crevier-Denoix, N. (2010). A Linear Laser Scanner to Measure Cross-Sectional Shape and Area

of Biological Specimens During Mechanical Testing. *Journal of Biomechanical Engineering*, *132*(10), 105001. https://doi.org/10.1115/1.4002374

Wang, X. T., & Ker, R. F. (1995). Creep rupture of wallaby tail tendons. *Journal of Experimental Biology*, *198*(3), 831–845. https://doi.org/10.1242/jeb.198.3.831

Wang, X. T., Ker, R. F., & Alexander, R. M. (1995). Fatigue rupture of wallaby tail tendons. *The Journal of Experimental Biology*, *198*(Pt 3), 847–852.

Wang, X. T., Ruister, M. R., Alexander, R., & Ker, R. F. (1991). The effect of temperature on the tensile stiffness of mammalian tail tendons. *Journal of Zoology*, *223*(3), 491–497. https://doi.org/10.1111/j.1469-7998.1991.tb04779.x

Weisstein, E. W. (2024, May 30). *Simpson's Rule*. "Simpson's Rule." From MathWorld--A Wolfram Web Resource. https://mathworld.wolfram.com/SimpsonsRule.html

Wren, T. A. L., Lindsey, D. P., Beaupré, G. S., & Carter, D. R. (2003). Effects of Creep and Cyclic Loading on the Mechanical Properties and Failure of Human Achilles Tendons. *Annals of Biomedical Engineering*, *31*(6), 710–717. https://doi.org/10.1114/1.1569267

Wren, T. A. L., Yerby, S. A., Beaupré, G. S., & Carter, D. R. (2001). Mechanical properties of the human achilles tendon. *Clinical Biomechanics*, *16*(3), 245–251. https://doi.org/10.1016/S0268-0033(00)00089-9

Wright, J. K., Carroll, L. J., Sham, T.-L., Lybeck, N. J., & Wright, R. N. (2016). Determination of the Creep-Fatigue Interaction Diagram for Alloy 617. *Volume 5: High-Pressure Technology; Rudy Scavuzzo Student Paper Symposium and 24th Annual Student Paper Competition; ASME Nondestructive Evaluation, Diagnosis and Prognosis Division (NDPD); Electric Power Research Institute (EPRI) Creep Fatigue Workshop*, V005T12A004. https://doi.org/10.1115/PVP2016-63704

Yung, M., Dale, A. M., Kapellusch, J., Bao, S., Harris-Adamson, C., Meyers, A. R., Hegmann, K. T., Rempel, D., & Evanoff, B. A. (2019). Modeling the Effect of the 2018 Revised ACGIH ® Hand Activity Threshold Limit Value ® (TLV) at Reducing Risk for Carpal Tunnel Syndrome. *Journal of Occupational and Environmental Hygiene*, *16*(9), 628–633. https://doi.org/10.1080/15459624.2019.1640366

Zitnay, J. L., Jung, G. S., Lin, A. H., Qin, Z., Li, Y., Yu, S. M., Buehler, M. J., & Weiss, J. A. (2020). Accumulation of collagen molecular unfolding is the mechanism of cyclic fatigue damage and failure in collagenous tissues. *Science Advances*, *6*(35), eaba2795. https://doi.org/10.1126/sciadv.aba2795

Appendix A

Table 23: Donor Demographics

Donor	Age	Sex	Race	Height (m)	Weight (kg)	BMI	Primary COD	Secondary COD
1	67	F	White	1.65	41.28	15	Cerebral Infarction	
2	75	F	White	1.65	81.65	30	Acute Coronary Syndrome, Respiratory Failure	
3†	48	F	Mexican, Mexican-America	1.55	88.90	37	Acute Hypoxemic Respiratory Failure, Hepatorenal Syndrome	Decompensated Liver Cirrhosis
4	66	M	White	1.78	63.96	20	Acute Renal Failure; ESRD; IgA Nephropathy	

Note. † Donor with known history of smoking.

Table 24: Average Cross-Sectional Area Measurements

Donor	Type	Digit	Tendon	Average CSA (mm^2)	CSA Measurement Method
1	LFDS	3	20	14.84	CT
1	LFDS	3	20	6.84	Volumetric
1	LFDS	3	20	8.68	Ker
1	RFPD	5	30	9.90	CT
1	RFPD	5	30	9.41	Volumetric
1	RFPD	5	30	7.09	Ker
1	RFDS	2	32	8.40	CT
1	RFDS	2	32	9.57	Volumetric
1	RFDS	2	32	7.43	Ker
1	RFPD	4	38	12.95	CT
1	RFPD	4	38	8.54	Volumetric
1	RFPD	4	38	8.82	Ker
1	LFDS	5	41	5.18	CT
1	LFDS	5	41	1.00	Volumetric
1	LFDS	5	41	1.16	Ker
1	RFDS	4	44	11.12	CT
1	RFDS	4	44	7.52	Volumetric
1	RFDS	4	44	7.97	Ker
1	RFDS	3	49	17.08	CT
1	RFDS	3	49	10.19	Volumetric
1	RFDS	3	49	12.93	Ker
1	LFPD	5	50	8.21	CT
1	LFPD	5	50	8.75	Volumetric
1	LFPD	5	50	5.76	Ker
1	RFPD	3	51	19.06	CT
1	RFPD	3	51	17.05	Volumetric
1	RFPD	3	51	12.83	Ker
1	LFPD	4	56	13.74	CT
1	LFPD	4	56	10.75	Volumetric
1	LFPD	4	56	9.24	Ker
1	LFDS	4	62	10.95	CT
1	LFDS	4	62	8.54	Volumetric
1	LFDS	4	62	8.44	Ker
1	LFPD	2	63	15.40	CT
1	LFPD	2	63	12.31	Volumetric
1	LFPD	2	63	10.44	Ker
2	LFPD	4	25	10.20	CT

Donor	Type	Digit	Tendon	Average CSA (mm^2)	CSA Measurement Method
2	LFPD	4	25	14.33	Volumetric
2	LFPD	4	25	8.11	Ker
2	LFDS	4	27	9.50	CT
2	LFDS	4	27	8.82	Volumetric
2	LFDS	4	27	7.08	Ker
2	LFPD	5	35	9.35	CT
2	LFPD	5	35	7.33	Volumetric
2	LFPD	5	35	7.10	Ker
2	RFDS	3	46	11.55	CT
2	RFDS	3	46	7.37	Volumetric
2	RFDS	3	46	5.60	Ker
2	RFPD	5	47	7.91	CT
2	RFPD	5	47	8.53	Volumetric
2	RFPD	5	47	7.13	Ker
2	LFPD	2	53	17.13	CT
2	LFPD	2	53	11.16	Volumetric
2	LFPD	2	53	13.43	Ker
2	RFDS	2	60	7.80	CT
2	RFDS	2	60	0.97	Volumetric
2	RFDS	2	60	7.42	Ker
2	LFDS	3	61	12.68	CT
2	LFDS	3	61	8.65	Volumetric
2	LFDS	3	61	8.89	Ker
3	LFPD	3	17	16.57	CT
3	LFPD	3	17	9.79	Volumetric
3	LFPD	3	17	13.29	Ker
3	LFPD	2	21	15.80	CT
3	LFPD	2	21	7.37	Volumetric
3	LFPD	2	21	8.08	Ker
3	LFPD	5	23	8.26	CT
3	LFPD	5	23	8.72	Volumetric
3	LFPD	5	23	4.62	Ker
3	RFPD	4	24	14.73	CT
3	RFPD	4	24	10.69	Volumetric
3	RFPD	4	24	11.34	Ker
3	LFDS	5	26	4.10	CT
3	LFDS	5	26	1.99	Volumetric
3	LFDS	5	26	3.00	Ker
3	LFDS	4	37	9.95	CT

Donor	Type	Digit	Tendon	Average CSA (mm^2)	CSA Measurement Method
3	LFDS	4	37	9.74	Volumetric
3	LFDS	4	37	7.78	Ker
3	RFDS	4	39	9.55	CT
3	RFDS	4	39	8.88	Volumetric
3	RFDS	4	39	7.50	Ker
3	RFDS	5	40	2.68	CT
3	RFDS	5	40	1.99	Volumetric
3	RFDS	5	40	5.57	Ker
3	RFPD	3	42	13.44	CT
3	RFPD	3	42	17.02	Volumetric
3	RFPD	3	42	10.38	Ker
3	LFDS	2	43	8.51	CT
3	LFDS	2	43	8.91	Volumetric
3	LFDS	2	43	7.68	Ker
3	RFPD	5	58	7.91	CT
3	RFPD	5	58	2.96	Volumetric
3	RFPD	5	58	6.06	Ker
3	RFDS	2	59	14.15	CT
3	RFDS	2	59	11.78	Volumetric
3	RFDS	2	59	6.52	Ker
4	RFPD	4	18	15.55	CT
4	RFPD	4	18	14.78	Volumetric
4	RFPD	4	18	11.69	Ker
4	RFPD	3	19	21.58	CT
4	RFPD	3	19	22.93	Volumetric
4	RFPD	3	19	15.64	Ker
4	LFPD	2	28	15.80	CT
4	LFPD	2	28	11.64	Volumetric
4	LFPD	2	28	16.21	Ker
4	LFDS	2	29	12.70	CT
4	LFDS	2	29	10.28	Volumetric
4	LFDS	2	29	10.44	Ker
4	RFPD	2	31	18.57	CT
4	RFPD	2	31	16.23	Volumetric
4	RFPD	2	31	13.98	Ker
4	LFPD	3	34	22.37	CT
4	LFPD	3	34	19.84	Volumetric
4	LFPD	3	34	16.73	Ker
4	LFPD	5	36	10.84	CT

Donor	Type	Digit	Tendon	Average CSA (mm^2)	CSA Measurement Method
4	LFPD	5	36	9.43	Volumetric
4	LFPD	5	36	7.48	Ker
4	RFDS	2	52	8.50	CT
4	RFDS	2	52	10.79	Volumetric
4	RFDS	2	52	12.32	Ker
4	LFDS	5	54	5.06	CT
4	LFDS	5	54	0.95	Volumetric
4	LFDS	5	54	3.46	Ker
4	RFDS	4	55	14.31	CT
4	RFDS	4	55	9.10	Volumetric
4	RFDS	4	55	11.42	Ker
4	LFDS	3	57	14.01	CT
4	LFDS	3	57	19.87	Volumetric
4	LFDS	3	57	18.47	Ker
4	RFDS	5	64	2.68	CT
4	RFDS	5	64	2.78	Volumetric
4	RFDS	5	64	3.83	Ker

Table 25: Fatigue Test Results

Donor	Type	Digit	Rand	Study #	% of UTS	Mass (g)	Length (cm)	Max Load (N)	Max Stress (MPa)	Time to Failure (hrs.)	Completed Cycles to Failure	Average Work per Cycle (J)	Failure Strain
1	LFDS	3	0.39	20	20	1.42	14.61	183.13	13.64	14.02	27619	0.011	0.19
2	LFDS	3	0.94	61	20	1.04	10.4	248.91	22.66	6.55	11301	0.004	0.14
1	RFPD	5	0.49	30	40	0.84	10.63	242.33	28.23	0.31	401	0.072	0.14
3	RFDS	5	0.65	40	40	0.63	10.04	100.90	47.23	0.24	184	0.014	0.14
2	LFPD	2	0.87	53	40	1.62	10.75	238.99	15.86	0.42	868	0.052	0.10
4	RFDS	4	0.88	55	40	1.41	10.99	251.28	19.49	6.55	11301	0.021	0.22
3	LFPD	3	0.34	17	60	1.52	10.22	214.91	22.99	0.22	353	0.065	0.12
2	LFPD	4	0.43	25	60	0.95	10.47	203.75	24.84	0.09	162	0.061	0.22
4	LFPD	3	0.60	34	60	1.89	10.08	348.18	17.49	5.58	12012	0.056	0.22
1	RFPD	4	0.64	38	60	1.04	10.54	292.55	28.19	0.22	424	0.086	0.15
4	RFPD	2	0.57	31	80	1.74	11.09	357.21	20.67	0.51	1096	0.080	0.16
1	RFDS	2	0.57	32	80	0.87	10.45	213.28	27.68	0.44	780	0.036	0.14
3	LFDS	2	0.73	43	80	0.87	10.11	295.92	39.58	0.07	104	0.105	0.20
2	RFPD	5	0.77	47	80	0.84	10.56	264.08	34.79	0.004	7	0.478	0.20

Appendix B

Table 26: Creep Test Results

Donor	Type	Digit	Rand	Study #	% of UTS	Mass (g)	Length (cm)	Min CSA (mm^2)	Max Load (N)	Max Stress (MPa)	Time of Test (hrs.)	Strain
4	RFPD	4	0.28	18	20	1.42	10.83	11.14	50.32	4.52	16	0.009
3	LFPD	5	0.86	23	20	0.53	10.32	7.17	40.63	5.67	16	0.007
1	RFPD	3	0.73	51	20	1.52	10.56	10.19	74.01	7.27	16	0.011
4	LFDS	5	0.59	54	40	0.41	10.53	4.08	37.46	9.18	16	0.008
1	LFPD	2	0.95	63	40	1.24	10.56	11.52	160.33	13.92	16	0.019
3	LFPD	2	0.16	21	60	1.48	16.29	9.46	146.86	15.52	16	0.013
2	LFPD	5	0.70	35	60	0.87	10.91	8.47	169.71	20.04	16	0.015
1	LFDS	5	0.19	41	60	0.13	10.02	2.59	60.29	23.24	16	0.016
4	RFPD	3	0.38	19	80	1.91	10.91	14.92	253.38	16.99	16	0.04
3	RFPD	3	0.04	42	80	1.23	10.58	7.82	158.81	20.31	16	0.11

Note. The table contains data for tendons that did not fail during the 16-hr. test.

Table 27: Creep Test Results

Donor	Type	Digit	Rand	Study #	% of UTS	Mass (g)	Length (cm)	Min CSA (mm^2)	Max Load (N)	Max Stress (MPa)	Time to Failure (hrs.)	Failure Strain
1	RFDS	4	0.37	44	80	0.95	10.64	9.84	279.80	28.43	1.05	0.21
2	RFDS	3	0.38	46	80	1.02	16.29	9.73	249.60	25.66	10.70	0.40

Note. Table contains data for tendons that failed during the 16-hr. test.

Appendix C

Table 28: Donor Demographics

Donor	Age	Height (in)	Weight (lbs)	Sex	Race	Height (m)	Weight (kg)	BMI	Primary COD	Secondary COD
1	61	62	83	F	Korean	1.57	37.65	15	Metastatic Malignant Neoplasm of the Lung	
2	70	62	147	F	White	1.57	66.68	27	Cardiac Arrest; Chronic Obstructive Pulmonary Disease (COPD)	Cor pulmonale
3†	50	67	191	F	White	1.70	86.64	30	Malignant Neoplasm of Ovary, Hyperlipidemia, Hypertension	
4†*	41	62	210	F	Hispanic or Latino	1.57	95.25	38	Pending	
5	77	72	226	M	Mexican, Mexican-American	1.83	102.51	31	Cardiac Arrest; Respiratory Failure; Pneumonia	Metastatic Lung Cancer
6†*	30	68	180	M	Mexican, Mexican-American	1.73	81.65	27	Deferred	
7†	45	68	125	M	White	1.73	56.70	19	Pancreatic Cancer	
8	56	62	198	F	White	1.57	89.81	36	Cardiac Arrest, Myocardial Infarction, Coronary Artery Disease	Diabetes Mellitus
9†	70	66	150	M	White	1.68	68.04	24	Hypertensive Arteriosclerosis, Congestive heart failure, COPD	Type II Diabetes Mellitus
10†	50	66	115	F	White	1.68	52.16	19	Metastatic Lung Cancer	Bilateral cerebellar resection of tumor

Note. † Donor with known history of smoking, * Cause of death not provided.

Table 29: R Code J CSA Measurement Code

ImageJ CSA Measurement Code

```
run("Set Measurements...", "area mean centroid center perimeter bounding shape feret's redirect=None decimal=4");
waitForUser("choose location of program ROIs");
Program_ROIs = getDirectory("choose file location of ROIs");
class_loc = getDirectory("choose location of classifier");
img_loc = getDirectory("choose file location of images");
save_loc =  getDirectory("choose file location to save spare images to");

dir=getDirectory("choose a folder to save data to");
newDir= dir + "/analyzed data/";
File.makeDirectory(newDir);

Dialog.create("Number of images");
Dialog.addMessage ("input the number of images you have");
Dialog.addNumber("Image count", 200);
Dialog.addNumber("Image start", 1);
Dialog.show();
img_count=Dialog.getNumber();
img_start=Dialog.getNumber();

////////////////////////////////////////////////////////////////////////////

for (iter=img_start;iter<=img_count;iter++){
newImage("roi", "8-bit black", 3, 3, 1);
run("Set Scale...", "distance=2.3273 known=1 unit=mm"); // this scale should be right

run("Trainable Weka Segmentation");
wait(1000);
TWS=getTitle();
selectWindow(""+TWS+"");
call("trainableSegmentation.Weka_Segmentation.loadClassifier", class_loc + "tray_outline.model");
call("trainableSegmentation.Weka_Segmentation.applyClassifier", img_loc, iter+".dcm", "showResults=true",
"storeResults=false", "probabilityMaps=false", "");
//
wait(10000);
selectWindow("Classification result");
run("8-bit");
run("Threshold...");
setMinAndMax(-461, 129);
run("Convert to Mask");

  if (isOpen("ROI Manager")) {
     selectWindow("ROI Manager");
     run("Close");
  }

run("Analyze Particles...", "size=1000-Infinity pixel circularity=0-1.00 show=Outlines display summarize add");
selectWindow(iter+".dcm"); // name
setMinAndMax(-461, 129);
roiManager("Select", 0);
run("Copy");

width = getWidth();
```

```
height = getHeight();
newImage("roi", "8-bit black", width, height, 1);
run("Paste");

  if (isOpen("ROI Manager")) {
     selectWindow("ROI Manager");
     run("Close");
  }
selectWindow("Classification result");
run("Close");

roiManager("Open", Program_ROIs + "divet_rois_test.zip");
  if (isOpen("Results")) {
     selectWindow("Results");
     run("Close");
  }
roiManager("Select", 30);

for (i=-10;i<0;i++){
   roiManager("Measure");
   roiManager("translate", 0, -1);
}
roiManager("translate", 0, 10);
for (i=0;i<10;i++){
   roiManager("Measure");
   roiManager("translate", 0, 1);
}

run("Summarize");
Mean = getResult("Mean");

for (i=0;i<20;i++){
   g=getResult("Mean",i);
   if (g==Mean) {
     maxMean=i+1;
   }
}

if (maxMean>10) {
   translate_fact_Y=maxMean-11;
}
if (maxMean<=10) {
   translate_fact_Y=(maxMean)-(2*maxMean)+1;
}
print(translate_fact_Y);
////////////////////////////////////////////////////////////////////////////////

roiManager("Select", 31);
  if (isOpen("Results")) {
     selectWindow("Results");
     run("Close");
  }

for (i=-10;i<0;i++){
   roiManager("Measure");
   roiManager("translate", -1, 0);
```

```
}
roiManager("translate", 10, 0);
for (i=0;i<10;i++){
   roiManager("Measure");
   roiManager("translate", 1, 0);
}

run("Summarize");
MeanX = getResult("Mean");

for (i=0;i<20;i++){
   g=getResult("Mean",i);
   if (g==MeanX) {
     maxMeanX=i+1;
   }
}

if (maxMeanX>10) {
   translate_fact_X=maxMeanX-11;
}
if (maxMeanX<=10) {
   translate_fact_X=(maxMeanX)-(2*maxMeanX)+1;
}
print("max mean intensity index");
print(maxMean);
print("max mean intensity index X");
print(maxMeanX);
print("translate factor X");
print(translate_fact_X);
print("translate factor Y");
print(translate_fact_Y);

  if (isOpen("ROI Manager")) {
     selectWindow("ROI Manager");
     run("Close");
  }

  if (isOpen("Results")) {
     selectWindow("Results");
     run("Close");
  }

////////////////////////////////////////////////////////////////////////////

roiManager("Open", Program_ROIs + "divet_rois_test.zip");

ROIArr = newArray("0");
for (i=1;i<roiManager("count");i++){
      ROIArr = Array.concat(ROIArr,i);
      }
roiManager("select", ROIArr);
roiManager("translate", translate_fact_X, translate_fact_Y);
rename("roi with overlay");
////////////////////////////////////////////////////////////////////////////
newImage("tray eliminated", "8-bit black", width, height, 1);
```

```
roiManager("Deselect");

for (i=0;i<2;i++){
   roiManager("Select", 30);
   roiManager("Delete");
}

selectWindow("roi with overlay");
roiManager("Combine");
run("Copy");
selectWindow("tray eliminated");
run("Paste");
saveAs("Tiff", save_loc + "roi with overlay");

  if (isOpen("ROI Manager")) {
     selectWindow("ROI Manager");
     run("Close");
  }
////////////////////////////////////////////////////////////////////////////
selectWindow(""+TWS+"");
wait(1000);
call("trainableSegmentation.Weka_Segmentation.loadClassifier", class_loc + "tendon classifier.model");
call("trainableSegmentation.Weka_Segmentation.applyClassifier", save_loc, "roi with overlay.tif",
"showResults=true", "storeResults=false", "probabilityMaps=false", "");
wait(10000);
selectWindow("Classification result");
run("8-bit");
run("Threshold...");
setThreshold(100, 255);//setThreshold(1, 255);
run("Convert to Mask");
run("Invert");
run("Analyze Particles...", "size=3-Infinity pixel circularity=0-1.00 show=Outlines display summarize add");

ROIArr = newArray("0");;
for (i=1;i<roiManager("count");i++){
      ROIArr = Array.concat(ROIArr,i);
}
roiManager("select", ROIArr);

ntendons=roiManager("count");
if (ntendons > 0) {
      selectWindow("ROI Manager");
      for (i=0 ; i<ntendons; i++) {
         roiManager("select", i);
         run("Enlarge...", "enlarge=1");
         roiManager("Add")
      }
}
roiManager("Delete");

newImage("tendons classified", "8-bit black", width, height, 1);

selectWindow("roi with overlay.tif");
roiManager("Combine");
run("Copy");
selectWindow("tendons classified");
```

```
run("Paste");

selectWindow("Results");
run("Close");

selectWindow("tendons classified");
run("Duplicate...", "tendons classified original");
selectWindow("tendons classified");
run("Threshold...");
setThreshold(1, 255);
run("Convert to Mask");

  if (isOpen("ROI Manager")) {
     selectWindow("ROI Manager");
     run("Close");
  }
roiManager("Open", Program_ROIs + "tray_array_rois.zip");

for (i=0;i<3;i++){
   roiManager("Select", i);
   run("Copy");
   width = getWidth();
   height = getHeight();
   newImage("tendon row "+i, "8-bit black", width, height, 1);
   run("Paste");
   run("Rotate 90 Degrees Right");
   selectWindow("tendons classified");
}
selectWindow("ROI Manager");
run("Close");
  if (isOpen("Results")) {
     selectWindow("Results");
     run("Close");
  }

for (i=0;i<3;i++){
   selectWindow("tendon row "+i);
   makeRectangle(0, 0, 512, 512);
   run("Set Scale...", "distance=2.3273 known=1 unit=mm");
   run("Analyze Particles...", "size=2-Infinity pixel circularity=0-1.00 show=Outlines display summarize add");
}
////////////////////////////////////////////////////////////////////////////
dataDir= newDir + "/"+iter+"/";
File.makeDirectory(dataDir);

roiManager("Save", dataDir + "ROI_"+iter+".zip");
saveAs("Results", dataDir + "Results_"+iter+".xls");

for (i=0;i<3;i++){
   selectWindow("tendon row "+i);
   saveAs("Tiff", dataDir + "Tendon_Mask_Row_"+i+"_img_"+iter);

}
selectWindow("tendons classified-1");
saveAs("Tiff", dataDir + "Tendons_Classified"+iter);
////////////////////////////////////////////////////////////////////////////
```

```
print("Image "+iter+" is done analyzing... analyzing next image");

run("Close All");
selectWindow("Results");
run("Close");
selectWindow("ROI Manager");
run("Close");
}
```

Note. This code was only for the stack of 3 trays.

Table 30: R Code CSA Measurement

```
ImageJ CSA Measurement Code
run("Set Measurements...", "area mean centroid center perimeter bounding shape feret's redirect=None decimal=4");
waitForUser("choose location of program ROIs");
Program_ROIs = getDirectory("choose file location of ROIs");
class_loc = getDirectory("choose location of classifier");
img_loc = getDirectory("choose file location of images");
save_loc =  getDirectory("choose file location to save spare images to");

dir=getDirectory("choose a folder to save data to");
newDir= dir + "/analyzed data/";
File.makeDirectory(newDir);

Dialog.create("Number of images");
Dialog.addMessage ("input the number of images you have");
Dialog.addNumber("Image count", 200);
Dialog.addNumber("Image start", 1);
Dialog.show();
img_count=Dialog.getNumber();
img_start=Dialog.getNumber();

////////////////////////////////////////////////////////////////////////////

for (iter=img_start;iter<=img_count;iter++){
newImage("roi", "8-bit black", 3, 3, 1);
run("Set Scale...", "distance=2.3273 known=1 unit=mm"); // this scale should be right

run("Trainable Weka Segmentation");
wait(1000);
TWS=getTitle();
selectWindow(""+TWS+"");
call("trainableSegmentation.Weka_Segmentation.loadClassifier", class_loc + "tray_outline.model");
call("trainableSegmentation.Weka_Segmentation.applyClassifier", img_loc, iter+".dcm", "showResults=true",
"storeResults=false", "probabilityMaps=false", "");
//
wait(10000);
selectWindow("Classification result");
run("8-bit");
run("Threshold...");
setMinAndMax(-461, 129);
run("Convert to Mask");

  if (isOpen("ROI Manager")) {
```

```
    selectWindow("ROI Manager");
    run("Close");
  }

run("Analyze Particles...", "size=1000-Infinity pixel circularity=0-1.00 show=Outlines display summarize add");
selectWindow(iter+".dcm"); // name
setMinAndMax(-461, 129);
roiManager("Select", 0);
run("Copy");

width = getWidth();
height = getHeight();
newImage("roi", "8-bit black", width, height, 1);
run("Paste");

  if (isOpen("ROI Manager")) {
    selectWindow("ROI Manager");
    run("Close");
  }
selectWindow("Classification result");
run("Close");

roiManager("Open", Program_ROIs + "divet_rois_test_4tray.zip");
  if (isOpen("Results")) {
    selectWindow("Results");
    run("Close");
  }
roiManager("Select", 41);

for (i=-10;i<0;i++){
  roiManager("Measure");
  roiManager("translate", 0, -1);
}
roiManager("translate", 0, 10);
for (i=0;i<10;i++){
  roiManager("Measure");
  roiManager("translate", 0, 1);
}

run("Summarize");
Mean = getResult("Mean");

for (i=0;i<20;i++){
  g=getResult("Mean",i);
  if (g==Mean) {
    maxMean=i+1;
  }
}

if (maxMean>10) {
  translate_fact_Y=maxMean-11;
}
if (maxMean<=10) {
  translate_fact_Y=(maxMean)-(2*maxMean)+1;
}
print(translate_fact_Y);
```

```
////////////////////////////////////////////////////////////////////////

roiManager("Select", 40);
  if (isOpen("Results")) {
     selectWindow("Results");
     run("Close");
  }

for (i=-10;i<0;i++){
   roiManager("Measure");
   roiManager("translate", -1, 0);
}
roiManager("translate", 10, 0);
for (i=0;i<10;i++){
   roiManager("Measure");
   roiManager("translate", 1, 0);
}

run("Summarize");
MeanX = getResult("Mean");

for (i=0;i<20;i++){
   g=getResult("Mean",i);
   if (g==MeanX) {
     maxMeanX=i+1;
   }
}

if (maxMeanX>10) {
   translate_fact_X=maxMeanX-11;
}
if (maxMeanX<=10) {
   translate_fact_X=(maxMeanX)-(2*maxMeanX)+1;
}
print("max mean intensity index");
print(maxMean);
print("max mean intensity index X");
print(maxMeanX);
print("translate factor X");
print(translate_fact_X);
print("translate factor Y");
print(translate_fact_Y);

  if (isOpen("ROI Manager")) {
     selectWindow("ROI Manager");
     run("Close");
  }

  if (isOpen("Results")) {
     selectWindow("Results");
     run("Close");
  }

////////////////////////////////////////////////////////////////////////

roiManager("Open", Program_ROIs + "divet_rois_test_4tray.zip");
```

```
ROIArr = newArray("0");
for (i=1;i<roiManager("count");i++){
	ROIArr = Array.concat(ROIArr,i);

}
roiManager("select", ROIArr);
roiManager("translate", translate_fact_X, translate_fact_Y);
rename("roi with overlay");
////////////////////////////////////////////////////////////////////////
newImage("tray eliminated", "8-bit black", width, height, 1);

roiManager("Deselect");

for (i=0;i<2;i++){
   roiManager("Select", 40);
   roiManager("Delete");
}

selectWindow("roi with overlay");
roiManager("Combine");
run("Copy");
selectWindow("tray eliminated");
run("Paste");
saveAs("Tiff", save_loc + "roi with overlay");

  if (isOpen("ROI Manager")) {
     selectWindow("ROI Manager");
     run("Close");
  }
////////////////////////////////////////////////////////////////////////
selectWindow(""+TWS+"");
wait(1000);
call("trainableSegmentation.Weka_Segmentation.loadClassifier", class_loc + "tendon classifier.model");
call("trainableSegmentation.Weka_Segmentation.applyClassifier", save_loc, "roi with overlay.tif",
"showResults=true", "storeResults=false", "probabilityMaps=false", "");
wait(10000);
selectWindow("Classification result");
run("8-bit");
run("Threshold...");
setThreshold(100, 255);
run("Convert to Mask");
run("Invert");
run("Analyze Particles...", "size=3-Infinity pixel circularity=0-1.00 show=Outlines display summarize add");

ROIArr = newArray("0");;
for (i=1;i<roiManager("count");i++){
	ROIArr = Array.concat(ROIArr,i);
}
roiManager("select", ROIArr);

ntendons=roiManager("count");
if (ntendons > 0) {
	selectWindow("ROI Manager");
	for (i=0 ; i<ntendons; i++) {
	   roiManager("select", i);
```

```
            run("Enlarge...", "enlarge=1");
            roiManager("Add")
        }
}
roiManager("Delete");

newImage("tendons classified", "8-bit black", width, height, 1);

selectWindow("roi with overlay.tif");
roiManager("Combine");
run("Copy");
selectWindow("tendons classified");
run("Paste");

selectWindow("Results");
run("Close");

selectWindow("tendons classified");
run("Duplicate...", "tendons classified original");
selectWindow("tendons classified");
run("Threshold...");
setThreshold(1, 255);
run("Convert to Mask");

  if (isOpen("ROI Manager")) {
     selectWindow("ROI Manager");
     run("Close");
  }
roiManager("Open", Program_ROIs + "tray_array_rois_4tray.zip");

for (i=0;i<4;i++){
   roiManager("Select", i);
   run("Copy");
   width = getWidth();
   height = getHeight();
   newImage("tendon row "+i, "8-bit black", width, height, 1);
   run("Paste");
   run("Rotate 90 Degrees Right");
   selectWindow("tendons classified");
}
selectWindow("ROI Manager");
run("Close");
  if (isOpen("Results")) {
     selectWindow("Results");
     run("Close");
  }

for (i=0;i<4;i++){
   selectWindow("tendon row "+i);
   makeRectangle(0, 0, 512, 512);
   run("Set Scale...", "distance=2.3273 known=1 unit=mm");
   run("Analyze Particles...", "size=2-Infinity pixel circularity=0-1.00 show=Outlines display summarize add");
}
////////////////////////////////////////////////////////////////////////////
dataDir= newDir + "/"+iter+"/";
File.makeDirectory(dataDir);
```

```
roiManager("Save", dataDir + "ROI_"+iter+".zip");
saveAs("Results", dataDir + "Results_"+iter+".xls");

for (i=0;i<4;i++){
   selectWindow("tendon row "+i);
   saveAs("Tiff", dataDir + "Tendon_Mask_Row_"+i+"_img_"+iter);

}
selectWindow("tendons classified-1");
saveAs("Tiff", dataDir + "Tendons_Classified"+iter);
////////////////////////////////////////////////////////////////////////////////

print("Image "+iter+" is done analyzing... analyzing next image");

run("Close All");
selectWindow("Results");
run("Close");
selectWindow("ROI Manager");
run("Close");
}
```

Note. This code is only for the stack of four trays.

Table 31: Load and Load Rate Calculation for Cyclic → Creep

Sequential Load Testing (Cyclic → Creep)							
Donor	**Study #**	**Type**	**Digit**	**% of UTS**	**Max Load (N)**	**Load Rate 1 Hz (N/s)**	**Min CSA (mm^2)**
5	46	RFDS	4	55	300.87	601.74	11.08
1	47	RFDP	5	55	205.59	411.19	7.57
2	52	RFDP	2	25	82.06	164.11	6.65
2	54	RFDP	4	25	52.42	104.85	4.25
6	55	LFDP	5	55	130.38	260.75	4.80
10	56	LFDS	2	25	63.82	127.64	5.12
2	57	RFDS	4	25	75.22	150.43	6.09
9	58	RFDP	5	55	175.51	351.01	6.46
9	59	RFDS	3	25	86.61	173.23	7.02
3	62	LFDS	2	25	75.22	150.43	6.09
4	63	LFDP	2	25	61.54	123.08	4.98
2	64	LFDP	2	25	72.94	145.88	5.91
8	65	LFDP	5	25	54.70	109.41	4.43
2	66	RFDS	3	55	220.64	441.28	8.12
1	67	RFDS	4	55	35.10	70.20	1.29
8	68	RFDS	2	55	145.42	290.84	5.35
3	69	RFDP	5	55	185.54	371.07	6.83
2	70	LFDS	2	55	105.31	210.61	3.87
10	71	RFDP	5	55	155.45	310.90	5.72
5	72	LFDS	2	25	123.08	246.17	9.97
7	73	RFDP	5	55	245.71	491.42	9.05
5	74	LFDP	3	55	80.23	160.46	2.95
9	75	RFDS	4	25	63.82	127.64	5.17
1	76	LFDS	3	55	30.09	60.18	1.11
9	78	LFDP	2	25	107.13	214.26	8.68
2	79	RFDP	3	55	90.26	180.52	3.32
1	81	RFDS	3	25	79.78	159.55	6.46
10	82	RFDP	4	55	185.54	371.07	6.83
5	84	LFDP	2	55	190.55	381.10	7.02

Table 32: Load and Load Rate Calculation for Creep → Cyclic

Sequential Load Order Testing (Creep → Cyclic)							
Donor	**Study #**	**Type**	**Digit**	**% of UTS**	**Max Load (N)**	**Load Rate 1Hz (N/s)**	**Min CSA (mm^2)**
6	85	LFDS	5	55	30.09	60.18	1.11
10	86	RFDS	3	55	215.62	431.25	7.94
6	87	RFDS	3	55	170.49	340.98	6.27
10	88	RFDP	2	25	72.94	145.88	5.91
7	89	LFDP	2	25	100.29	200.58	8.12
8	90	LFDP	4	55	135.39	270.78	4.98
1	91	LFDP	5	55	110.32	220.64	4.06
9	92	LFDS	5	55	30.09	60.18	1.12
8	93	RFDS	3	25	79.78	159.55	6.46
7	94	LFDS	5	55	45.13	90.26	1.66
3	95	RFDP	4	55	220.64	441.28	8.12
10	97	LFDP	5	55	105.31	210.61	3.88
9	98	LFDP	4	25	157.27	314.55	12.74
4	99	RFDS	3	25	136.76	273.52	11.08
4	100	LFDS	5	25	13.68	27.35	1.12
8	102	LFDS	3	25	109.41	218.81	8.86
10	103	RFDP	3	25	59.26	118.52	4.80
9	105	RFDP	2	25	109.41	218.81	8.86
7	109	LFDP	5	25	84.33	168.67	6.83
8	110	LFDP	2	55	155.45	310.90	5.72
7	111	RFDP	3	25	175.51	351.01	14.22
7	112	LFDS	2	55	155.45	310.90	5.72
6	113	RFDS	4	55	140.41	280.81	5.17
1	114	RFDP	3	55	170.49	340.98	6.28
10	116	LFDS	5	55	25.07	50.14	0.92
7	117	RFDS	2	25	98.01	196.02	7.94
1	120	LFDP	2	55	80.23	160.46	2.95
3	121	RFDS	3	55	155.45	310.90	5.72
8	122	LFDS	5	55	35.10	70.20	1.29
9	123	LFDP	3	25	177.79	355.57	14.40
9	124	RFDP	4	25	129.92	259.84	10.52

Table 33: R Code: Code for Calculating Strain Differences for Each Load Sequence

```
################################### Cr 55 ###################################
cr55 <- read.csv("CrCy55Full.csv", header=TRUE)
# Code treatment cyclic = 1, creep = 0
# == creates a boolean (meaning there are two possible values, true or false)
#operator which ensures that the values on the left side are the exact same as the values on the right
cr55$Trt <- as.integer(cr55$Trt == "Cyclic")
# Find the last index(row #) of where tendons change
lastind <- cumsum(rle(cr55.1$Tendon)$lengths)
# Find the first index (row #) of where tendons(testing number) change
firstind <- c(0,lastind[-length(lastind)]) + 1
# Drop the first row for each tendon
cr55.2 <- cr55.1[-firstind, ]
# Drop the last row for each tendon
cr55.3 <- cr55.1[-lastind, ]

# Create new dataframe with differences creates strain and Trt differences between the end of each event of the
sequence
cr55new <- cr55.2
cr55new$Trt <- cr55.2$Trt - cr55.3$Trt
cr55new$Strain <- cr55.2$Strain - cr55.3$Strain
# Scale time
cr55new$Time <- scale(cr55new$Time)
# If you need time differences then do the following
cr55new$Time <- cr55.2$Time - cr55.3$Time
# Trt = -1 if creep -> cyclic, Trt = 1 if cyclic -> creep Result of differenced Trt
# Change to Trt = 0 if creep -> cyclic, Trt = 1 if cyclic -> creep
cr55new$Trt <- as.factor(cr55new$Trt == 0)
################################### Cr 25 ###################################
cr25 <- read.csv("CrCy55Full.csv", header=TRUE)
# Code treatment cyclic = 1, creep = 0
cr25$Trt <- as.integer(cr25$Trt == "Cyclic")
# find the last index of where tendons change
lastind <- cumsum(rle(cr25.1$Tendon)$lengths)
# Find the first index of where tendons change
firstind <- c(0,lastind[-length(lastind)]) + 1
# Drop the first row for each tendon
cr25.2 <- cr25.1[-firstind, ]
# Drop the last row for each tendon
cr25.3 <- cr25.1[-lastind, ]
# Create new dataframe with differences (for Markov)
cr25new <- cr25.2
cr25new$Trt <- cr25.2$Trt - cr25.3$Trt
cr25new$Strain <- cr25.2$Strain - cr25.3$Strain
# Scale time
cr25new$Time <- scale(cr25new$Time)
# If you need time differences then do the following
cr25new$Time <- cr25.2$Time - cr25.3$Time
# Trt = -1 if creep -> cyclic, Trt = 1 if cyclic -> creep
# Change to Trt = 0 if creep -> cyclic, Trt = 1 if cyclic -> creep
cr25new$Trt <- as.factor(cr25new$Trt == 0)
################################## Cy 55 ##################################
cy55 <- read.csv("CyCr55Full.csv", header=TRUE)
# Code treatment cyclic = 1, creep = 0
```

```
cy55$Trt <- as.integer(cy55$Trt == "Cyclic")
# Find the last index of where tendons change
lastind <- cumsum(rle(cy55.1$Tendon)$lengths)
# Find the first index of where tendons change
firstind <- c(0,lastind[-length(lastind)]) + 1
# Drop the first row for each tendon
cy55.2 <- cy55.1[-firstind, ]
# Drop the last row for each tendon
cy55.3 <- cy55.1[-lastind, ]
# Create new dataframe with differences (for Markov)
cy55new <- cy55.2
cy55new$Trt <- cy55.2$Trt - cy55.3$Trt
cy55new$Strain <- cy55.2$Strain - cy55.3$Strain
# Scale time
cy55new$Time <- scale(cy55new$Time)
# If you need time differences then do the following
cy55new$Time <- cy55.2$Time - cy55.3$Time
# Trt = -1 if creep -> cyclic, Trt = 1 if cyclic -> creep
# Change to Trt = 0 if creep -> cyclic, Trt = 1 if cyclic -> creep
cy55new$Trt <- as.factor(cy55new$Trt == 1)
########################## Cy 25 ################################
cy25 <- read.csv("CyCr25Full.csv", header=TRUE)
# Code treatment cyclic = 1, creep = 0
cy25$Trt <- as.integer(cy25$Trt == "Cyclic")
# Find the last index of where tendons change
lastind <- cumsum(rle(cy25.1$Tendon)$lengths)
# Find the first index of where tendons change
firstind <- c(0,lastind[-length(lastind)]) + 1
# Drop the first row for each tendon
cy25.2 <- cy25.1[-firstind, ]
# Drop the last row for each tendon
cy25.3 <- cy25.1[-lastind, ]
# Create new dataframe with differences (for Markov)
cy25new <- cy25.2
cy25new$Trt <- cy25.2$Trt - cy25.3$Trt
cy25new$Strain <- cy25.2$Strain - cy25.3$Strain
# Scale time
cy25new$Time <- scale(cy25new$Time)
# If you need time differences then do the following
cy25new$Time <- cy25.2$Time - cy25.3$Time
# Trt = -1 if creep -> cyclic, Trt = 1 if cyclic -> creep
# Change to Trt = 0 if creep -> cyclic, Trt = 1 if cyclic -> creep
cy25new$Trt <- as.factor(cy25new$Trt == 1)
############## Creating new data frame with all required variables #################
cy25new2 <- data.frame(Time=cy25new$Time, Trt=cy25new$Trt, Strain=cy25new$Strain,
Tendon=cy25new$Tendon, Donor=cy25new$Donor,  Load = rep(25, dim(cy25new)[1]))
cr25new2 <- data.frame(Time=cr25new$Time, Trt=cr25new$Trt, Strain=cr25new$Strain,
Tendon=cr25new$Tendon, Donor=cr25new$Donor,  Load = rep(25, dim(cr25new)[1]))
cy55new2 <- data.frame(Time=cy55new$Time, Trt=cy55new$Trt, Strain=cy55new$Strain,
Tendon=cy55new$Tendon, Donor=cy55new$Donor,  Load = rep(55, dim(cy55new)[1]))
cr55new2 <- data.frame(Time=cr55new$Time, Trt=cr55new$Trt, Strain=cr55new$Strain,
Tendon=cr55new$Tendon, Donor=cr55new$Donor,  Load = rep(55, dim(cr55new)[1]))
cycr <- rbind(cr25new2, cy25new2, cr55new2, cy55new2)
```

Table 34: R Code: Code for Model and Analysis

```
#Testing of Linear Models
library(lme4)
library(sjPlot)
library(ggplot2)
library(splines)
library(sjlabelled)
library(tidyverse)

#Other Libraries
library(patchwork)

#Mixed Effect

library(readr)
cycr <- read_csv("cycr2.csv")
#cycra <- read_csv("cycr.csv")
View(cycr)

cycr$Hand <- as.factor(cycr$Hand == "Right")
#This makes Right = TRUE
cycr$Type <- as.factor(cycr$Type == "FDP")
#Makes FDP = TRUE
cycr$Digit <- as.factor(cycr$Digit)
cycr$Fail<- as.factor(cycr$Fail)
cycr$Load <- as.factor(cycr$Load)
cycr$Direction <- as.factor(ifelse(cycr$Trt == TRUE, "Creep -> Cycle", "Cycle -> Creep"))
cycr3<-cycr

cycr3.mod <- lmer(Wren ~ Direction + Load + (1|Donor/Tendon) + Adj_Time + Load*Adj_Time , data = cycr3,
REML = TRUE, verbose = FALSE)
tab_model(cycr3.mod, digits = 6, digits.re = 6, dv.labels = c("Strain Difference"),
CSS=css_theme("cells"),auto.label = "", show.fstat = TRUE)

#simple main effects analysis
#Create subset of data only using 25% (3a) Load=25
cycr3a<-cycr3 %>% filter(Load==25)

my_model <- lmer(Wren ~ Direction  + (1|Donor/Tendon), data = cycr3a)
tab_model(my_model, digits = 6, digits.re = 8, dv.labels = c("Delta Strain"), CSS=css_theme("cells"),auto.label =
"", title = "25%UTS",show.df = TRUE)

#Create subset of data only using 55% (3b) Load=55
cycr3b<-cycr3 %>% filter(Load==55)

my_model2 <- lmer(Wren ~ Direction  + (1|Donor/Tendon) , data = cycr3b)
tab_model(my_model2, digits = 6, digits.re = 6, dv.labels = c("Delta Strain"), CSS=css_theme("cells"),auto.label =
"", title = "55%UTS")
```

Table 35: Load Transition Test Results Cyclic → Creep.

Sequential Load Order Testing (Cyclic → Creep)												
Donor	**Type**	**Digit**	**Study #**	**Rand**	**% of UTS**	**Mass (g)**	**Length (cm)**	**Max load (N)**	**Max Stress (MPa)**	**Time till Failure (hrs.)**	**Completed Sequences**	**Failure Strain**
2	RFDP	2	52	0.3271	25	0.814	8	83.50	12.56	1032.24	255	0.22
2	RFDP	4	54	0.3404	25	0.798	8.1	53.50	12.60	1339.98	280	0.09
10	LFDS	2	56	0.3756	25	0.643	8.1	64.79	12.53	2498.91	620	0.08
3	LFDS	2	62	0.4754	25	0.639	8.1	76.39	12.54	1509.74	369	0.10
2	LFDP	2	64	0.5288	25	0.839	8.4	77.32	13.09	207.62	49	0.08
8	LFDP	5	65	0.5523	25	0.573	8.3	55.46	12.52	1390.46	321	0.09
5	LFDS	2	72	0.6245	25	1.094	8.2	124.56	12.49	153.51	38	0.13
9	RFDS	4	75	0.6652	25	0.723	8.2	65.14	12.60	5304.87	1317	0.13
5	RFDS	4	46	0.298	55	1.238	8.2	303.57	27.40	0.46	0	0.07
1	RFDP	5	47	0.3004	55	0.444	8	207.59	27.42	0.048	0	0.03
6	LFDP	5	55	0.3536	55	0.681	8.4	132.22	27.54	150.51	35	0.12
9	RFDP	5	58	0.4064	55	0.595	8.1	178.25	27.58	0.45	0	0.08
2	RFDS	3	66	0.56	55	1.098	8.3	223.80	27.55	85.55	21	0.17
1	RFDS	4	67	0.569	55	-	-	35.54	27.50	495.13	125	0.07
8	RFDS	2	68	0.5876	55	0.713	8.5	148.03	27.65	49.17	12	0.09
3	RFDP	5	69	0.5986	55	0.62	8.4	188.41	27.58	0.14	0	0.06
2	LFDS	2	70	0.6081	55	0.594	8.3	107.48	27.72	14.78	3	0.12
10	RFDP	5	71	0.6195	55	0.611	8.2	157.15	27.46	17.40	4	0.16
7	RFDP	5	73	0.6307	55	0.648	8.2	248.61	27.48	4.68	1	0.10
5	LFDP	3	74	0.6409	55	1.895	7.8	81.71	27.66	4250.46	976	0.09
1	LFDS	3	76	0.6689	55	0.781	8	30.11	27.18	121.59	30	0.08
2	RFDP	3	79	0.6994	55	0.881	8	91.73	27.60	646.27	149	0.09
10	RFDP	4	82	0.7204	55	0.898	8.5	191.25	28.00	5.34	1	0.13
5	LFDP	2	84	0.6778	55	1.567	8.5	193.03	27.50	109.56	26	0.14

Note. This data table is the result of load sequence test where the test begins with cyclic loading.

Table 36: Load Transition Test Results Creep → Cyclic.

Sequential Load Order Testing (Creep → Cyclic)												
Donor	**Type**	**Digit**	**Study #**	**Rand**	**% of UTS**	**Mass (g)**	**Length (cm)**	**Max load (N)**	**Max Stress (MPa)**	**Time till Failure (hrs.)**	**Completed Sequences**	**Failure Strain**
7	LFDP	2	89	0.35	25	0.774	8.4	101.67	12.52	323.04	70	0.09
8	RFDS	3	93	0.42	25	0.869	8.2	81.04	12.54	3692.88	920	0.14
9	LFDP	4	98	0.49	25	1.365	8.1	161.04	12.64	758.42	163	0.16
4	LFDS	5	100	0.5	25	0.113	8.3	14.06	12.70	2.24	0	0.03
8	LFDS	3	102	0.52	25	0.773	8	111.11	12.54	340.88	84	0.12
7	LFDP	5	109	0.59	25	0.556	8.5	85.50	12.52	313.82	74	0.09
7	RFDP	3	111	0.61	25	1.057	8.5	177.97	12.36	85.55	18	0.11
9	RFDP	4	124	0.79	25	1.273	8.3	132.45	12.59	5507.53	1359	0.12
6	LFDS	5	85	0.29	55	0.139	8.4	32.71	29.53	3.68	0	0.10
10	RFDS	3	86	0.32	55	1.16	8	224.43	27.29	111.08	27	0.19
6	RFDS	3	87	0.33	55	0.846	8.5	172.80	27.53	91.77	21	0.12
8	LFDP	4	90	0.36	55	0.772	8	136.77	27.44	19.50	3	0.04
1	LFDP	5	91	0.36	55	0.47	8.2	111.65	27.49	2.34	0	0.08
9	LFDS	5	92	0.36	55	0.139	8.2	56.72	51.20	2.41	0	0.11
7	LFDS	5	94	0.45	55	0.22	8.2	45.73	27.52	43.97	8	0.09
3	RFDP	4	95	0.46	55	1.228	8.3	223.45	27.51	109.57	23	0.12
10	LFDP	5	97	0.47	55	0.509	8.2	106.84	27.56	68.93	13	0.10
8	LFDP	2	110	0.61	55	0.688	8.2	157.81	27.57	140.26	31	0.12
7	LFDS	2	112	55	55	-	-	160.01	27.96	2.15	0	0.02
6	RFDS	4	113	0.61	55	0.633	7.8	142.28	27.52	59.51	13	0.13
1	RFDP	3	114	0.63	55	1.086	8.4	172.50	27.48	51.92	11	0.11
10	LFDS	5	116	0.7	55	0.186	8.1	25.59	27.73	43.77	7	0.07
8	LFDS	5	122	0.78	55	0.19	8.1	35.52	27.48	25.84	4	0.05

Note. This data table is the result of load sequence test where the test begins with creep loading.

Table 37: Data table of Censored Tendons

Survived Tendons: Sequential Load Order Testing (Creep → Cyclic)													
Donor	**Type**	**Digit**	**Study #**	**Rand**	**% of UTS**	**Mass (g)**	**Length (cm)**	**Max load (N)**	**Min CSA (mm^2)**	**Max Stress (MPa)**	**Time (hrs.)**	**Completed Sequences**	**Strain**
10	RFDP	2	88	0.332	25	0.994	8.2	73.59	5.9081	12.46	120.47	1861	0.07
10	RFDP	3	103	0.533	25	0.94	8.1	59.97	4.8003	12.49	119.34	1810	0.05
1	LFDP	2	120	0.758	55	0.804	8	81.38	2.954	27.55	265.22	3543	0.11

Note. The tendons in this table did not fail, strain reference to the peak strain when the test was stopped.

Figure 28: Strain Time Curve Example 55% Creep → Cyclic

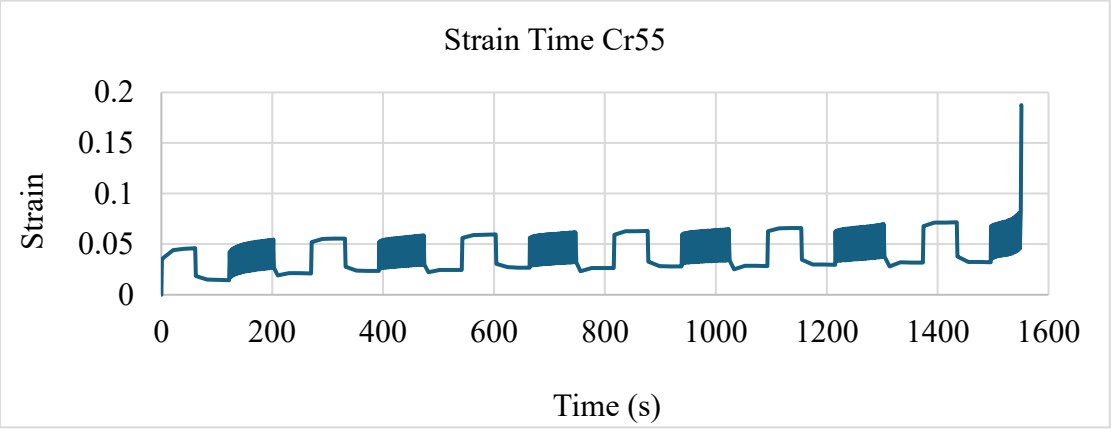

Note. This figure is an example of a tendon tested at 55% UTS and with the starting phase being creep.

Figure 29: Strain Time Curve Example 55% Cyclic → Creep

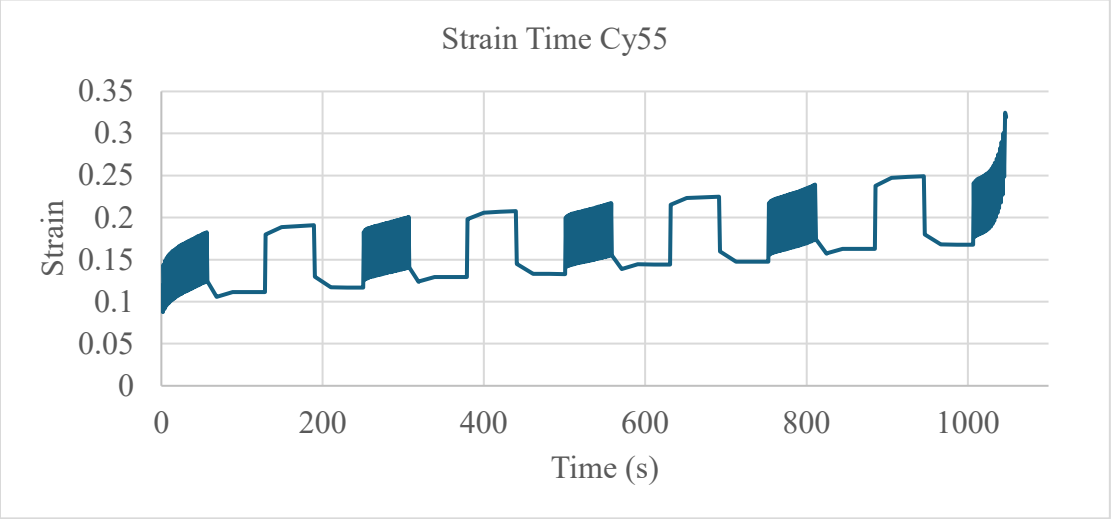

Note. This figure is an example of a tendon tested at 55% UTS and with the starting phase being cyclic.

Figure 30: Strain Time Curve Example 25% Cyclic → Creep

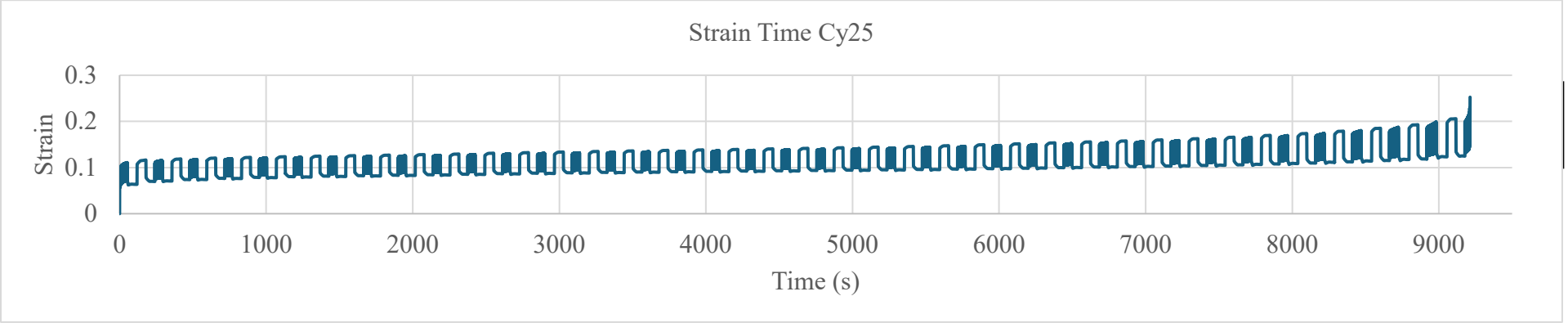

Note. This figure is an example of a tendon tested at 25% UTS and with the starting phase being cyclic.

Figure 31: Strain Time Curve Example 25% Cyclic → Creep

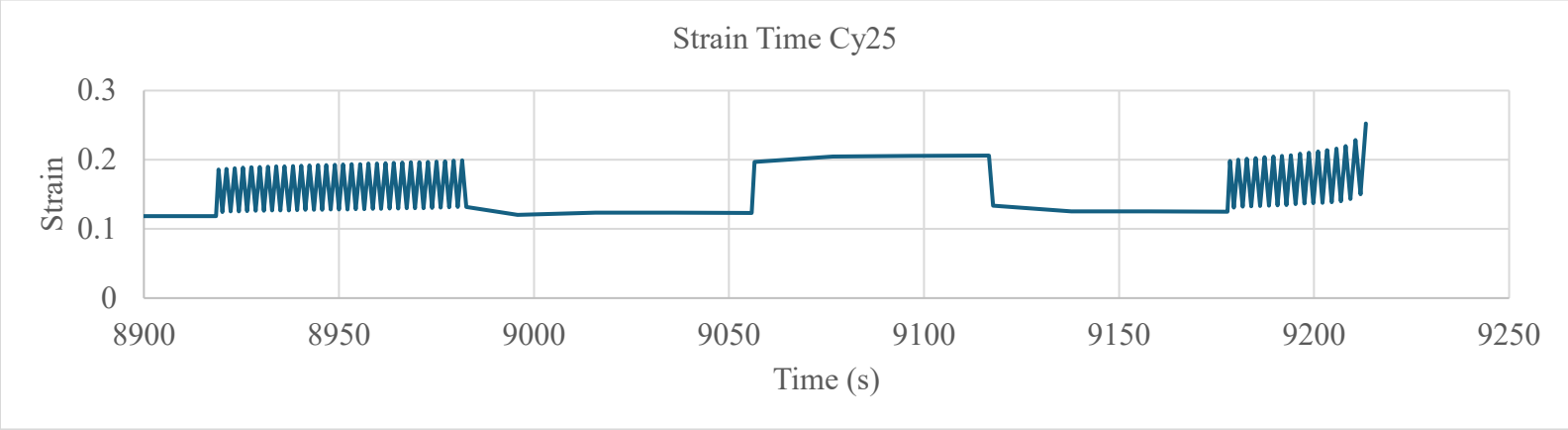

Note. This is a zoomed in version of Figure 30 showing the last sequence and when the sample failed.

Figure 32: Strain Time Curve Example 25% Creep → Cyclic

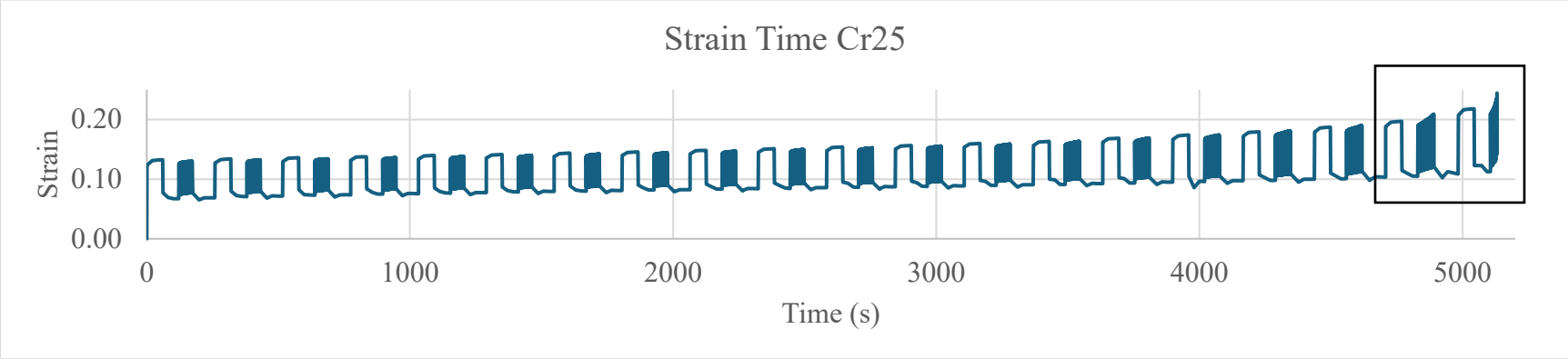

Note. This figure is an example of a tendon tested at 25% UTS and with the starting phase being cyclic.

Figure 33: Strain Time Curve Example 25% Creep → Cyclic

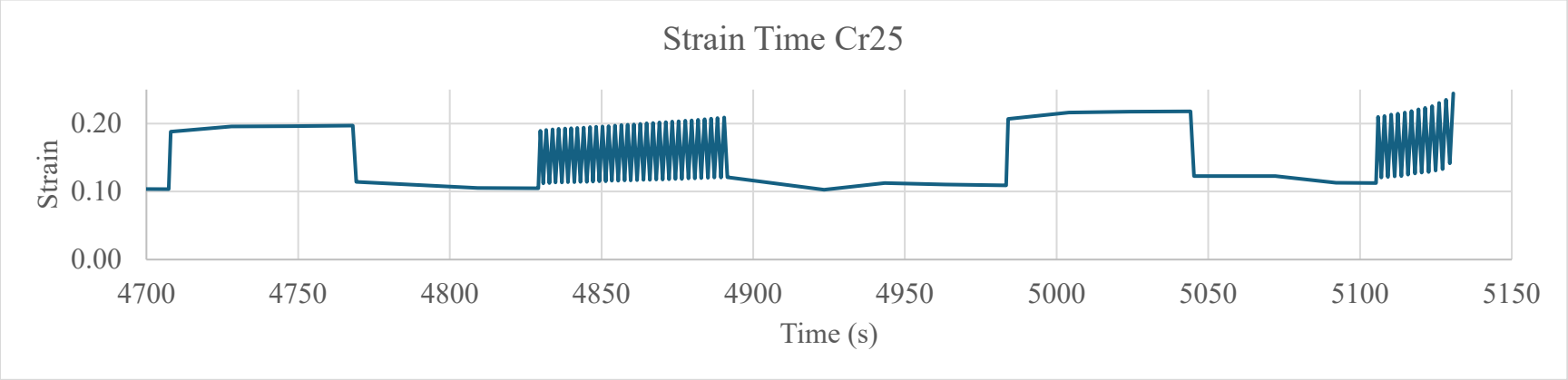

Note. This is a zoomed in version of Figure 32 showing the last sequence and when the sample failed.